Effect of Creep Loading on the Nanostructure of Tendons

Khaled Marwan Anis Hijazi

A Thesis Submitted to Saint Marys University, Halifax, Nova Scotia in Partial Fulfillment
of the Requirements for the Degree of
Master of Science in Applied Science

© Khaled Marwan Anis Hijazi, 2017

Approved by:

Dr. Samuel P. Veres
Supervisor

Dr. Laurent Kreplak
External Examiner

Dr. J. Michael Lee
Examiner

Dr. Kathy L. Singfield
Examiner

Date: Friday August 25, 2017

'I dedicate this work to my parents and family, for whom I am indepted with everything I was, everything I am, and everything I will ever be.'

Abstract

Effect of Creep Loading on the Nanostructure of Tendons

By: Khaled Marwan Anis Hijazi

This thesis focused on exploring ultrastructural damage to tendons during low strain-rate loading at overload and suboverload levels. In the first experiment, tendons were either statically loaded at overload stress until rupture, ramp loaded to yield and then unloaded, or ramp loaded until rupture. In the second experiment, tendons were statically loaded at suboverloaded stress for different periods of time, after which they were unloaded. Structural assessments of loaded tendons and matched-pair controls were conducted using scanning electron microscopy and differential scanning calorimetry. Rupturing tendons at low strain-rate created significant ultrastructural damage to the packing of collagen molecules within fibrils. Only when rupture occurred during static loading, though, were significant quantities of denatured collagen created. Sustained loading at suboverload levels was found to disrupt collagen fibrils when applied for durations >2 hours.

Date Submitted: Friday August 25, 2017

Acknowledgments

I'd like to acknowledge my supervisors Samuel Veres, Kathy Singfield and Michael Lee for the quality and consistency of their support, their ongoing enthusiasm, and their patience. I'd like to thank all the faculty at Saint Mary's University's Division of Engineering and Faculty of Science, for supporting me and all the other students, both on the graduate and the undergraduate levels. I'd also like to acknowledge my lab partners both at our lab at Saint Mary's University and our sister Tissue Mechanics lab at Dalhousie University for their consistent support and help. In particular, I'd like to thank Michael Morgan, Brendan Grue, and Samuel Baldwin all of whom offered great assistance to me during the different steps of conducting my experiments.

Contents

List of Tables vii

List of Figures viii

1 Background 1

1.1 Anatomy and Physiology of Tendons . . . 1

1.1.1 Tendons and their Structural Hierarchy . . . 1

1.1.2 Crosslinks . . . 4

1.1.3 Non-Collagenous Components of tendons . . . 4

1.2 Mechanical Properties of Tendons . . . 5

1.2.1 Viscoelasticity . . . 5

1.2.2 Response of Tendons to Applied Tension at Suboverload Stress Levels . . . 5

1.2.3 Response of Tendons to Applied Tension at Overload Stress Levels 7

1.3 Creep Testing of Tendons . . . 13

1.4 Stress Relaxation . . . 18

2 Literature Summary and Thesis Objectives 19

2.1 Outcome of the Previous Literature . . . 19

2.2 Objectives . . . 20

3 Building and Testing the Mechanical Creep System 22

3.1 Hardware . . . 22

3.2 Software . . . 24
3.3 Testing and Calibrating the Mechanical Creep System . . . 28
3.3.1 Confirming the Linearity of Load Cell Readings . . . 28
3.3.2 Confirming Optical Encoder Readings . . . 29
3.3.3 Confirming Functionality of Ramp Loading . . . 30
3.3.4 Confirming the Functionality of the Static Creep Test . . . 31

4 Overload Creep Rupture's Effect on the Nanostructure of Tendons 36
4.1 Introduction and Research Question . . . 36
4.2 Hypotheses and Rationale . . . 37
4.3 Methodology . . . 39
4.3.1 Tendon Preparation and Geometrical Dimensions' Measurement 40
4.3.2 Mechanical Loading Tests . . . 41
4.3.3 Determination of the Yield Point of Tendons . . . 43
4.3.4 DSC Thermoanalysis . . . 47
4.3.5 SEM Nanostructural Analysis . . . 49
4.3.6 Statistical Analysis . . . 51
4.4 Results . . . 52
4.4.1 Mechanical Properties . . . 52
4.4.2 Macrostructural Rupture Properties . . . 55
4.4.3 DSC Thermoanalysis . . . 56
4.4.4 SEM Nanostructural Analysis . . . 60
4.5 Discussion . . . 72
4.5.1 The Relationship Between Fibrillar- and Molecular-level Structural Alterations . . . 72
4.5.2 The Role of Strain Rate in Nanostructural Damage Formation 75
4.5.3 Possible Differences in Other Tendon Models . . . 77

5 Suboverload Creep Rupture's Effect on the Nanostructure of Tendons 78
5.1 Introduction and Research Question . . . 78
5.2 Hypotheses and Rationale . . . 79

5.2.1 Hypotheses . . . 79
5.2.2 Rationale . . . 79
5.3 Methodology . . . 80
5.3.1 Mechanical Loading Tests . . . 80
5.3.2 Post-Test Mechanical Analysis . . . 81
5.3.3 Analysis of the Samples: SEM and DSC Tests . . . 82
5.3.4 Statistical Analysis . . . 84
5.4 Results . . . 84
5.4.1 Mechanical Properties . . . 84
5.4.2 DSC Thermoanalysis . . . 85
5.4.3 SEM Nanostructural Analysis . . . 86
5.5 Discussion . . . 97
5.5.1 Time Dependence of both Macroscale and Nanoscale damage formation . . . 97
5.5.2 The Relationship between Molecular and Fibrillar Damage . . . 97
5.5.3 Creep Loading Induced Nanostructural Disruption . . . 102
5.5.4 Structural Continuity of Collagen Fibrils . . . 104
5.5.5 Physiological Relevance of this Study's Results . . . 106

6 Summary and Conclusion **109**
6.1 Summary of Results . . . 109
6.2 Significance . . . 110
6.3 Next Steps . . . 111

Bibliography **113**

List of Tables

1.1 Collagen content measured in human and bovine tendons. 2

4.1 Comparison of the yield points of tendons determined through different methods. 46
4.2 Average yield stress and yield strain values from tested tendons. . . . 55
4.3 A summary of the first experiment's DSC thermoanalysis. 57
4.4 Comparison between the DSC analysis of this study and that of a previous study. 76

5.1 Fit tests of creep strain vs. creep duration 86
5.2 Maximum stress experienced by human and cow tendons *in vivo* . . . 107

List of Figures

1.1 Schematic diagram of the structure of rat tail tendons. 2
1.2 Axial structure of D-periodic collagen fibrils, showing the dark and light appearance of the D-banding. 3
1.3 Typical stress-strain response observed in rat tail tendons. 6
1.4 Representative stress-strain curves of ramp loaded rabbit anterior cruciate ligaments and patellar tendons at different strain rates. 8
1.5 SEM: Differences in fibril structure before and after overloading . . . 9
1.6 SEM images showing differences in structural changes caused by overloading CDETs and overloading SDFTs 10
1.7 The progression of discrete plasticity under repetitive stress 11
1.8 SEM images showing the discrete plasticity effect in collagen fibrils, along with the effect of trypsin digestion on overloaded tendon fibrils 12
1.9 A Typical strain-time curve of a static creep loading session. 14
1.10 Variation in creep lifetime with different stress levels for wallaby tail tendons. 15
1.11 Lifetime (s)-Temperature (°C) chart of results of the static creep loading done on wallaby tails. 15
1.12 Lifetime (s)-Length graph(mm) of results of static creep loading, at different stress levels. 16
1.13 Creep lifetime vs. initial strain, failure strain and applied stress level. 17

3.1 Mechanical Creep System (MCS) hardware assembly. 23
3.2 The front panel of the main VI (OCR). 25

3.3 The front panel of the main VI (SCL). 26
3.4 Linearity test: Representative stress-strain chart of loading a plastic bar 29
3.5 Comparison between the displacement recorded by the MCS and the caliper measured displacement after the last calibration. 31
3.6 Stress-strain curves of the two ramp loaded tendons. 32
3.7 Strain-time curves of the two ramp loaded tendons. 33
3.8 Stress-strain curves of both creep overloaded tendons. 34
3.9 Strain-time curves of both creep overloaded tendons. 35

4.1 The flowchart of the procedure of the first experiment. 40
4.2 Creep overloaded tendon's stress-strain curve. 43
4.3 A magnified region of the creep loading phase in Figure 4.2 44
4.4 A representative highly stressed and then unloaded tendon's stress-strain curve. 45
4.5 A representative ramp ruptured tendon's stress-strain curve. 46
4.6 An RR Stress Strain curve with the slope change percentage readings superimposed. 47
4.7 A representative ramp rupture's stress-strain presenting the yield point determination's analysis. 48
4.8 Two representative DSC office 50
4.9 Representative SEM image of a panoramic scan of a tendon sample. . 51
4.10 Representative Stress-Strain and Strain-Time charts an OCR sample 53
4.11 Representative Stress-Strain and Strain-Time charts an OCR sample 54
4.12 Representative DSC endotherms of an OCR sample compare to that of a matched pair control 56
4.13 Representative DSC endotherms of an HS sample compare to that of a matched pair control 57
4.14 Representative DSC endotherms of an RR sample compare to that of a matched pair control 58
4.15 DSC test result: comparisons of the DSC thermal analysis of the three mechanical protocols 59
4.16 SEM images of a high stress sample and its matched pair control. . . 61

4.17 SEM images of a high stress sample and its matched pair control. . . 62
4.18 SEM image of a creep overloaded sample vs. a matched pair control. 63
4.19 SEM image of a creep overloaded sample vs. a matched pair control. 64
4.20 SEM image of a creep overloaded sample vs. a matched pair control. 65
4.21 SEM image of a creep overloaded sample vs. a matched pair control. 66
4.22 SEM image of a creep overloaded sample vs. a matched pair control. 67
4.23 SEM image of a ramp loaded sample vs. an unloaded control sample. 68
4.24 SEM image of a ramp loaded sample vs. an unloaded control sample. 69
4.25 SEM image of a ramp loaded sample vs. an unloaded control sample. 70
4.26 SEM image of a ramp loaded sample vs. an unloaded control sample. 71

5.1 The flowchart of the methodology of the SCL experiment. 81
5.2 Illustration of the process of calculating the secondary creep loading start and end points. 83
5.3 Creep Strain vs. Creep Duration plot with the logarithmic fit shown. 85
5.4 Differential Scanning Calorimetry Endotherms of different SCL samples. 87
5.5 Changes in the DSC parameters vs. creep strain (ϵ_{creep}) 88
5.6 SEM image of the first creep suboverloaded five hour sample vs. a matched pair control. 89
5.7 SEM image of the first creep suboverloaded five hour sample vs. a matched pair control. 90
5.8 SEM image of the first creep suboverloaded five hour sample vs. a matched pair control. 91
5.9 SEM image of the second creep suboverloaded five hour sample vs. a matched pair control. 92
5.10 SEM image of the second creep suboverloaded five hour sample vs. a matched pair control. 93
5.11 SEM image of one of the creep suboverloaded four hour sample vs. a matched pair unloaded control. 94
5.12 SEM image of one of the creep suboverloaded four hour sample vs. a matched pair unloaded control. 95

5.13 SEM image of one of the creep suboverloaded four hour sample vs. a matched pair unloaded control. 96
5.14 SEM image of one of the creep suboverloaded two hour sample vs. a matched pair unloaded control. 98
5.15 SEM image of one of the creep suboverloaded two hour sample vs. a matched pair unloaded control. 99
5.16 SEM image of one of the creep suboverloaded two hour sample vs. a matched pair unloaded control. 100

Chapter 1

Background

1.1 Anatomy and Physiology of Tendons

1.1.1 Tendons and their Structural Hierarchy

Tendons are hierarchically structured and collagenous connective tissues, whose main function is to transmit force from muscles to bones, allowing the movement of skeletal systems[1–3]. To perform their physiological functions, tendons are required to withstand high uniaxial tensile forces, resisting catastrophic failure in the process[4]. The structural hierarchy of tendons has been studied intensively, with the most common model studied being rat tail tendons (Figure 1.1)[5–8]. Collagen molecules and fibrils form the nanostructural level, while fibers and fascicles form the microstructural level. Finally, groups of fascicles or whole tendons may be referred to as the macrostructural level.

Collagen is the main structural component of tendons[6,9–11]. Collagen molecules are triple-helical proteins that are approximately 300 nm in length and 1 nm in diameter[12–15]. While many types of collagen exist, type I collagen is the most prominent in tendons, making up to 70%-80% of the dry mass of most tendons[16]. The triple helix of type I collagen consists of three amino acid chains known as α-chains, two

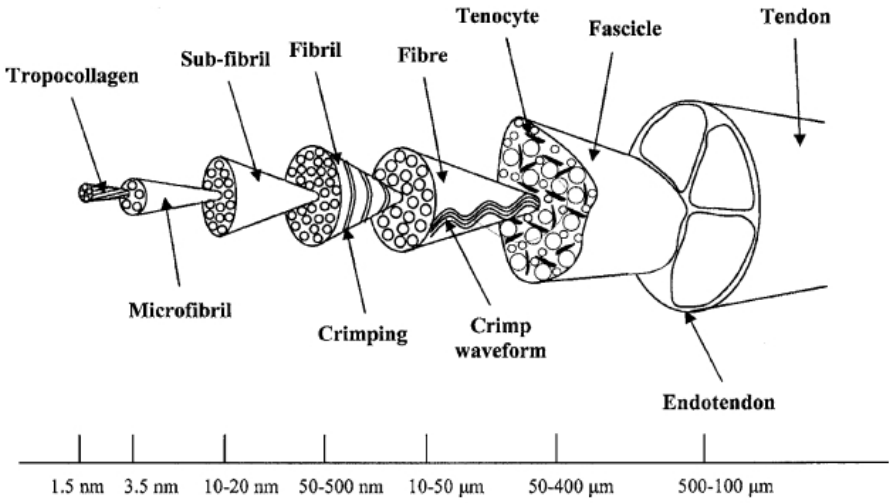

Figure 1.1: Schematic diagram of the structural hierarchy of rat tail tendons[8].

Table 1.1: Collagen content measured in human and bovine tendons.

Tendon Type	Type I Collagen Dry Mass (%)
Human supraspinatus tendon	67[23]
Human biceps flexor tendon	65[23]
Bovine tail tendon	80[24]

α1-chains and one α2-chain, which are held together via hydrogen bonds[17]. Table 1.1 shows type I collagen content found in some human tendons and steer tail tendons. Type I collagen appears to be the major contributor to the mechanical properties of tendons[12,18,19]. Traces of other collagen types, most notably type III collagen, can be found in tendons[20–22].

Tendons are composed of a longitudinal arrangement of collagen fibrils. Collagen fibrils are linear aggregates of collagen molecules[25,26]. Fibrils are approximately 50 to 500 nm in diameter[16,27]. Collagen fibrils in tendons have a cross-striated pattern with 67 nm repeat, better known as D-banding[28,29]. D-banding is formed due to the quarter stagger and semi-crystalline packing of collagen molecules with repeating gap and

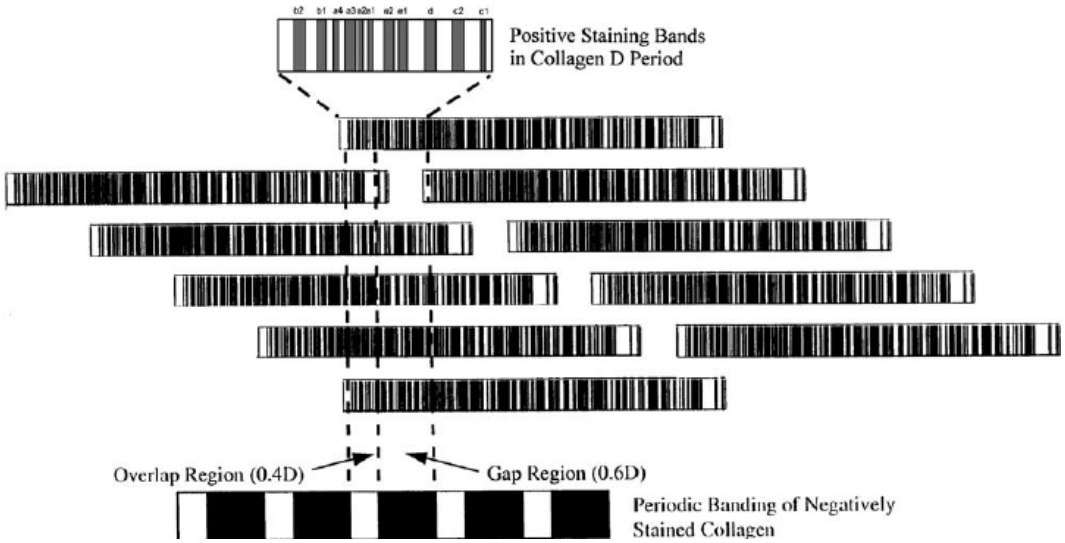

Figure 1.2: Axial structure of D-periodic collagen fibrils, showing the dark and light appearance of the D-banding[29].

overlap regions within fibrils[28,29] (Figure 1.2). Groups of five collagen molecules are packed into microfibrils and joined via intermolecular crosslinking[20,27,30]. Microfibrils are bundled into subfibrils[31]. Subfibrils are wound around the fibril's axis during fibril formation[32]. This orientation pattern is reminiscent of that of a rope[33–35].

A subject debated in the field of tendon research revolves around the question of whether fibrils are continuous along the length of tendons. Many studies indicated that fibrils are more likely to be discontinuous[3,8,28,36–40]. It was initially thought that a physical intermediate, such as proteoglycans link adjacent fibrils[41,42]. However, several investigations reported that proteoglycans do not perform a fundamental role in load transfer within ligaments and tendons[43–45]. Alternatively, a recent study done by Szczesny et al.[40] suggested that interfibrillar load transfer is provided by small diameter fibrils[40]. Szczesny et al.[38,46] suggested that discontinuous fibrils in tendons would experience shear stress when loaded in tension, causing interfibrillar sliding, an event that was well documented and measured in recent studies[38,46]. Such interfibrillar sliding is thought to be the cause of fibrillar damage in loaded tendons[38]. On the other hand, recent studies have pointed towards the fibrils in tendons being longitudinally

continuous[7,47]. In a recent study, Svensson et al.[47] used serial block-face images of mouse tendons, human hamstring tendons, and human patellar tendons to determine their fibrils' lengths. In total, 67.5 mm of fibril length was tracked, with only one fibril end found[47]. These new results suggest that fibrils are in fact structurally continuous[47].

1.1.2 Crosslinks

A major contribution to the mechanical properties of tendon is the presence of crosslinks. Collagen fibrils were reported to be assembled and then bound together using crosslinks[12]. Crosslinks have been shown to affect the overall mechanical strength of tendons[48–50]. Crosslinks are formed either enzymatically via lysyl oxidase or by aging-induced glycation[11,51–53]. Crosslinks are known to prevent slippage of collagen molecules within fibrils when under tension, increasing fibrils' elastic modulus, tensile strength, and toughness[11]. Kastelic et al.[11] previously reported that loading rat tail tendons from different age groups causes them to present different levels of fibrillar structure damage, with older tendons being more resistant to fibril disintegration.

1.1.3 Non-Collagenous Components of tendons

McCarthy and Hannafin[16] cited in their review that about 20%-30% of the dry mass of tendons is composed mainly of proteoglycans, and elastin[5,6,14,16,26]. The normal human tendon may contain around 2% dry mass of elastin[14]. Proteoglycans contain glycoseaminoglycan (GAG) subunits bound to a protein core, with a majority of proteoglycans in tendons being leucine-rich[26]. Proteoglycans play a role in fibrillogenesis, regulation of collagen fibril diameters, and may influence the water content of the matrix[26]. Water is a major constituent of tendons. Water accounts for as much as 65% - 75% of the wet weight of tendons' ECM[26]. Water is known to play a role in the specialized mechanical properties of tendons[53–55].

1.2 Mechanical Properties of Tendons

The mechanical properties of tendons have been studied at different levels of hierarchy and under different types of loading[12,44,56]. Tendons are known to have a wide variation in mechanical properties depending species, age, and anatomical location[7,57,58].

1.2.1 Viscoelasticity

Tendons are known to be viscoelastic[59–61]. By definition, a tendon being viscoelastic means that its mechanical properties are loading rate dependent[62]. Previous studies done by Haut et al.[63] and Yamamoto et al.[64], among others, have shown that decreasing loading rate, decreases both stress and strain levels at failure. All levels of structural hierarchy in tendons are thought to display viscoelasticity, including molecules[3,19], fibrils[65], and fascicles[59,66,67]. It has also been reported that significant differences in molecular-level damage occurs in tendons at different loading rates, with slower loading causing more molecular level damage than faster loading[68].

1.2.2 Response of Tendons to Applied Tension at Suboverload Stress Levels

The mechanical response of tendons to tensile loading can be studied through analyzing their stress-strain behavior. The stress-strain behavior of tendons can be divided into two regions, overload and suboverload regions. The suboverload region is the portion of the mechanical response below the yield point. The suboverload region can be divided into three regions: the toe, the heel, and the linear region[69,70].

Figure 1.3 shows a representative stress-strain curve from rat tail tendon, along with the structural changes to crimp representation and the collagen molecules at each stage of the suboverload region. The toe region is the first part of the deformation curve, in which tendons can be extended with very low force. Microscopy experiments

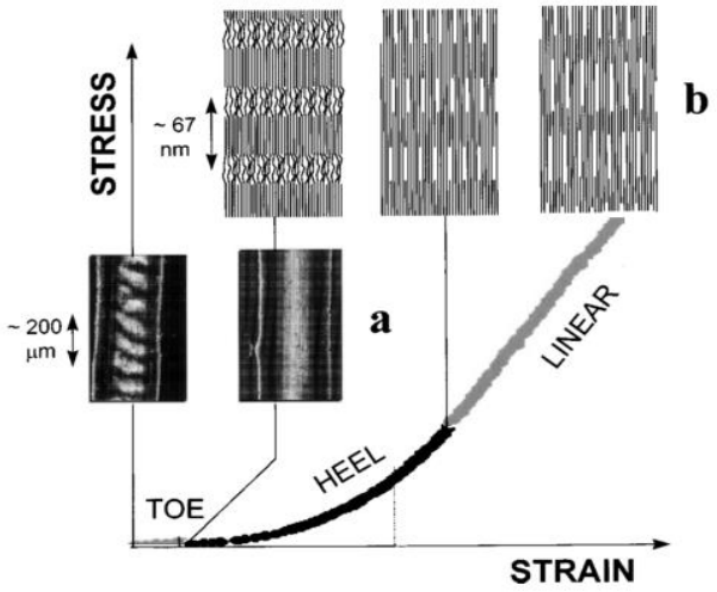

Figure 1.3: Typical stress-strain response observed in rat tail tendons[71]. Figures above the chart represent: (a) The straightening of fibrils and disappearance of the crimp as tendons reach the heel region. (b) the straightening of molecular kinks in the gap region within the heel region[72] and the gliding of molecules as tendons reach the linear region[37].

show that the straightening of microscale waveform crimp present in tendons produces this portion of the curve[56,71,72] (Figure 1.3a). The heel region corresponds to the straightening of the collagen helices within the gap region[69,72] (Figure 1.3b). The linear region is caused by a side by side gliding of molecules[72], the stretching of the collagen triple helices, and the cross-links between helices[56,71,72] (Figure 1.3b). X-ray diffraction experiments indicate that when loaded within the linear region and immediately unloaded, no permanent nanoscale damage appears to occur[37].

1.2.3 Response of Tendons to Applied Tension at Overload Stress Levels

Tendons are known to fail and rupture due to overload stress levels[41,63,73]. Representative stress-strain curves of tendons ramp loaded to rupture at different strain rates can be seen in Figure 1.4.

Earlier studies investigated overloaded rat tail tendons using transmission electron microscopy (TEM). Many of these studies reported that overloaded rat tail tendon fibrils dissociated into subfibrils[9,11,75,76]. Other studies have looked into molecular alterations, using X-ray diffraction, in overloaded rat tail tendons[75,77]. Knörzer et al.[76] used X-ray diffraction to investigate the molecular level structure of overloaded rat tail tendons. This study reported that localized molecular level damage occurred prior to any interfibrillar sliding occurring. This means that shear stress from interfibrillar sliding is not likely to be the cause of fibrillar damage[76]. An early study done by Nemetschek et al.[75] which employed both X-ray diffraction and TEM, reported the presence of fibrillar kinking in rat tail tendons due to overloading and then unloading. Nemetschek et al.[75] suggested that this kinking was more likely to occur in older tendons than in younger ones.

More recent studies have been done to determine the nanostructural damage created by tendon overloading. Veres et al.[56] used scanning electron microscopy (SEM) to analyze the fibrillar structure in overloaded tendons. Veres et al.[56] reported that tensile overloading has a distinct effect on tendons fibrils and on the collagen molecules within them. Overloading tendons caused fibrils to develop characteristic repeating kinks[56]. This kinking formation was given the term discrete plasticity[56,69,78] (Figure 1.5). In the same study, Veres et al.[56] assessed collagen denaturation[56]. Kinks exhibited in overloaded tendon fibrils were found to contain denatured collagen molecules, as shown via trypsin digestion, which specifically removes denatured collagen from fibrils[24,56]. While fibrillar kinking was previously reported in earlier studies[75], Veres et al.[56] was able to investigate the spread of fibrillar damage along the length of tendons. The presence of discrete plasticity damage caused by loading of whole tendons

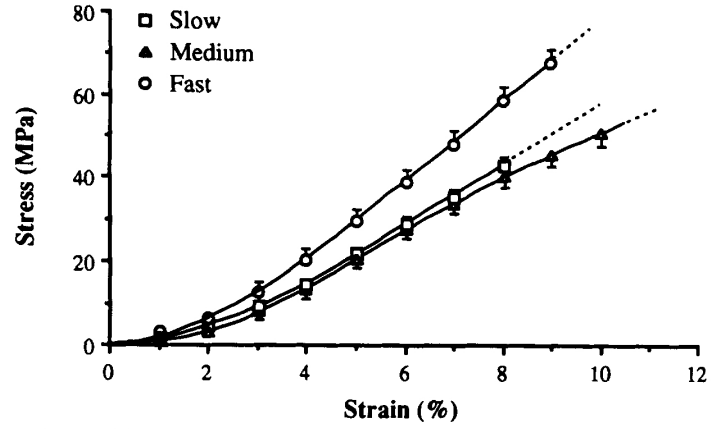

(A) ACL

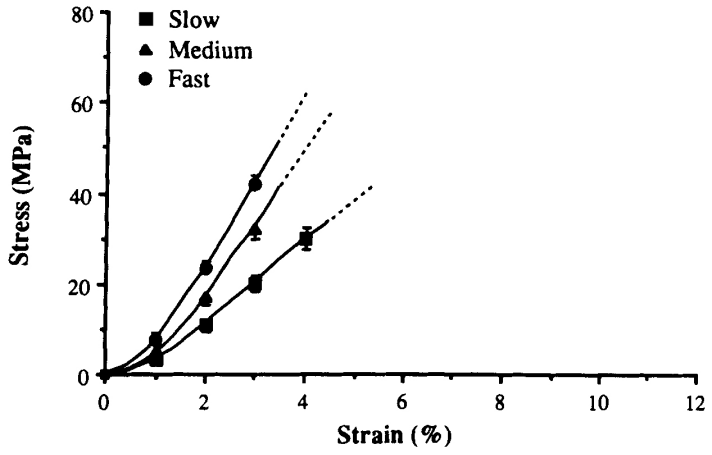

(B) PT

Figure 1.4: Representative stress-strain curves of ramp loaded rabbit (A) anterior cruciate ligaments and (B)patellar tendons at different strain rates[74].

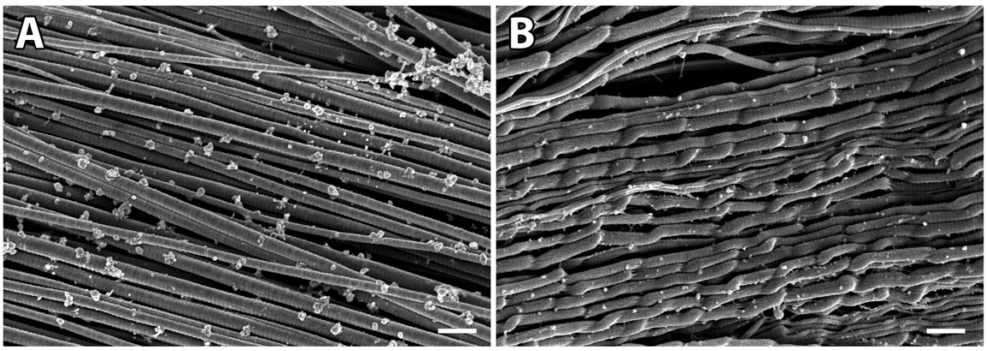

Figure 1.5: SEM: Differences in fibril structure before and after overloading. (A) The unloaded collagen fibrils as seen with a Scanning Electron Microscope. (B) The kinking formation of the loaded collagen fibrils[56].

is unlikely to have been caused by interfibrillar sliding[47,56]. Instead, discrete plasticity damage appears to occur because fibrils are loaded to their mechanical limits[47].

It appears that the formation of longitudinal kinking depends on the amount of crosslinking found in different tendons. Herod et al.[79] studied changes in the nanostructure of bovine superficial flexor tendons (SDFT) and common digital extensor tendons (CDET) due to overloading[79]. It was reported that CDETs presented similar structural changes to those found in overloaded steer tail tendons, while SDFTs did not show any significant fibrillar changes (Figure 1.6)[79]. It should be noted steer flexor tendons have a higher amount of crosslinking than extensor tendons[79]. Using atomic force microscopy (AFM), Quigley[80] found that single SDFT fibrils loaded to rupture did not show significant damage, which is not the case with CDET[80]. Second harmonic generation (SHG) microscopy investigation of the molecular organization showed that overloaded flexor tendons did not have any molecular damage, while overloaded extensor tendons suffer molecular disruption[80].

It has been observed by Veres et al.[4,69], after applying repeated overloading on tendons, that fibrils become progressively more damaged, with additional kinks forming between the original kinks. Fibrils were also found to lose their D-banding due to progressive overloading (Figure 1.7). Eventually, the D-banding pattern is completely lost

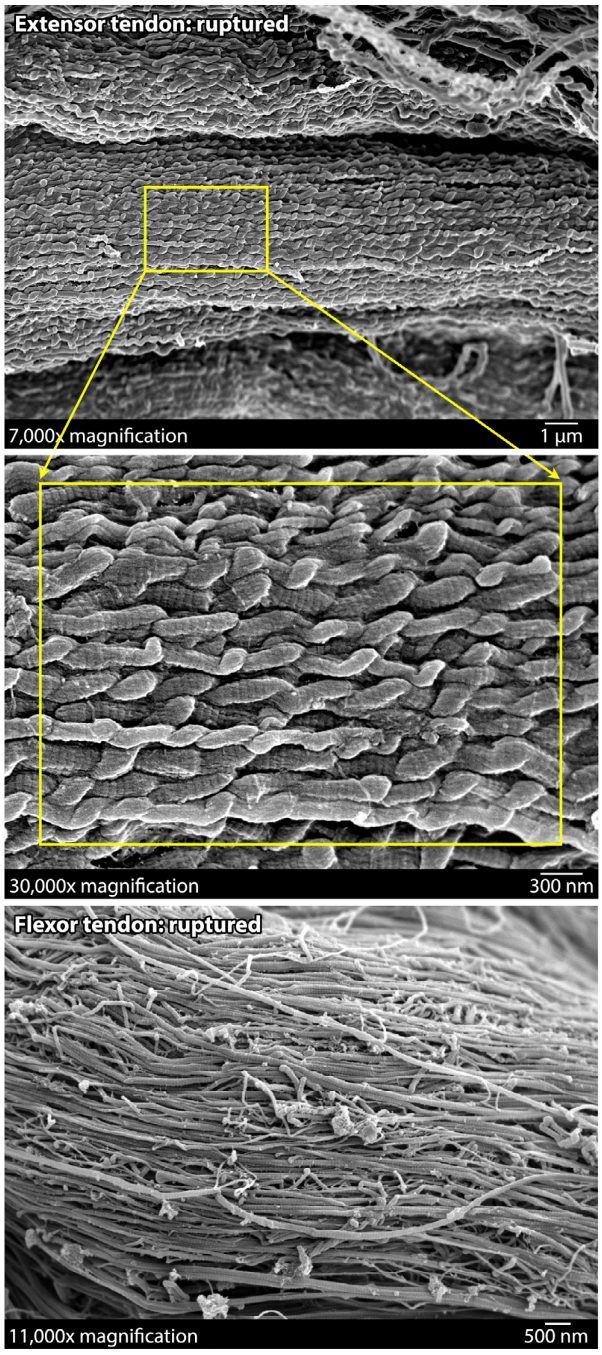

Figure 1.6: SEM images showing differences in structural changes caused by overloading CDET (top and middle) and overloading SDFT (bottom)[56].

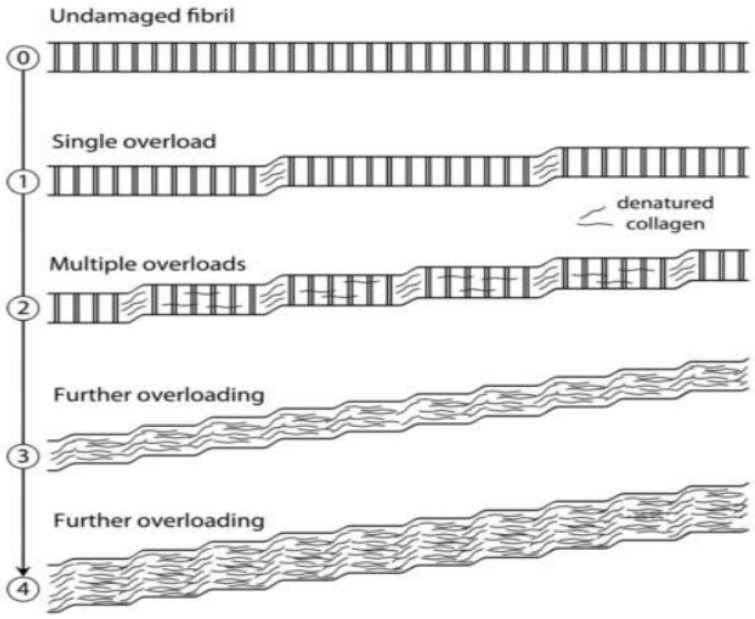

Figure 1.7: The progression of discrete plasticity under repetitive stress[78].

due to progressive overloading, resulting in the collagen fibrils showing an expanded, fibrous appearance as the lateral cohesion between subfibrils is lost (Figure 1.7). The change in fibril structure between control samples and repeatedly overloaded tendons can be seen in Figure 1.5.

Thermal parameters of loaded tendons were previously used to assess nanostructural alterations. Using differential scanning calorimetry (DSC), two important molecular-level alterations can be assessed: molecular packing and collagen denaturation[68,69,81]. Molecular packing in this context refers to the lateral spacing of collagen molecules within fibrils[17,68,69]. According to what is termed as 'polymer-in-a-box' stabilization, the thermal stability of collagen molecules is supported by their lateral packing within fibrils[17]. The proximity of neighboring molecules causes restriction of the conformational freedom of individual α-chains[17,69]. Loss of thermal stability, as measured through DSC, indicates that molecular packing disruption has occurred. Willett et al.[68] used DSC to analyze the molecular level changes resulting from rupture. Results of Willet et al.'s study[68] indicates a significant increase in the lateral spacing

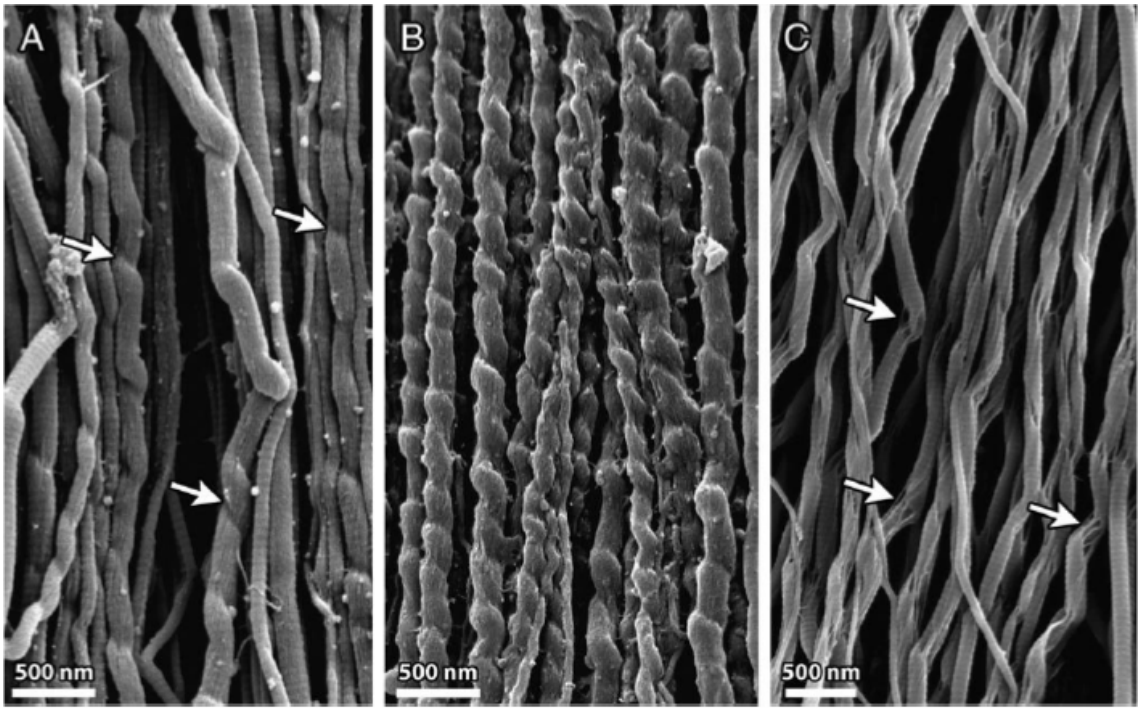

Figure 1.8: SEM images showing the discrete plasticity effect in collagen fibrils. (A) Pulling tendons to rupture causes fibrils to develop kinks in a periodic pattern that repeat every 300800 nm along their length (×30,000). (B) Repetitive overloading causes fibrils to develop additional kinks between the kinks caused by the initial overload cycle (×30,000). (C) Trypsin digestion causes the removal of all of the non-helical collagen content, keeping the intact collagen that was not damaged while causing a partial dissolution of kinks (×25,000).[56].

of adjacent molecules, indicating that overloading can cause molecular unpacking. Consistent with this, SEM of overloaded tendons shows that fibrils dissociate into subfibrils as longitudinal kinking density increases[4,56].

Using DSC, collagen denaturation can be assessed through the specific enthalpy value[17]. Previous studies have reported that a decrease in the specific enthalpy value in loaded tendons means that the amount of energy required to break intramolecular collagen hydrogen bonding has also decreased, indicating that fewer collagen molecules have been uncoiled from their original state due to DSC heating[68,69]. Previous studies have reported that no significant decrease in specific enthalpy occurred in steer ten-

dons as a result of ramp rupture[68]. Collagen denaturation in overloaded tendons was indicated using other methods of collagen denaturation detection[4,56]. The insignificance of the drop of specific value as seen by Willett et al.[68] could indicate a lower level of denaturation due to these mechanical regimes.

1.3 Creep Testing of Tendons

Creep is defined as applying a constant force to a material over a period of time[82]. Creep can be applied via two different methods, static or cyclic loading[83]. A static creep test is done by loading a material up to a stress level, and then keeping the material at that stress level for a period of time[28,82–84]. A cyclic creep test is done by repeatedly loading a material up to a given stress level for a period of time[83].

A typical strain-time diagram for a static creep test of tendon to failure is shown in Figure 1.9[58]. Static loading causes the progressive recruitment and elongation of tendons' collagen fibers and effectively their constituent fibrils[83]. The response can be divided into three different phases[65,85]: the first phase is called primary creep, where the rate of elongation with time decreases. The second phase is called secondary creep, where the rate of elongation is approximately constant. The third phase is called tertiary creep, where elongation accelerates leading to failure. Due to tendons' viscoelasticity, they elongate when they are exposed to a constant load[62,86]. The elongation of tendons, which was found in all studies involving creep loading, may suggest that damage is occurring within the structure of the tendon[7,58,82]. Elongation can occur at all creep stages, but occurs most rapidly at the tertiary level, before tendon failure. The additional strain due to tertiary creep was investigated by Wang and Ker, who found that tertiary creep caused the greatest amount of damage accumulation within tendons[82].

Wang and Ker[82] studied static creep in wallaby tail tendons. In their work they investigated the impact of changing the length of the loaded specimen, the temperature at which loading was done, and the stress level that static loading was conducted

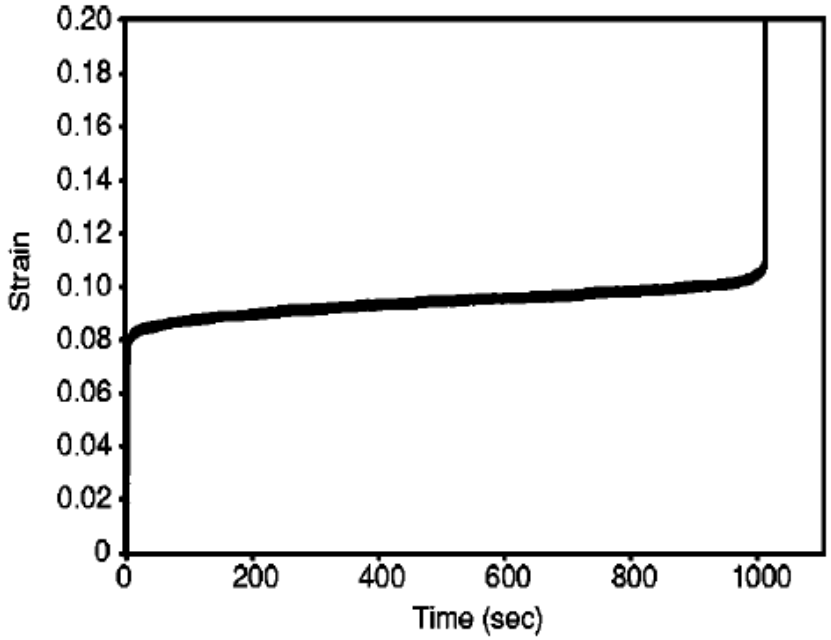

Figure 1.9: A Typical strain-time curve, showing the time dependent strain response of tendons to static creep loading[58].

at[82]. There were several important results found by Wang and Ker's study: 1) static loading at suboverload stress levels between 20 MPa and 80 MPa can cause wallaby tail tendons to fail, 2) increasing stress levels at which static loading is conducted can reduce the time to failure of tendons (Figure 1.10). 3) increasing the temperature of the medium at which tendons are loaded reduce the lifetime of tendons under creep (Figure 1.11), and 4) decreasing the length of tendons undergoing static loading increased the lifetime of tendons under creep (Figure 1.12)[82].

Wren et al.[58] studied the effect of static loading on human Achilles tendons. In their study, the effect of applied stress (Figure 1.13A), initial strain (Figure 1.13B), and failure strain (Figure 1.13C) on lifetime-to-rupture of tendons was investigated. The results showed that the best parameter for predicting creep lifetime is the initial strain at which the target stress level for the creep test was reached[58].

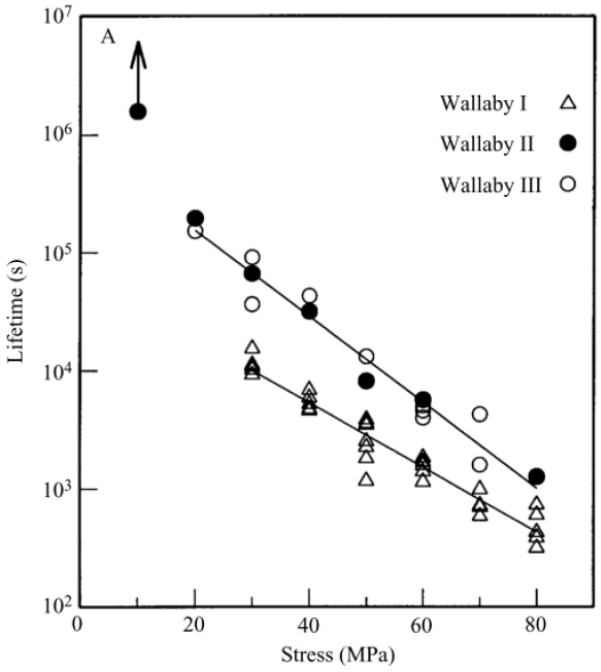

Figure 1.10: Variation in creep lifetime with different stress levels for wallaby tail tendons. The chart includes one specimen that underwent 10 MPa creep loading stress and never ruptured[82].

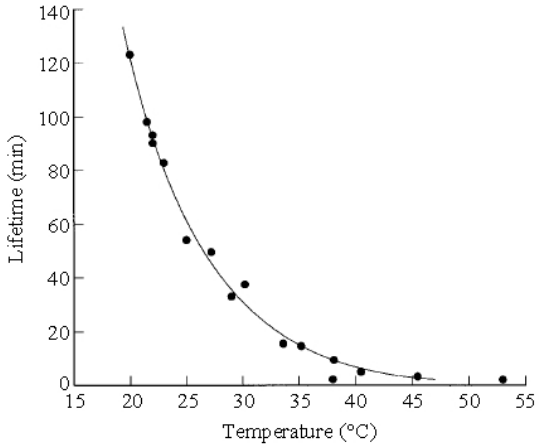

Figure 1.11: Lifetime (s)-Temperature (°C) chart of results of static creep loading done on wallaby tails. All the samples plotted in this chart were loaded at a constant stress level of 60 MPa[82].

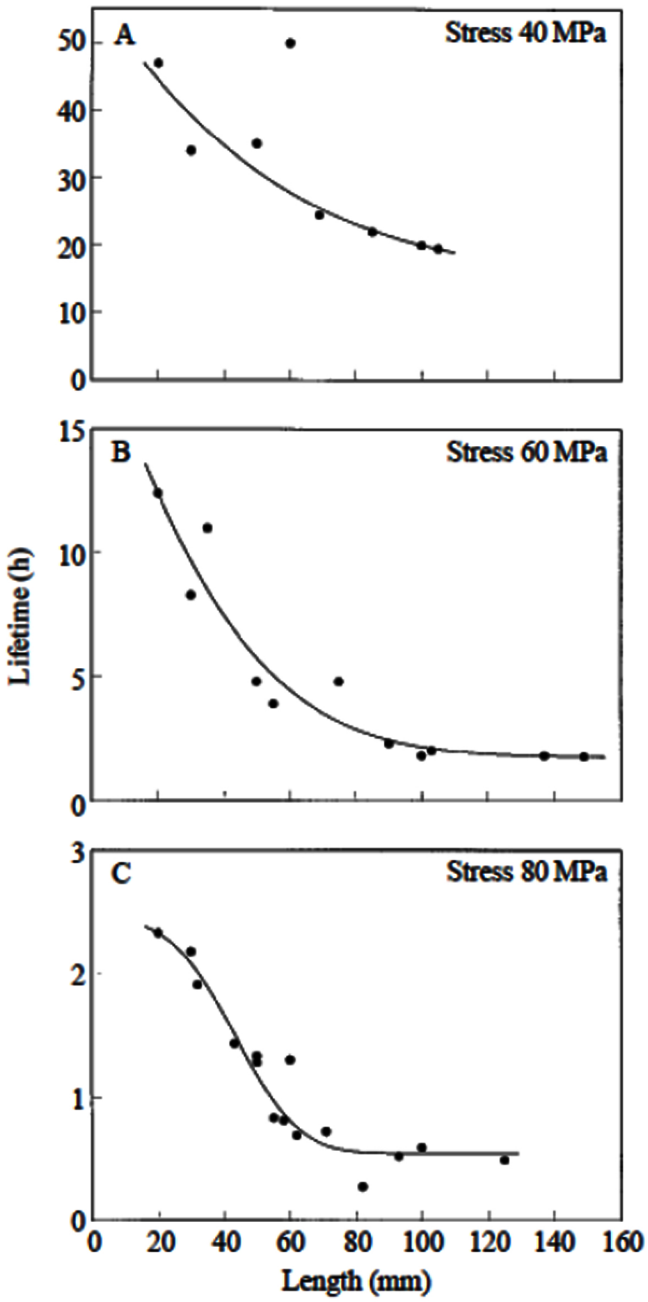

Figure 1.12: Lifetime (s)-Length graph(mm) of results of static creep loading, at different stress levels. It can be seen that at different stress levels, the lifetime of the tendon under creep loading was inversely related to the initial length of the tendon specimen. This was the case until tendons of more than 80 mm were tested, when the lifetime became constant with increasing tendon's length[82].

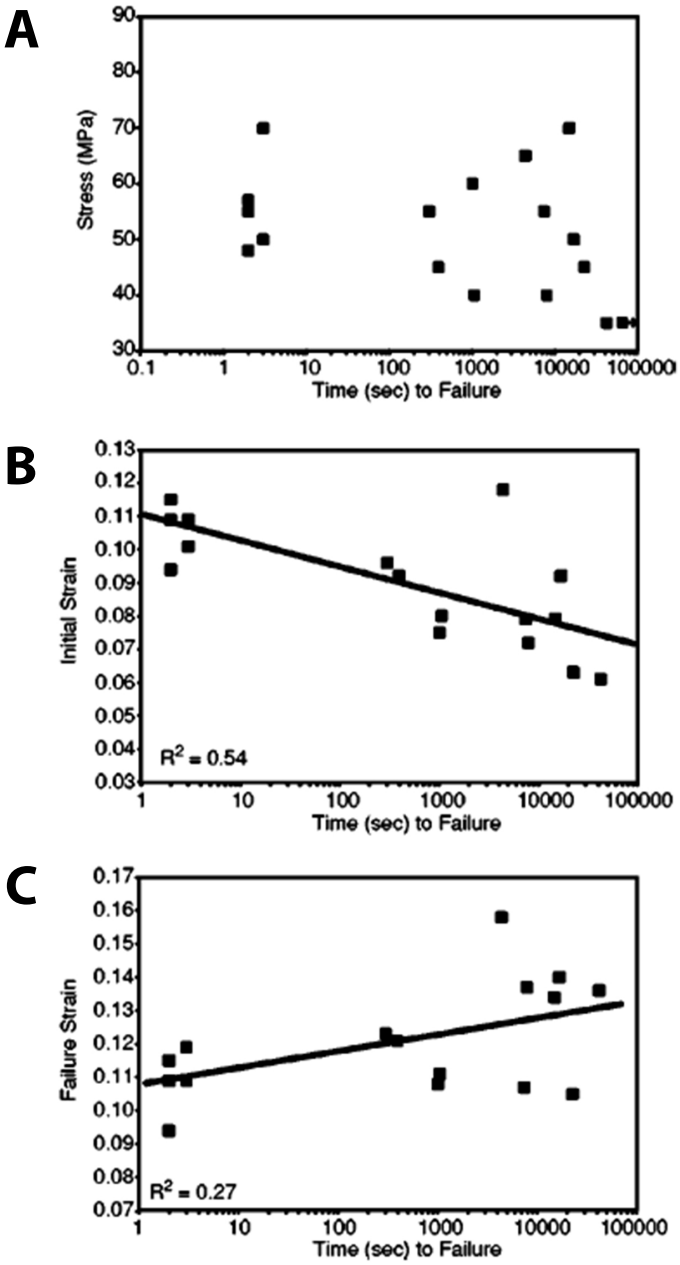

Figure 1.13: Creep lifetime results vs.: A) applied stress, B) initial strain, and C) failure strain. Initial strain was the best predictor of creep lifetime. There was no significant relationship between applied stress and creep lifetime[58].

While tendons and ligaments are physiologically distinct, they share similar structural mechanical characteristics[26,87]. Consequently, it is worth mentioning studies that explored creep in ligaments. Thornton et al.[88] investigated changes in the mechanical properties of rabbit medial collateral ligaments during static loading. In this study, static loading was applied to ligaments at the toe, heel, and linear regions of the suboverload deformation curve, hence assessing the different mechanical responses at different stresses within the suboverload region[88]. Thornton et al.[88] reported that ligaments ramp loaded to the linear region and then held under static load had a reduction of their modulus, when compared to samples that were statically loaded at their toe-heel region or were not loaded.

1.4 Stress Relaxation

When subjected to an applied deformation, the decrease in restoration force produced by a material is called stress relaxation[89]. Like creep, stress relaxation occurs in tendons and ligaments[62]. For ligaments, Provenzano et al.[91] and Thornton et al.[94] have both found that, stress relaxation proceeds at a faster rate than creep. Johnson et al.[92] studied stress relaxation in tendons of different age groups, finding that tendons from different age groups behave similarly. Screen et al.[95] studied the behavior of tendon fascicles during stress relaxation testing using confocal microscopy. They found that stress relaxation is dominated by fiber sliding mechanisms[8,95].

Chapter 2

Literature Summary and Thesis Objectives

2.1 Outcome of the Previous Literature

The mechanical and structural properties of tendons have long been the subject different studies over the past few years. Many of these studies were particularly targeted towards studying effects of loading on tendons and their structural properties. One of the loading regimes that was previously studied, in the context of its effect on tendons, was creep loading. Creep loading is known to cause failure of tendons[58,82] and ligaments[96] at stress levels that are considered to be in the suboverload region. Creep loading is also known to cause alterations in the mechanical properties of ligaments, such as the modulus of ligaments[94]. Creep loading is a low strain rate loading regime, which could explain its distinctive effect on the viscoelastic tendons[97]. Previous studies have clearly shown that tendons fail at lower stress and strain levels due to lower loading rate[63,64]. Willett et al.[68] have reported that tendons ruptured at lower strain rates present higher levels of collagen molecule unpacking. The complete scope of how nanostructural damage in tendons changes with lower strain rates have not been well investigated.

Veres et al.[56] found that fibrils of tendons that were ramp loaded until rupture featured heterogeneous plastic damage, which is characterized by longitudinal kinking. This nanostructural disruption feature was given the name discrete plasticity[4]. When repetitive overloading was applied by Veres et al.[4], fibrillar kinking was found to significantly increase. Increasing cycles of overloading was also linked to a significant increase of fibrillar dissociation and loss of D-banding[4]. These results were consistent with molecular level investigations of these overloaded tendons[68,69], which reported that molecular unpacking, as well as collagen denaturation, can occur due to overloading tendons. In all the cited nanostructural damage investigations[4,56,68,69], steer tail tendons were used, which have a low crosslinking concentration. Similar to steer tail tendons, steer extensor tendons were found to feature similar discrete plasticity features in their collagen fibrils[79]. Bovine flexor tendons, on the other hand, did not show significant nanostructural changes, indicating that discrete plasticity is more likely to occur in lower crosslinked tendons' nanostructure[79].

As mentioned, discrete plasticity was found in steer tail tendons and forelimb extensor tendons that were overloaded until rupture. With that said, if tendon failure due to tensile overloading causes discrete plastic damage to form, then it is possible that discrete plasticity is the characteristic feature of tendons creep loaded to rupture too. Prior to this study, the presence of discrete plasticity damage in creep tendons was not confirmed, whether on the molecular or fibrillar levels of structural hierarchy. Given the previous work done by others, understanding how collagen fibrils respond to low rate extension during creep may provide valuable insight into tendon and fibril structure and mechanics.

2.2 Objectives

The main objectives of this thesis were:

Objective 1: To determine if creep loading applied using an overload stress affects the structure of collagen fibrils and molecules within tendons.

Objective 2: To determine if creep loading applied using a suboverload stress affects the structure of collagen fibrils and molecules within tendons.

Chapter 3

Building and Testing the Mechanical Creep System

A custom-made mechanical loading device was assembled to perform the *in vitro* mechanical loading of tendons for the research experiments conducted as part of this thesis. This device, called the mechanical creep system (MCS), was an electromechanical tensile testing machine (Figure 3.1). The device was designed and programmed to perform ramp and creep loading of tendons.

3.1 Hardware

All components of the MCS were attached to a steel base. The base had a hole where an acrylic bath was positioned. The size of the base was designed so that the MCS could fit into a water-jacket incubator, allowing testing to be conducted at 37°C. The incubator was a Model Dual Chamber 3326 water jacketed incubator (Forma Scientific Inc., Marietta, OH, United States).

A linear actuator and a load cell were fixed to opposing sides of the base, with each

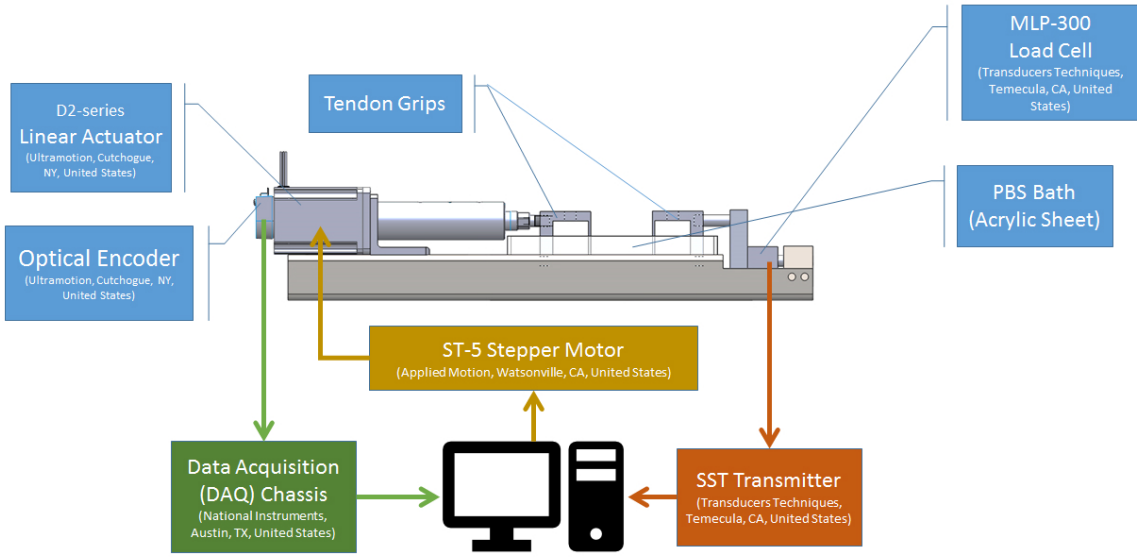

Figure 3.1: MCS hardware assembly. The labels show all the parts of the MCS with their components. The connections between the MCS and the computer were shown in the diagram. Arrows represent the connections that were used to present the data flow of the optical encoder's displacement readings (green), the linear actuator commands (gold), and the load cell's force readings (orange). The intermediate devices were shown and labeled along with the data flow.

having stainless steel grips attached (Figure 3.1). Each grip consists of a rectangular frame that holds a pair of jaws with waveform gripping surface coated with synthetic diamond. To avoid damaging tendons during gripping, small pieces of cotton were used to cover the top and bottom surfaces of the tendon before sandwiching the tendon in the waveform jaws. The top and bottom jaws of each grip were clamped to each other using a fastening bolt with a pressure pan.

An Ultra Motion D2 series linear actuator (Ultra Motion, Cutchogue, NY, United States) was used to stretch the tendons. This linear actuator moved one of the grips at a constant velocity. The linear actuator had a pre-installed optical encoder, which tracked the displacement of the linear actuator's arm. The displacement reading was acquired by a National Instruments USB data acquisition (DAQ) chassis with a NI 9218 DAQ module (National Instruments, Austin, TX, United States). The linear

actuator was controlled by a ST5-S stepper drive (Applied Motion, Watsonville, CA, United States), which used serial commands sent from a connected computer to operate the linear actuator. Commands were first sent to a National Instrument serial board (National Instruments, Austin, TX, United States), which was then transmitted into the stepper drive, which moves the linear actuator as per the given command.

A Transducers Techniques MLP-300 load cell with TEDs Plug and Play capability (Transducers Techniques, Temecula, CA, United States) was connected between the second grip and the base. The load cell was connected to a SST transmitter (Transducers Techniques, Temecula, CA, United States), which converted the incoming voltage signal from the load cell into pounds (lbs), which was then converted by the software system into newtons (N). Readings from the SST transmitter were sent via serial connection to the computer.

3.2 Software

Custom software to control the MCS system was programmed using LabVIEW 2014 (National Instruments, Austin, TX, United States). The software consists of a main Virtual Instrument (VI) and several sub-VIs that perform calculations and conversions.

Two different main VIs were written, one called Mechanical Creep System (OCR).vi and Mechanical Creep System (SCL).vi. The front panel of the Mechanical Creep System (OCR).vi can be seen in Figure 3.2, while the Mechanical Creep System (SCL).vi can be seen in Figure 3.3.

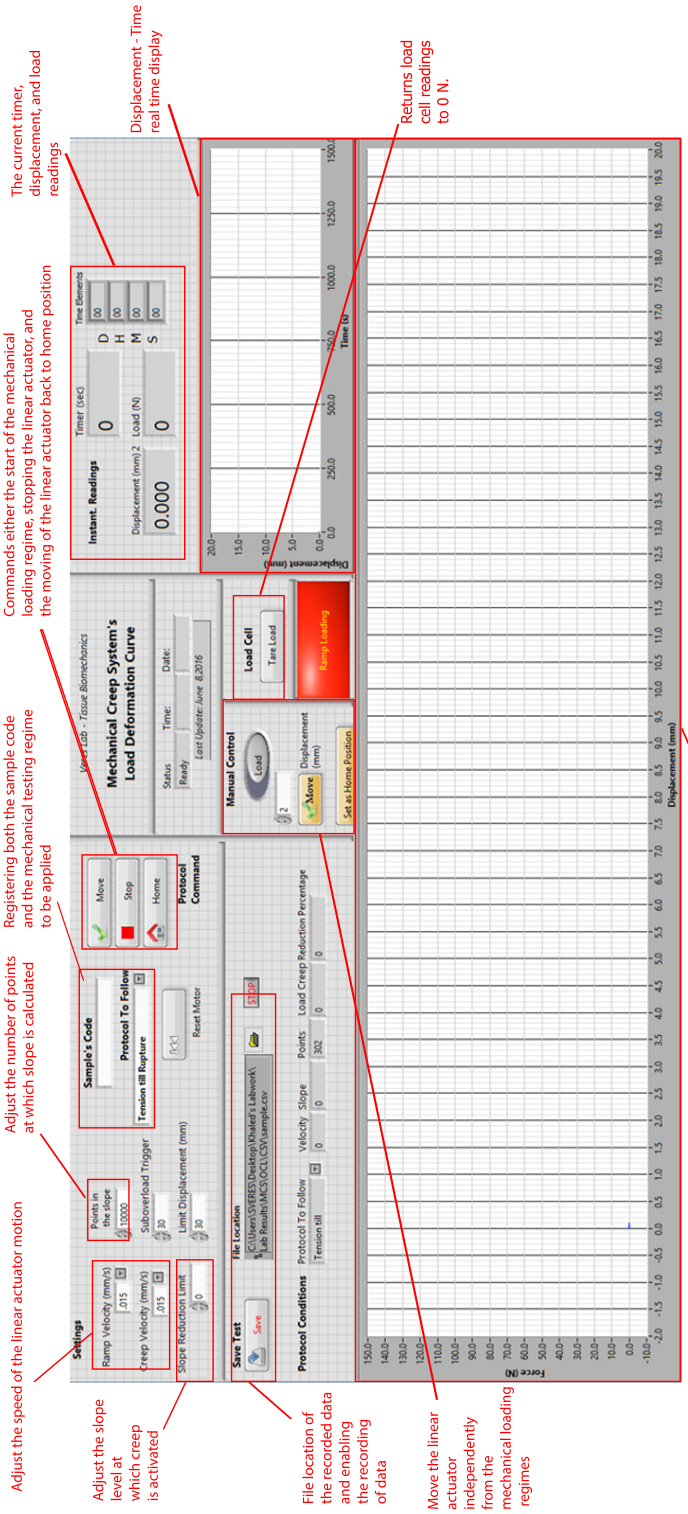

Figure 3.2: The front panel of the main VI (OCR).

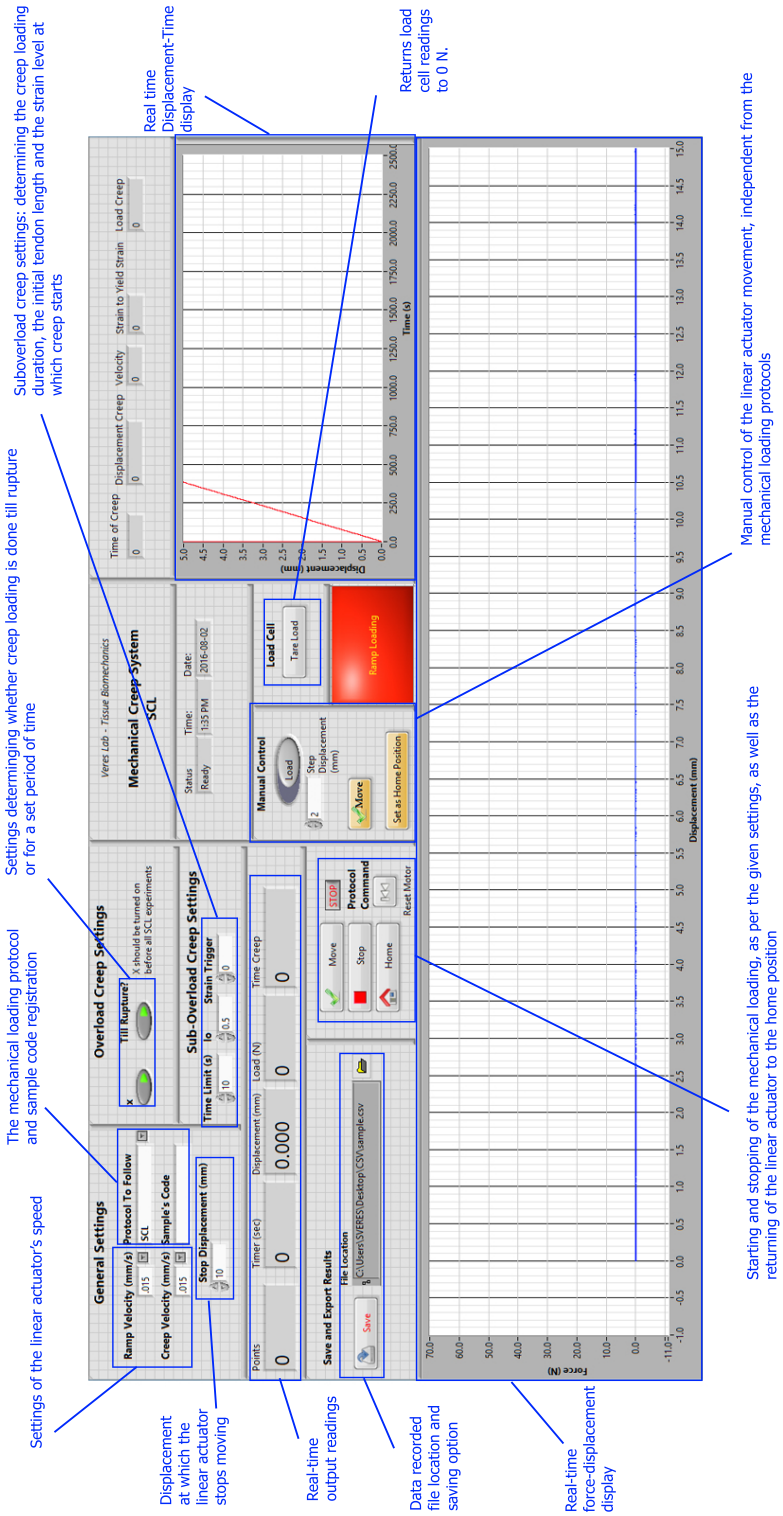

Figure 3.3: The front panel of the main VI (SCL).

The main VIs allowed the user to set up and monitor the test. The user provided information to the MCS prior to the mechanical test's start, including the ramp velocity, the mechanical test to use, tendon's sample name, limit of the actuator displacement, as well as other options depending on the mechanical test to be used. The main VIs acquired loading data from the load cell, displacement data from the optical encoder, and running time. All of these data were displayed on the front panel, and were also written to a spreadsheet using a sub-VI (To Excel.vi). The main VIs are set to activate one of four mechanical treatments on tested samples: Overload creep rupture (OCR), high stress loading (HS), ramp rupture (RR), and suboverload creep loading (SCL). Each of these mechanical treatments will be further explored in the next two chapters.

Within both main VIs was a second sub-VI, Applied Initiate Move.vi, which was used to convert displacement (mm), velocity (mm/s) and acceleration (mm/s^2) into steps, revolutions/s and revolutions/s^2 respectively. Each revolution of the stepper motor was set to include 20000 steps. Once activated, the stepper motor receives the necessary commands, which then moves the actuator at a user-set velocity, stretching the tendon sample in the process. The same VI was also used to stop the linear actuator both automatically as a part of a mechanical loading regime, or manually at the user's discretion.

For overload creep tests and high stress tests, the yield point was the condition to trigger creep or actuator reversal. A method to determine the yield point was implemented, which depended on tracking the change in the slope of the force-displacement curve. As tendons were ramp loaded, a sub-VI (slope fitting.vi) continuously calculated the slope of the force-displacement curve by applying least square linear regression to a set number of the force-displacement readings. After each recorded data point, the change in slope in consecutive slope values was calculated. When the change in slope reached a user-set level, the ramp loading protocols switched to either creep loading or unloading to the home position. For overload creep, the stress level read within the same loop iteration at which the change in slope value reached a set trigger point, which was set as the target creep stress. For the high stress tests, the

change in slope trigger caused the linear actuator to return to the home position at the same speed as during ramp loading. In the case of the suboverload creep tests, the strain level at which creep triggering occurred was set by the user, and hence the linear fitting was not used.

Once creep was activated, a sub-VI (Creep Mechanism.vi) controlled the creep loading mechanism of the MCS. The whole MCS program's dataflow was forced into a case structure, which commanded the MCS to stop the linear actuator when the load reading was equal or greater to the queued load level. When the load reading decreased by 0.2 N from the queued load level, the linear actuator arm was ordered to move until the load reading was equal to or greater than the target load. This mechanism was maintained until rupture in the case of overload creep tests, while it was stopped after a user set duration in the suboverload creep tests. In the case of suboverload creep tests, tendons were unloaded back to their home position when the set duration of creep loading was reached. The speed of unloading was the same as that used during ramp loading.

3.3 Testing and Calibrating the Mechanical Creep System

Once the initial assembly and programming of the MCS was done, testing was conducted to confirm the accuracy of the load cell readings, the displacement readings, the MCS's ability to detect the yield point, and finally the MCS ability to apply creep loading correctly. Adjustments were made to improve the functionality of the MCS.

3.3.1 Confirming the Linearity of Load Cell Readings

The load cell readings were tested prior to installing it to the MCS, using standard weights ranging between 20 g and 2000 g. The load cell readings and the standard

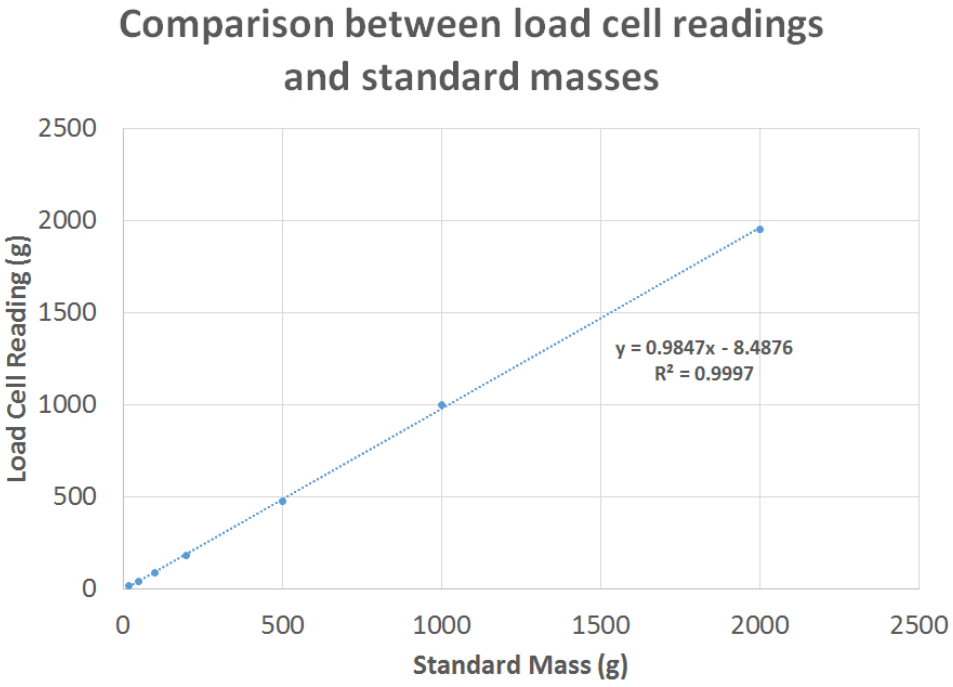

Figure 3.4: Linearity test: known standard masses vs. measured mass. The linear fit was added with the R^2 value, showing that the load readings were linear.

masses were plotted against each other (Figure 3.4). The results showed that the load cell readings were linear, functioning as expected. After installing the load cell, linearity was then again confirmed by performing a tensile test on a linear elastic material.

3.3.2 Confirming Optical Encoder Readings

The optical encoder sends the displacement readings as a waveform signal into the LabVIEW software, where the waveform peaks were counted by the software and converted into a number of points, which were then converted to displacement (mm). After installing the linear actuator, a test was conducted to find the conversion factor necessary to alter the counted number of input waveform peaks into displacement

values. Using this conversion factor, the accuracy of the optical reader's displacement readings was then tested using move commands for 5 mm, 10 mm, 15 mm, and 20 mm, with all the tests done starting from the home position (0 mm). The speed of the linear actuator was kept at 0.015 mm/s. Each of the movement orders was done three times. Once the linear actuator had completed its movement order, a micrometer caliper was used to measure the distance that the linear actuator had moved. Results of both digital readings from the MCS of the displacement and measurement of the caliper were recorded and plotted. These results were used to establish a linear relationship between optical encoder output and actuator displacement. After this was established, the relationship was then verified, as shown in Figure 3.5. This process was repeated prior to the start of the second experiment, as changes were made to the LabVIEW code to correct an inaccuracy in the readings of the displacement during creep loading, something that was detected after the first experiment was completed.

3.3.3 Confirming Functionality of Ramp Loading

Two tendons were used to test the system for ramp to rupture loading. The intergrip distance was set to 15 mm, and each tendon was then fixed into the grips. Each tendon was then fully unloaded by moving the actuator forward until the tendon was visibly slack. The load cell was then zeroed. Tested tendons were then stretched to 0.5 N, and the distance between grips measured and recorded as the intergrip gauge length, l_o. Time readings (s), load readings (N) and displacement readings (mm) were recorded and exported to a spreadsheet, where the load readings were converted to stress (MPa), by dividing each reading by the cross sectional area mm^2, and the displacement readings were converted to strain (%) by dividing the displacement readings by l_o. Stress-strain charts (Figure 3.6) and strain-time charts (Figure 3.7) were generated from these mechanical loading tests.

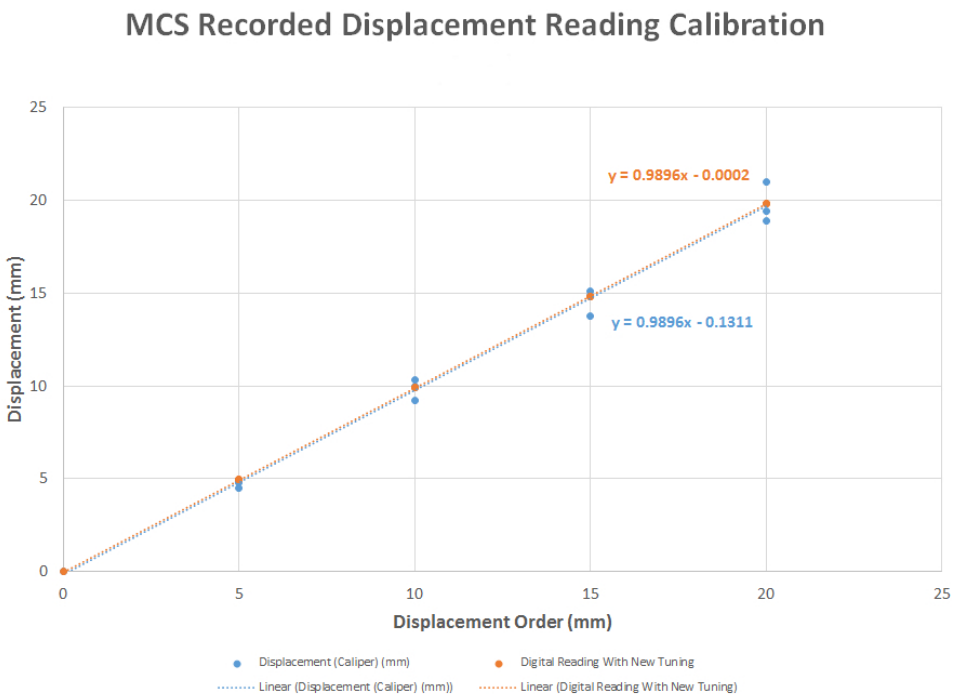

Figure 3.5: Comparison between the displacement recorded by the MCS and the caliper measured displacement after the last calibration. It can be seen that the linear actuator displacement measurement matched that of the optical encoder reading.

3.3.4 Confirming the Functionality of the Static Creep Test

The static creep loading test procedure was tested with two tendons. Initial setup was the same as described above. The ability of the system to apply static loading was tested and confirmed (Figure 3.8 and 3.9). Further details of the static creep test are given in sections 4.3.2 and 4.3.3.

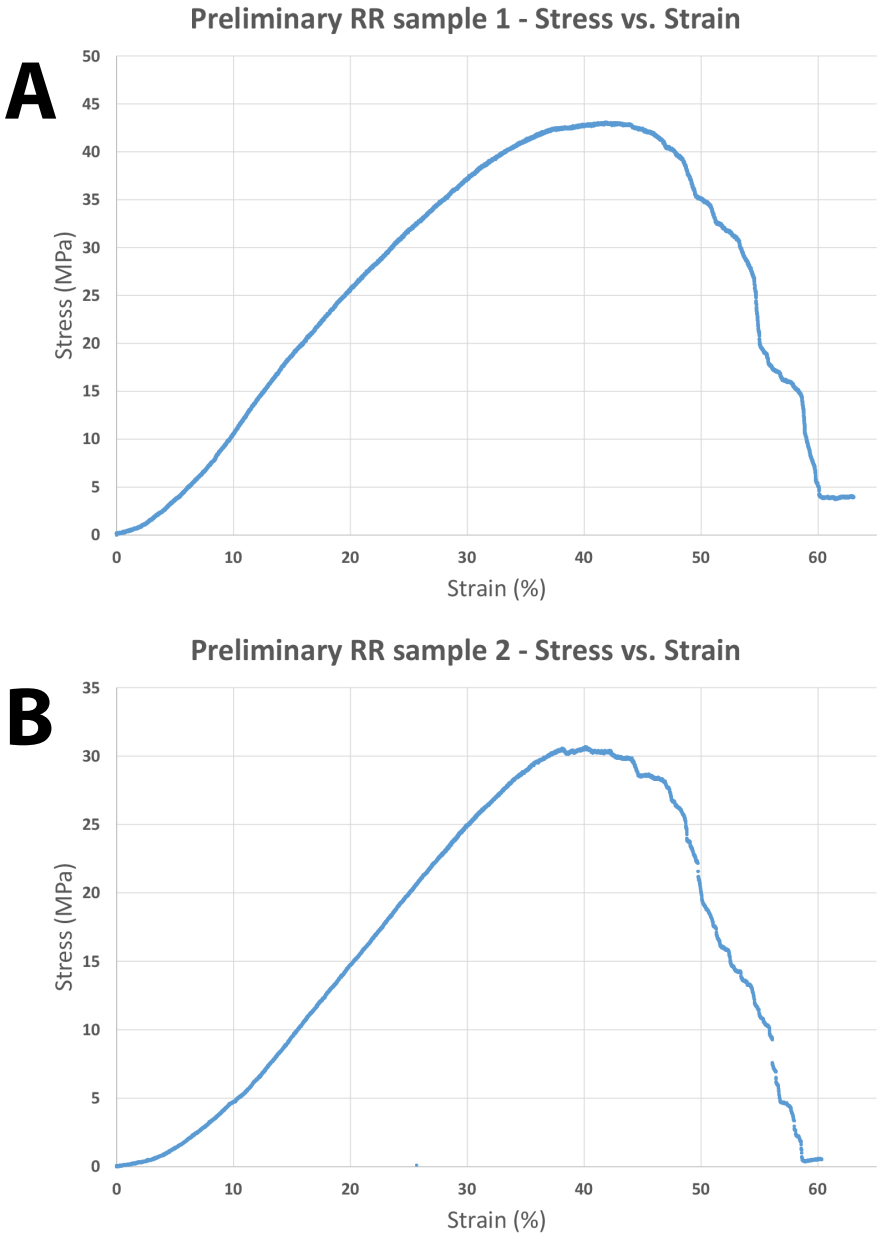

Figure 3.6: Stress-strain curves of both RR loaded tendons.

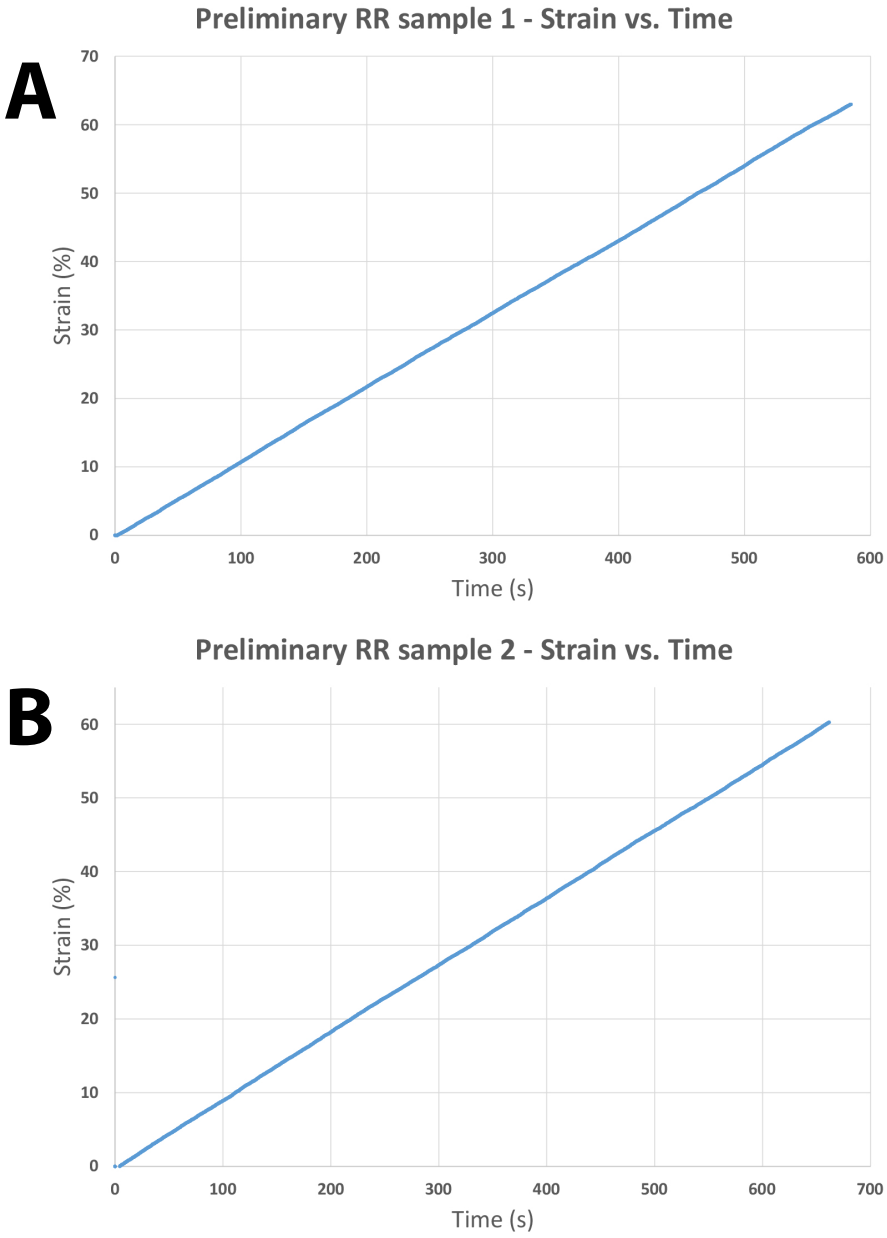

Figure 3.7: Strain-time curves of both RR loaded tendons.

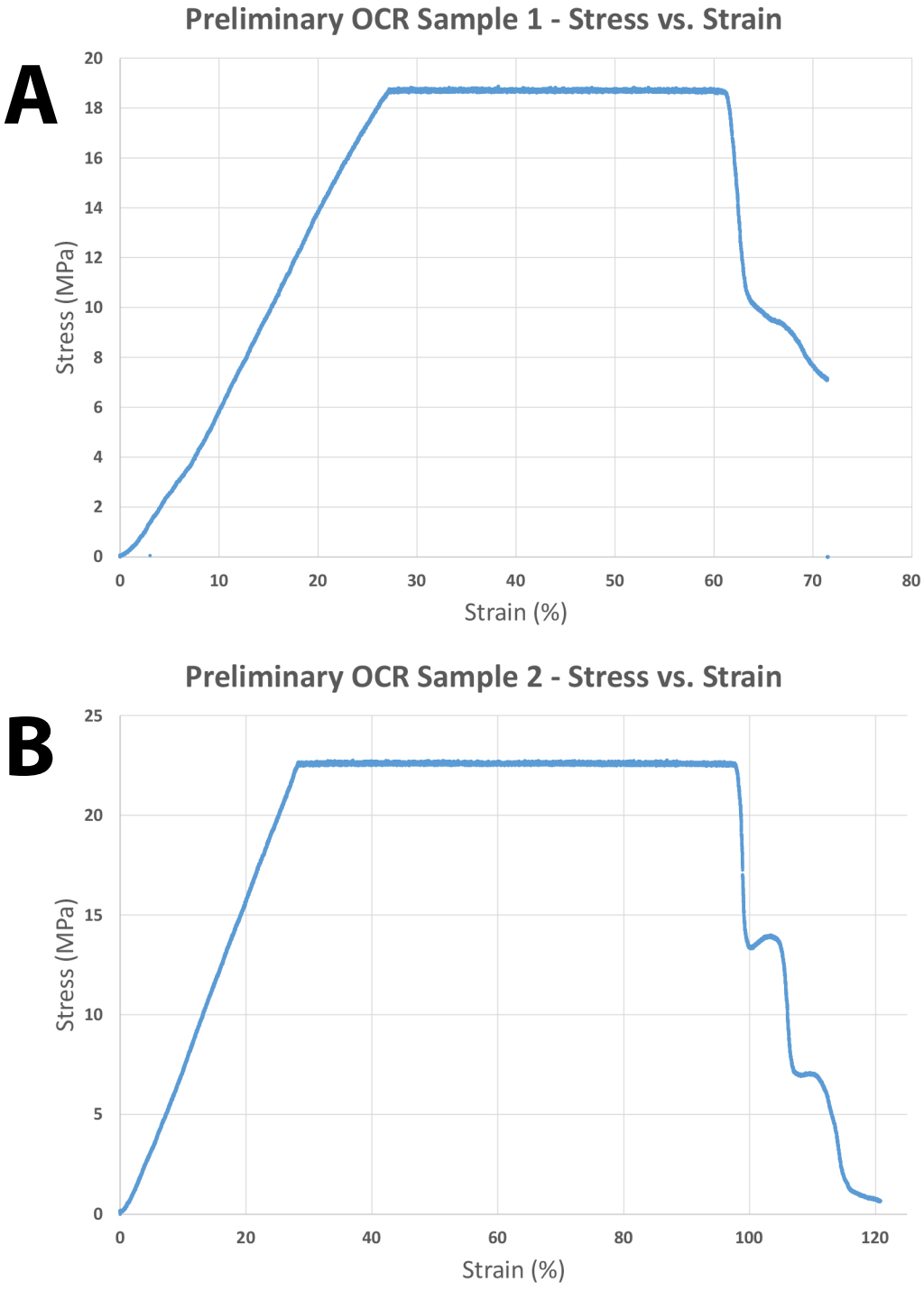

Figure 3.8: Stress-strain curves of both OCR loaded tendons.

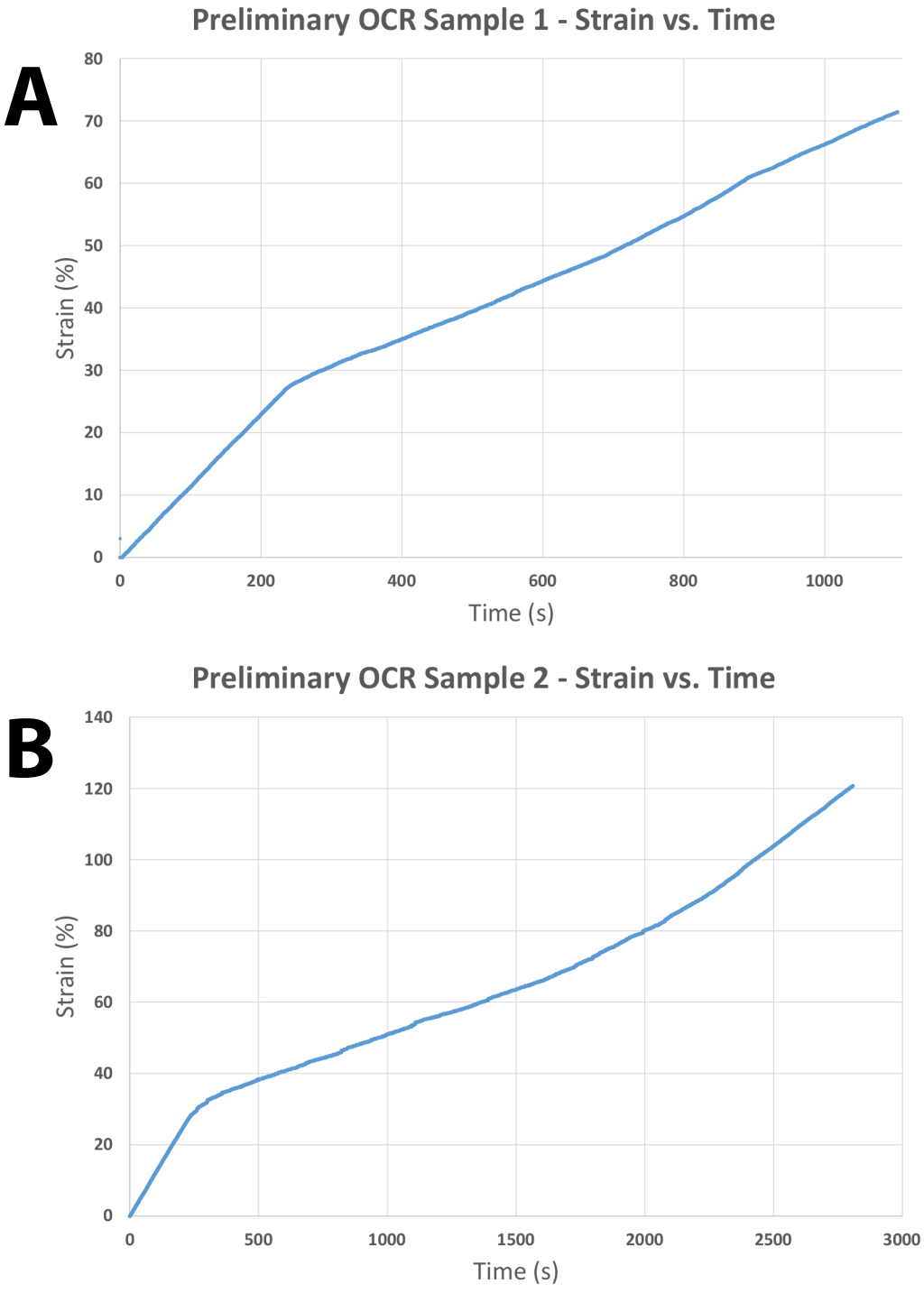

Figure 3.9: Strain-time curves of both OCR loaded tendons.

Chapter 4

Overload Creep Rupture's Effect on the Nanostructure of Tendons

4.1 Introduction and Research Question

Tendons that were overloaded at strain rates between 0.25%/s and 10%/s were found to contain unique nanostructural alterations[4,56,69,79]. Evidence from literature showed that these tendons' fibrils experienced repeating kinks along their length. This mode of damage, owing to it being permanent and having a heterogeneous nature, was given the name discrete plasticity[4,56,69]. Dissociation of fibrils into sub-fibrils and disappearance of D-banding on the loaded fibrils were other features found to occur in cyclically overloaded tendons[4]. The molecular packing was previously shown to be significantly disrupted within overloaded tendons[68,69]. Evidence of loading-induced collagen denaturation was detected in both ramp and cyclically overloaded tendons[56].

Tendons, like other soft tissues, are known to be viscoelastic[62], which means that their mechanical properties are affected by lowering or increasing the loading rate. On the macroscale, differences in the rupture mode of tendons was detected at different loading rates[24,98]. Low loading rates can cause tendons to fail at lower strain and stress levels[63], while higher strain rate loading was previously connected to an increase

in their ultimate tensile strength and strain levels at failure[64]. Some studies have hypothesized the presence of a connection between tendons' mechanical and structural properties[58,99]. Previous studies have shown that the disruption of molecular packing in tendons increased significantly when low loading rates are applied on tendons, as opposed to higher loading rates.[68].

The question of how lower strain rate loading, as in the case of either very slow tension to rupture or static creep loading, can affect the nanostructure of tendons is yet to be answered. Studying how the collagen fibrils in tendons respond to static load would allow a better understanding of the effect of sustained loading on tendons, establishing a comparison between damage due to this loading treatment and results from other loading treatments used in earlier studies. Hence, the research question that was asked in the first experiment of this thesis was whether or not nanostructural damage within tendons occurs during very slow, creep-based loading at high stress.

4.2 Hypotheses and Rationale

Hypothesis 1: Subjecting steer tail tendons to a static load until rupture at a stress slightly above the yield point will cause significant nanostructural alterations.

Sub-hypothesis 1a: After overload creep rupture, tendons examined with differential scanning calorimetry (DSC) will show significantly lower values of the T_{onset}, T_{peak} and specific enthalpy, as well as higher values of FWHM, when compared with their matched-pair, unloaded controls.

Rationale 1a: The thermal stability of the collagen molecules, exhibited in unloaded tendons, is expected to be disrupted due to static loading at overload stress levels. Previous tests have shown that tendons rupture when they are exposed to static loading[58,82]. Other research studies have shown that mechanically damaged tendons had structural alterations within their fibrils, including regions of denatured collagen[56], as well as disruption in the molecular packing of these tendons. When tested under DSC, it is expected that analyzed thermal parameters of ramp and creep loaded

tendons will show significant changes when compared to their match-paired control samples, in a similar trend to previously seen results from previous studies[17,68,69]. A reduction in the normalized enthalpy is expected to occur due to the denaturation of collagen molecules, as shown in previous studies[54,100]. Significant drops in onset and peak temperatures are expected due to the increase in the lateral spacing of collagen molecules, which decreases thermal stability, as shown previously by Miles and Ghelashvili[17]. The increase in the FWHM value, indicating a greater range of molecular stabilities, will occur due to the decrease in the onset temperature parameter without significant changes to the end of the endotherm signal, as seen previously[68,69].

Sub-hypothesis 1b: After overload creep rupture, tendons will show kinked fibrils under scanning electron microscopy (SEM), whereas unloaded tendons will not.

Rationale 1b: As seen in previous studies, loading tendons to rupture causes discrete plasticity, characterized by the formation of longitudinal kinking along collagen fibrils[56]. In addition, previous studies have shown that creep loading can cause tendon rupture[58,82]. Because discrete plasticity is known to occur in tendons as a response to ramp rupture, then presumably a similar observation will be found in tendons ruptured under creep loading.

Whether tendons could be loaded to their yield points without causing damage at the fibril and molecular levels was unknown prior to this study. Nanostructural alterations were observed in response to loading beyond the yield stress, either through tension to rupture or repetitive overloading. To determine the nanostructural effect of ramp loading tendons to the yield point, a new sample group was added, where tendons were loaded up to their yield points and then unloaded.

Hypothesis 2: Tendons loaded to their yield point, but unloaded immediately will not show changes in the DSC or SEM relative to unloaded controls.

Rationale 2: During ramp loading, collagen molecules within tendons straighten. Once straightened, intermolecular sliding occurs, causing the increase of the D-stagger[37,53]. Elongation of tendons and alterations in the molecular structure has been shown to

be reversible within the linear region of the mechanical response[37]. It is therefore expected that no structural alterations will occur in tendons that are loaded to yield and then unloaded. This will appear in both the DSC and SEM results, where these tests will produce statistically similar results to their unloaded, matched-pair controls.

In preliminary tests, the creep ruptured tendons showed striking differences in the DSC and SEM results in comparison to tendons pulled to rupture in previous studies[56,68,69]. To explore if this observation was simply caused by the slower strain rate applied through creep loading, a third hypothesis was proposed:

Hypothesis 3: Tendons exposed to low strain rate ramp rupture loading will show less significant fibrillar and molecular damage than found in their creep ruptured counterparts.

Rationale 3: Previous studies have shown that the mechanical responses of tendons depend on the loading rate applied on these tendons[63,101,102]. Willett et al.[68] have shown that the molecular structure of tendons is directly impacted by a decrease in the strain rate. Specifically, it has been found that the disruption of the molecular packing of tendons increases significantly when the strain rate is decreased[68]. With that in mind, it is expected that creep overloaded tendons, which are loaded at loading rates significantly lower than ramp ruptured samples, will have more significant nanostructural alterations.

4.3 Methodology

An overview of the experiment is shown in Figure 4.1.

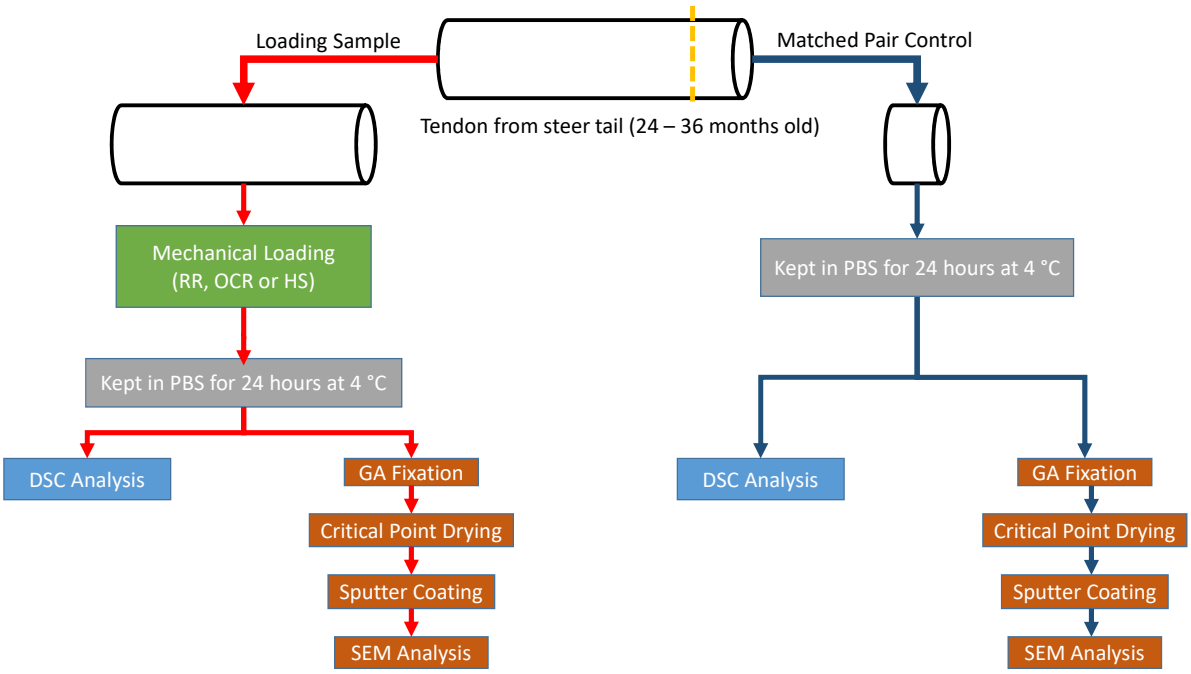

Figure 4.1: The flowchart of the procedure OCR experiment.

4.3.1 Tendon Preparation and Geometrical Dimensions' Measurement

Tails from adult steers (24 - 32 months old), which were killed for food, were collected from a local abattoir (Reids Meats, Wolfville, NS, Canada). Tendons were extracted from the dorsal, proximal part of collected steer tails and stored in a -86 °C freezer (Thermo Fischer Scientific, Waltham, MA, USA). Previous tests performed after freezing of tendons, for periods of less than 30 days, confirmed that this process

does not affect the mechanical response of tendons[57,103,104]. Evidence from the literature suggests that soft tissues, including tendons, from female mammals may have greater structural variability due to the side-effects of pregnancy[105–108]. Therefore, only steer tails were used in this study.

Prior to mechanical loading, tendons' cross-sectional area (CSA) values were measured and recorded. To perform this measurement, each tendon was first hung vertically using a binder clip, after which four consecutive photos of the hung tendon were taken, with the tendon rotated axially by 90° between each photo. The resulting photos were then imported into ImageJ (National Institutes of Health, Bethesda, MD, United States). For each of the tendons, the cross-sectional diameter was measured at three different locations along the tendon's longitudinal axis, after which these three values were averaged. This yielded four different diameter measurements, one for each photo. The mean major and minor diameters were calculated by finding the mean values of the two larger diameters and the two smaller diameters respectively, after which each tendon's CSA was finally calculated using the following formula:

$$CSA = \pi \times \frac{MeanMajorDiameter}{2} \times \frac{MeanMinorDiameter}{2} \tag{4.1}$$

Tendons were then laid on a dissection platform, where each tendon was cut to around 55 mm in length. Tendons were then gripped into the rig and then submerged in the PBS bath. The average CSA for all samples tested was 3.47± 0.84 mm^2.

4.3.2 Mechanical Loading Tests

Prior to starting each mechanical testing, a small piece of each tendon was dissected. These dissected samples formed the unloaded, matched-pair control sample group (n = 36). For the current experiment, each tendon was assigned to one of the following three mechanical tests: 1) Overload Creep Ruptured (OCR group, n=12): These samples were ramp loaded to their yield stress and maintained at this stress until rupture, (Figure 4.2 and Figure 4.3). 2) High-Stress Test (HS group, n=12): These samples

were ramp loaded to the yield stress and then unloaded immediately (Figure 4.4). 3) Ramp Rupture (RR group, n=12): These samples were ramp loaded to rupture, at the same rate used for the ramp portion of the OCR group (Figure 4.5).

Each tendon (length = 5.5 cm) was fixed into the MCS using crush grips. The samples were then submerged in a bath containing 250 ml of phosphate buffered saline (PBS) solution (0.15 M) during the test. An initial 0.5 N load was applied to each tendon, which was the starting point of all the mechanical tests. The intergrip distance, l_o, was then measured (l_o = 14.8 ± 0.3 mm). During each test, the optical encoder was set to read samples at a rate of 51 Hz.

Time readings (s), load readings (N) and displacement readings (mm) were exported to Microsoft Excel. Load readings were converted to stress (MPa), by dividing each reading by each tendon's pre-loading's cross-sectional area. Displacement readings were converted to strain (mm/mm and then converted to %) by dividing the displacement readings by l_o.

From the stress, strain and time readings, several mechanical properties were found or calculated and then recorded. The ramp loading's and the creep session's strain rates (both in mm/mm/s or %/s) were calculated by finding the slope of the strain vs. time curve during ramp loading and secondary creep loading phases respectively. The yield point was calculated using the slope change calculation method to be explained in the next section. Ultimate tensile strength (UTS) values were also recorded for the RR samples. The modulus value was also calculated, by calculating the slope of the linear region of the stress-strain curve.

For all tests, the ramp loading section was done at a deformation rate of 0.013 ± 0.001 mm/s, resulting in an average strain rate of 0.09 ± 0.01 %/s. The creep loading rate of tendons was calculated after the experiment and was found to be around 0.03 ± 0.01 %/s. Both the strain rates used in this experiment were lower than loading rates previously used during ramp or cyclic overloading tests of the same tendon model[4,56,68,69,79].

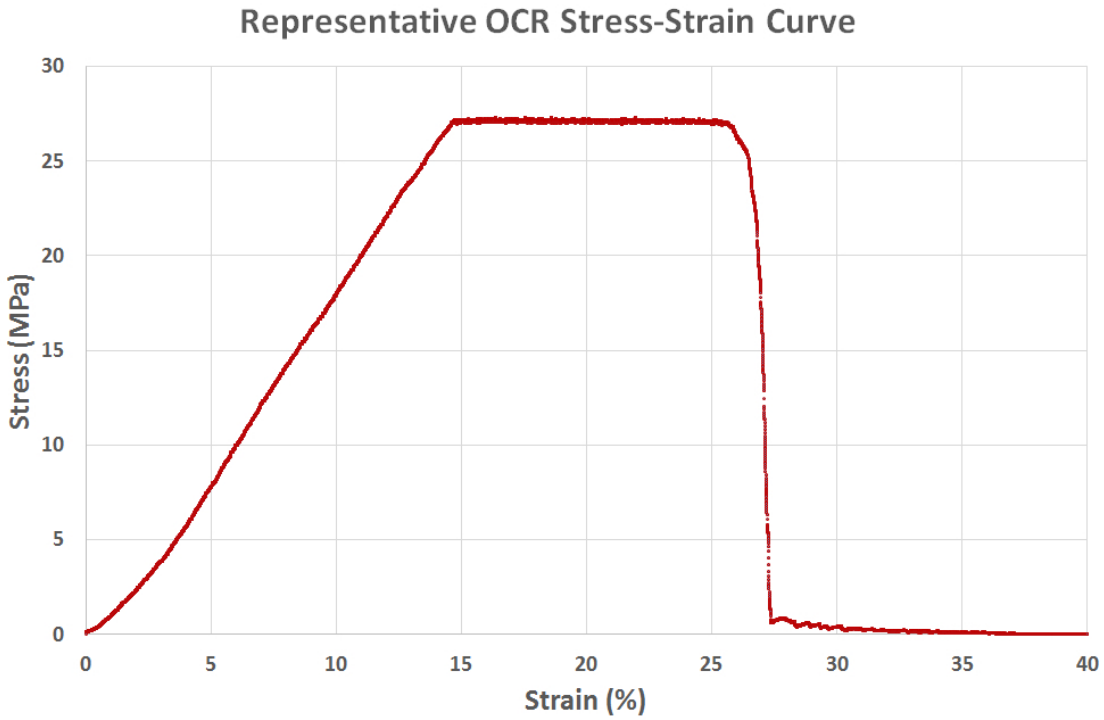

Figure 4.2: A representative stress-strain curve generated from an OCR loading test on a tendon. A zoomed in portion of this curve is shown Figure 4.3.

4.3.3 Determination of the Yield Point of Tendons

For the current experiment, the yield stress of tendons was the target stress level to either trigger creep loading in the case of the OCR loading, or to trigger the unloading of the tendon in HS loading. The yield point of tendons is typically defined as the end of the linear region when the slope of the stress-strain (or force-deformation) curve

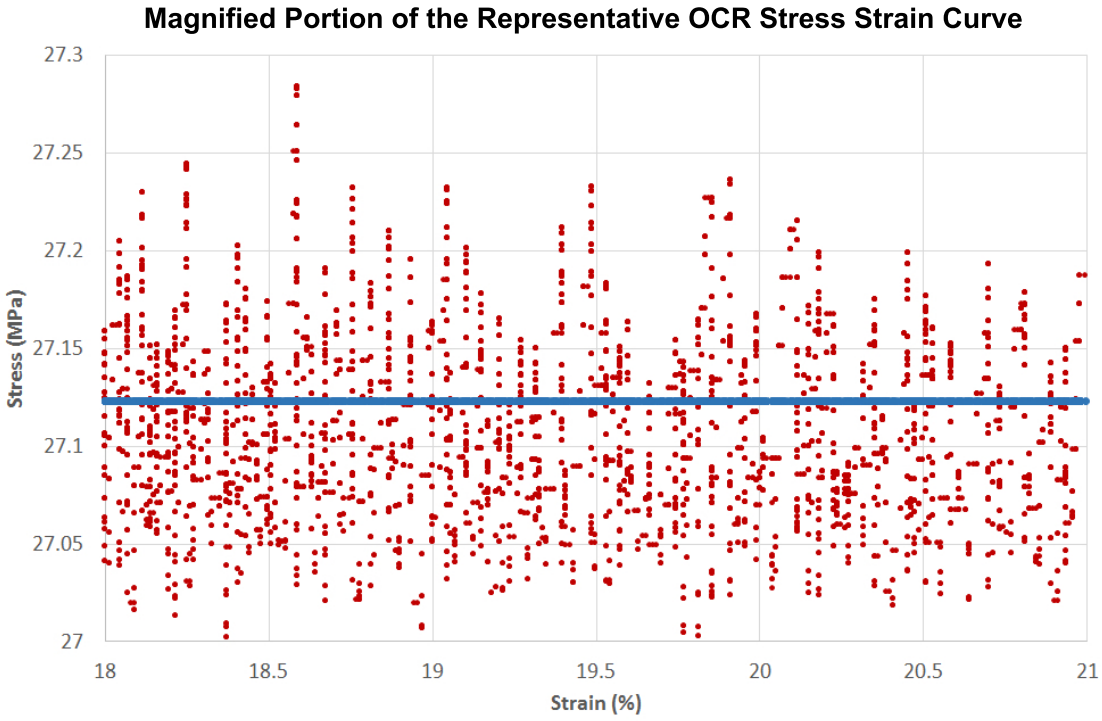

Figure 4.3: A magnified regions of the creep portion of Figure 4.2. The linear actuator loads the tendon when the force measured by the load cell falls below the trigger creep load by around 0.2 N.

begins to decrease. The following method was used to calculate each tendon's yield point:

During each mechanical test, the slope of the load-deformation curve was continuously calculated using the preceding 10000 data points, starting from the 10000th point of each test. The change between sequential slopes (ΔSlope, %) was calculated using the following formula:

$$\Delta Slope = \frac{NewSlope - OldSlope}{OldSlope} \times 100 \tag{4.2}$$

Tendons were considered to have yielded when the ΔSlope reached 0%, indicating

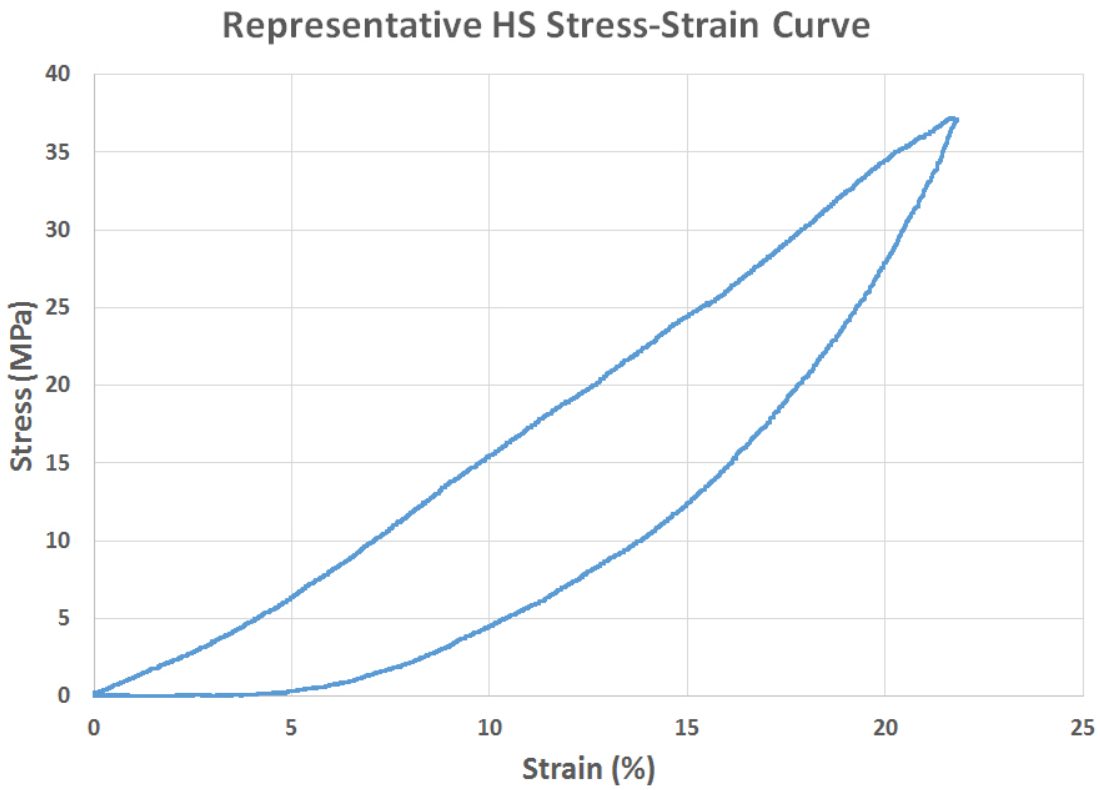

Figure 4.4: A representative stress-strain curve generated from an HS loading test on a tendon.

that the maximum linear slope had been reached (Figure 4.6).

The number of points used to calculate the slope, using this method, was initially determined based on trial and error. The yield point was then determined manually by fitting and overlapping a straight line through the linear region of the stress-strain curve, observing where the curve began to deviate from that line (Figures 4.7). An analysis of six RR samples showed that determination of the yield point using 10000 point slope calculation was consistent with the manual determination of the yield point. Results were tabulated in Table 4.1.

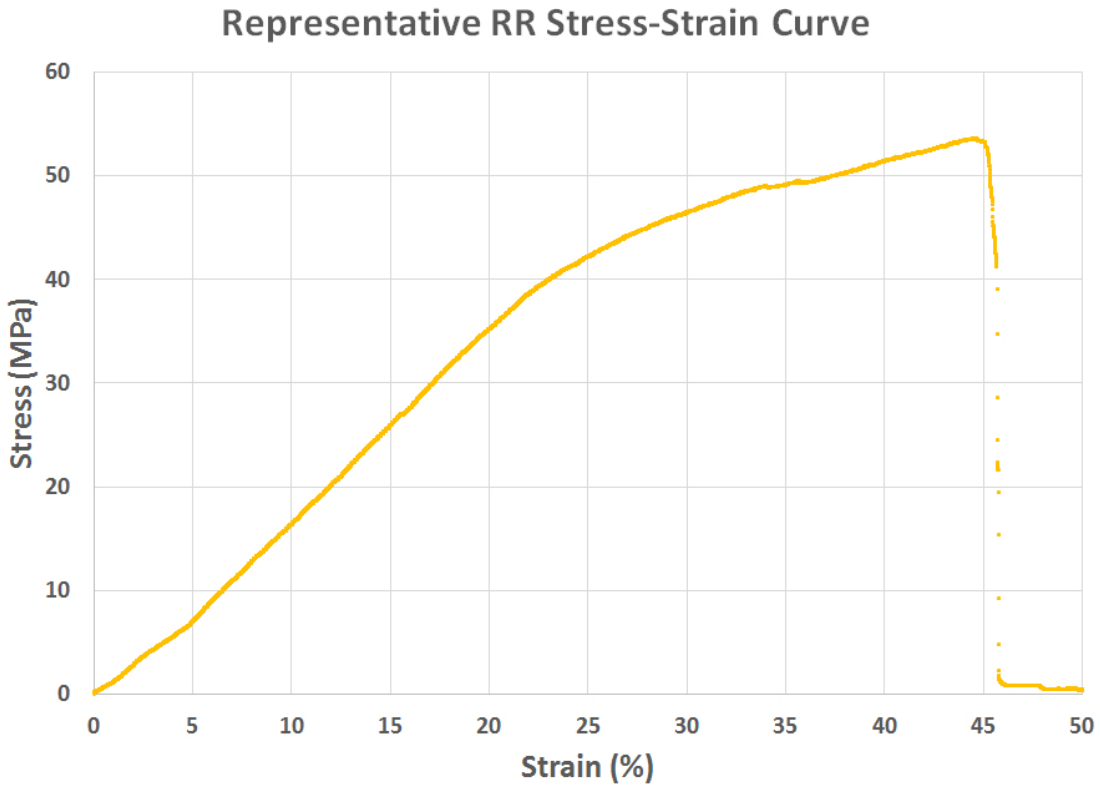

Figure 4.5: A representative stress-strain curve generated from an RR loading test on a tendon.

Table 4.1: The analysis of six RR samples' yield points by calculating slope using 5000 points and 10000 points slope calculation (as used for HS and OCR samples) and by manual observation.

	Calculation (5000 Points)		MCS Trigger (10000 Points)		Manual Observation	
Samples	**Strain (%)**	**Stress (MPa)**	**Strain (%)**	**Stress (MPa)**	**Strain (%)**	**Stress (MPa)**
ST13-T7	21.4	29.9	25.3	36.0	25.6	36.4
ST13-T10	23.4	29.4	23.4	29.4	26.2	32.5
ST13-T13	18.8	33.1	21.6	38.0	21.4	37.5
ST14-T1	13.2	14.3	20.9	23.4	20.9	23.4
ST14-T4	12.2	18.3	18.3	27.2	15.6	23.3
ST14-T7	18.4	29.1	22.6	35.6	21.1	33.5
Mean	17.9	25.7	22	31.6	21.8	31.1
Standard Deviation	4.0	6.9	2.2	5.3	3.5	5.7

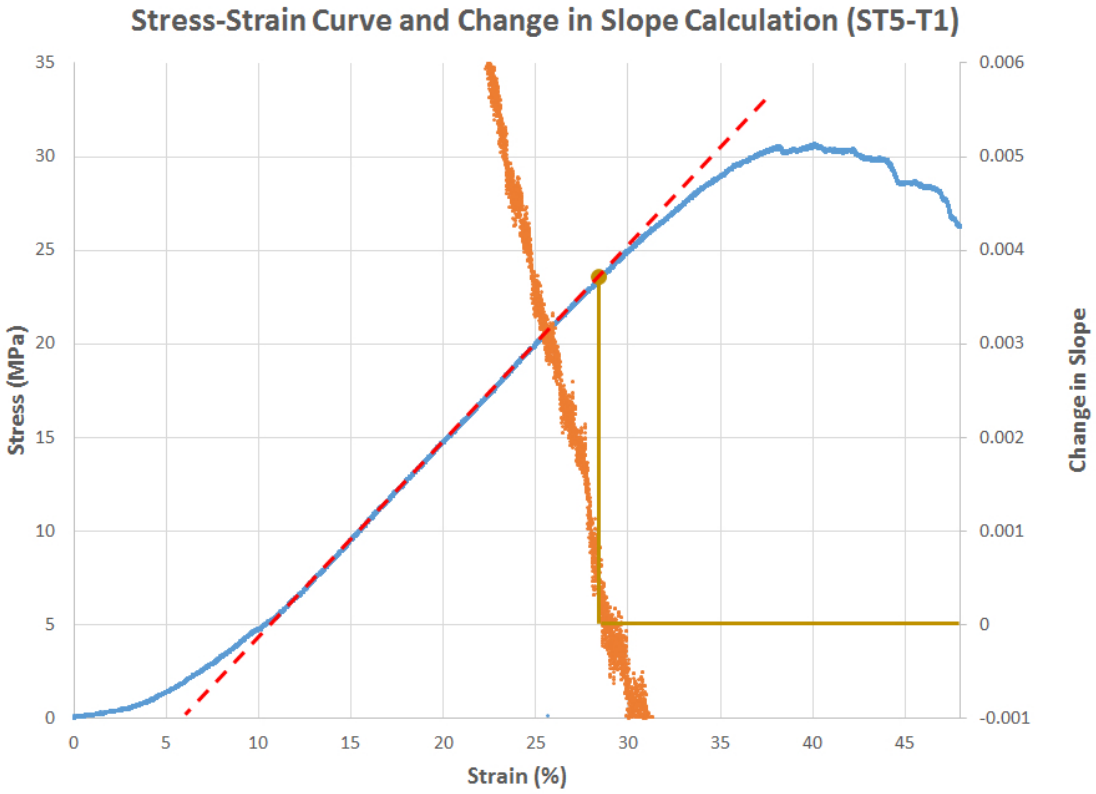

Figure 4.6: A tendon's stress strain curve, which underwent RR loading, is shown in blue, with the change in slope of that curve shown using orange points. Were this a static creep test, static loading would be triggered at the point indicated, where the change in slope reached 0%, which is the location of the maximum slope of the stress strain curve.

4.3.4 DSC Thermoanalysis

After each mechanical test, the tested tendon was unloaded from the rig and the gripped ends were cut off and discarded. Each of the loaded and control samples was then stored in 5 ml of PBS in the fridge overnight to await DSC analysis or preparation for SEM.

DSC analysis of all loaded samples, as well as their matched-pair controls, was done using a Q100 differential scanning calorimeter (TA Instruments, New Castle, DE).

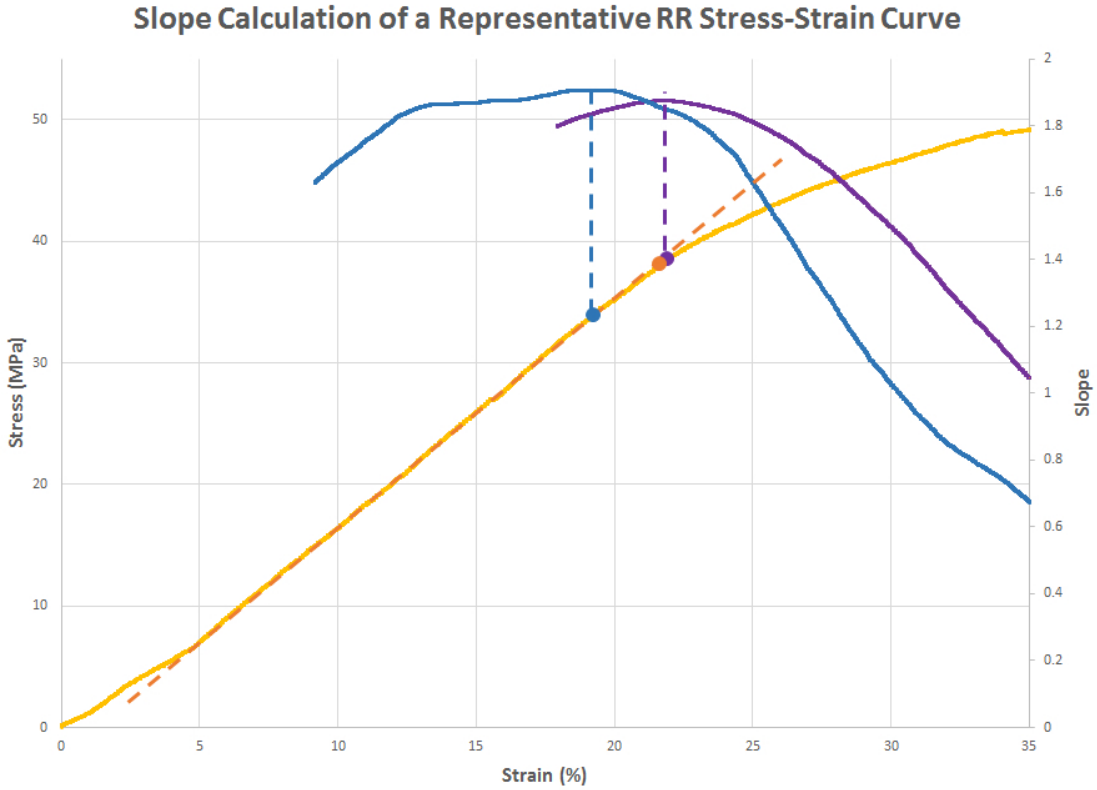

Figure 4.7: An RR stress-strain curve (yellow), with the different derivatives featuring the point at which the slope of 10000 points calculations reached its maximum value (purple) and 5000 points (blue). The manual calculation of the yield point is shown in the curve (orange). This chart shows clearly that the yield point was best predicted using 10000 points calculation.

Prior to starting the DSC tests, all samples were rinsed with ultrapure water, treated with reverse osmosis along with deionization. Samples were rinsed in 24 well-trays for 30 minutes, with three rinses in separate wells, each rinse was 10 minutes long. The DSC was calibrated using an indium sample (mass = 12.28 mg) placed in an aluminum pan and run against an empty pan. Eight tendons from each mechanical test, as well as their matched-pair control samples, were analyzed using DSC: RR samples (n=8), OCR samples (n=8), HS samples (n=8) and matched-paired controls (C, n=24). A small sample (mean ± SD: 11.72 ± 1.40 mg) was taken from each tendon, blotted to remove excess surface liquid, weighed, and placed in aluminum DSC pans. Each

pan was then hermetically sealed, prior to each DSC run. The samples were loaded against an empty sealed pan for each run.

Samples were equilibrated at 30 °C and then ramped to 90 °C at a rate of 5 °C/min. Endotherms were analyzed using Universal Analysis 2000 software (version 4.5A, TA Instruments, New Castle, DE, United States) for onset temperature (T_{onset}), peak temperature (T_{peak}), full width at half maximum (FWHM), and specific enthalpy of denaturation (Δh). Endotherms were generated from each of the DSC analysis tests (Figure 4.12). DSC tests were performed on two pieces from each tendon sample, the results of which were then averaged. In some cases, the result of DSC analysis yielded double peaked endotherms (Figure 4.8). In such cases, the analysis of double peaked endotherm was done in the same method done in single peaked endotherms. The T_{onset} and specific enthalpy results were calculated in the same way in both single and double peaked endotherms. The T_{peak} value of double peaked endotherms was identified for each of these samples as the higher value of T_{peak} recorded of both peaks in each of these samples. The FWHM value for these samples were calculated between the incline and decline of the endotherm manually.

For all DSC analysis tests of this experiments, Δh was calculated based on dry sample weight. After the DSC analysis, each tendon sample was left to dry in a vacuum desiccator with desiccant for 24 hours. Samples were then weighed for the first time. These samples were then dried for another 24 hours and reweighed. If the mass of the second measurement had not changed significantly, the average of these two masses was calculated and recorded as the dry mass. Otherwise, the samples were dried for an additional 24 hours and reweighed. In that case, the average of the last two dry masses was calculated.

4.3.5 SEM Nanostructural Analysis

SEM analysis was performed on four samples from each group: unloaded matched-paired control samples (n=4), RR samples (n=4), HS samples (n=4) and OCR samples (n=4).

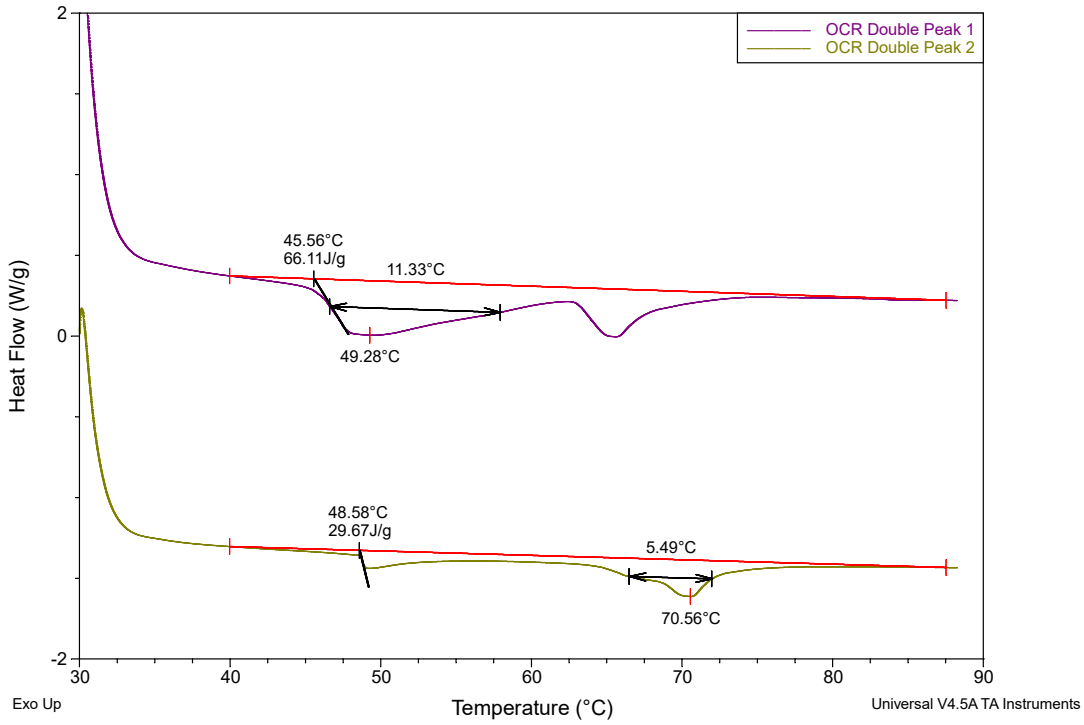

Figure 4.8: An RR stress-strain curve (yellow), with the different derivatives featuring the point at which the slope of 10000 points calculations reached its maximum value (purple) and 5000 points (blue). The manual calculation of the yield point is shown in the curve (orange). This chart shows clearly that the yield point was best predicted using 10000 points calculation.

Tendon samples to be analyzed using SEM were fixed using 2.5% EM-grade glutaraldehyde (GA) in cacodylate buffer (0.2 M). The GA fixation was done for a total of one hour for each of the tendon samples, at room temperature and was stirred using a shaker. After being GA fixed, tendons were bisected longitudinally, dehydrated in graded ethanol, and critical point dried. The samples were then mounted on SEM stubs with carbon tape, with their exposed, interior surface facing upward, after which the samples were sputter coated with gold-palladium.

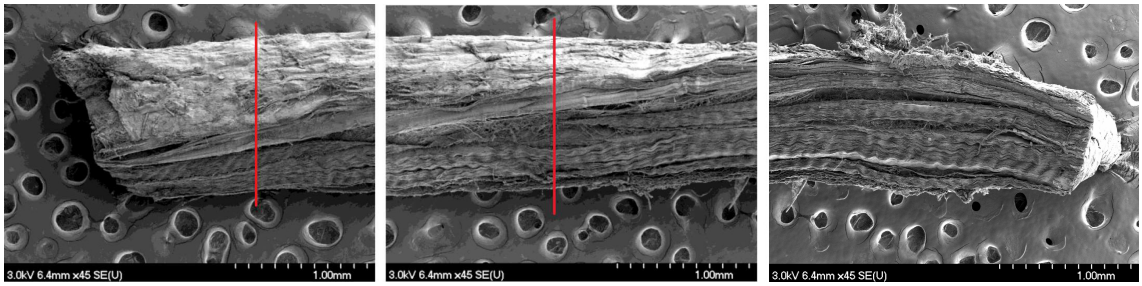

Figure 4.9: A representative panoramic scan of one of the tendon samples that was later scanned under high magnification. The red lines show both cross-sections where the scans were done.

Tendon samples were inspected using a model number S-4700 SEM (Hitachi, Chula Vista, CA) operating at 3 kV, 15 mA. A panoramic image was first taken for each sample at low magnification levels (Figure 4.9), after which each of the tendon samples was scanned at two different and distant cross sections at high magnifications that ranged between 10,000× and 45,000×. to determine the degree and consistency of structural alterations to the tendon. For each sample at least 10 high magnification representative images were taken.

4.3.6 Statistical Analysis

Statistical analysis procedures were done using JMP analysis software, in order to test the proposed hypothesis from this experiment. All data are presented as mean ± Standard Deviation (SD). All results with $p < 0.05$ were considered significant.

While tendons used in this experiment were all from steers of the same age range, nanostructural differences may occur between individual tendons from either the same or from different individual steers. To determine if the tendons from all animals were structurally similar and could, therefore, be viewed as independent samples, ANOVA statistical analysis was done on the DSC data from control samples, with their animal of origin set as the independent factor. Results of this analysis showed no significant

differences in the thermal parameters of the control samples, indicating that tendons from different tails were similar in structure. Each tendon was therefore considered an independent sample.

Matched-pair t-test was performed on DSC results. This was done to determine whether the thermal parameters were significantly altered due to each loading regimen, in comparison to that of their counterpart match-pair control samples' analysis. This analysis would assess indicators of either molecular packing disruption and/or collagen denaturation in loaded samples, in comparison to their matched pair controls. The results were first separated into three groups representing the types of mechanical loading applied on them. Shapiro-Wilk test was done on each of the sets of results to determine their goodness under a normal fit. A nonparametric Wilcoxon signed rank test was performed on any of the sets that showed a negative Shapiro-Wilk test result. Finally, T-test analysis was performed to compare the differences in thermal parameters results of the RR and OCR samples.

4.4 Results

4.4.1 Mechanical Properties

Several mechanical properties were calculated as part of the analysis. The yield strain and stress were similar for tendons in the OCR, HS, and RR groups, as shown in Table 4.2. The average time that OCR samples sustained static loading before rupture was 520.4 ± 217.2 seconds. While recorded, after this test was completed, the displacement readings during creep were found to be inaccurate (readings were $\sim 28\%$ higher than what they should have been). The displacement during creep should therefore be regarded as approximate (Figures 4.10 and 4.11). Note that for the OCR and RR samples, displacements recorded during the ramp portion of the test were not affected by this error and are accurate.

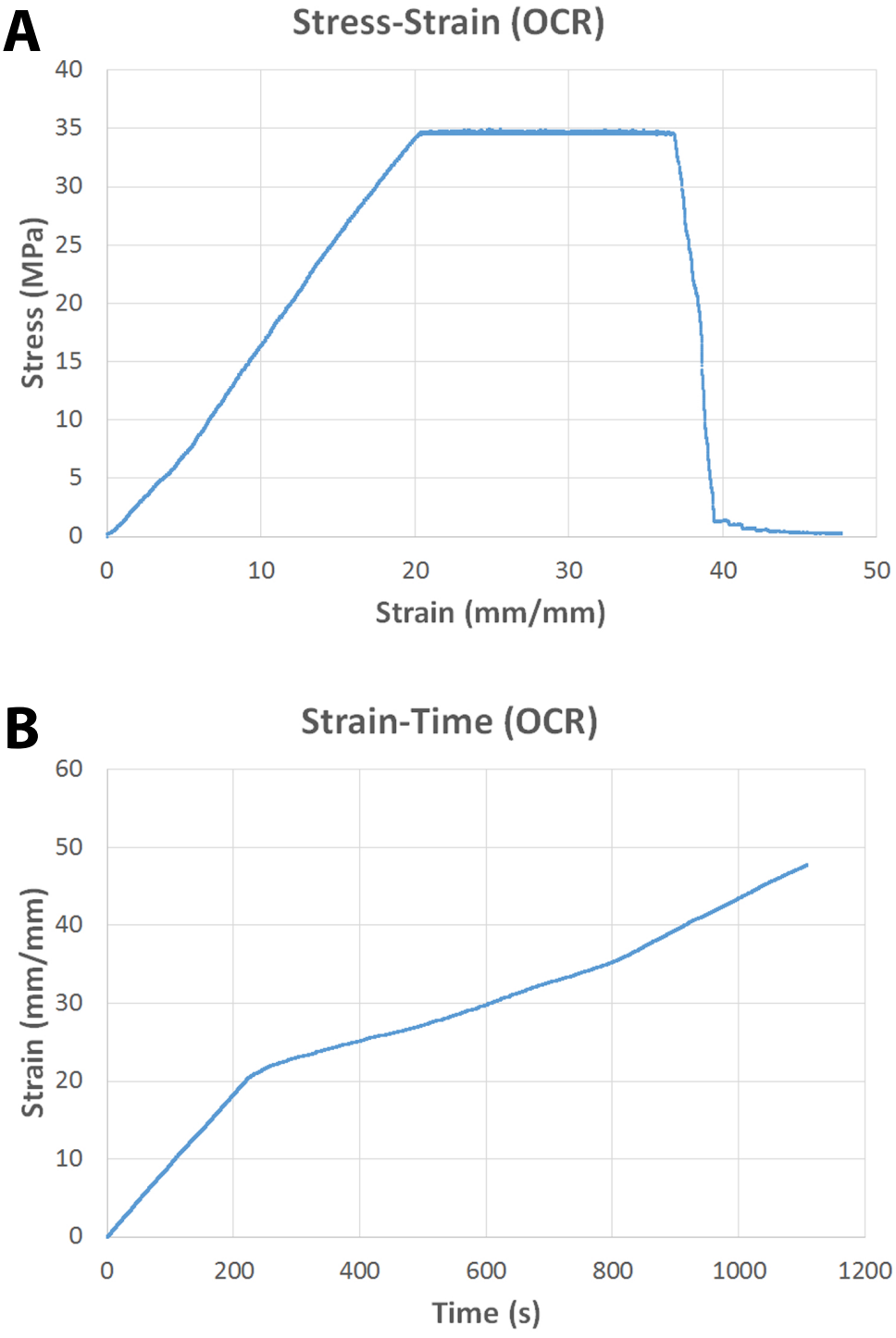

Figure 4.10: Representative Stress-Strain and Strain-Time charts an OCR sample.

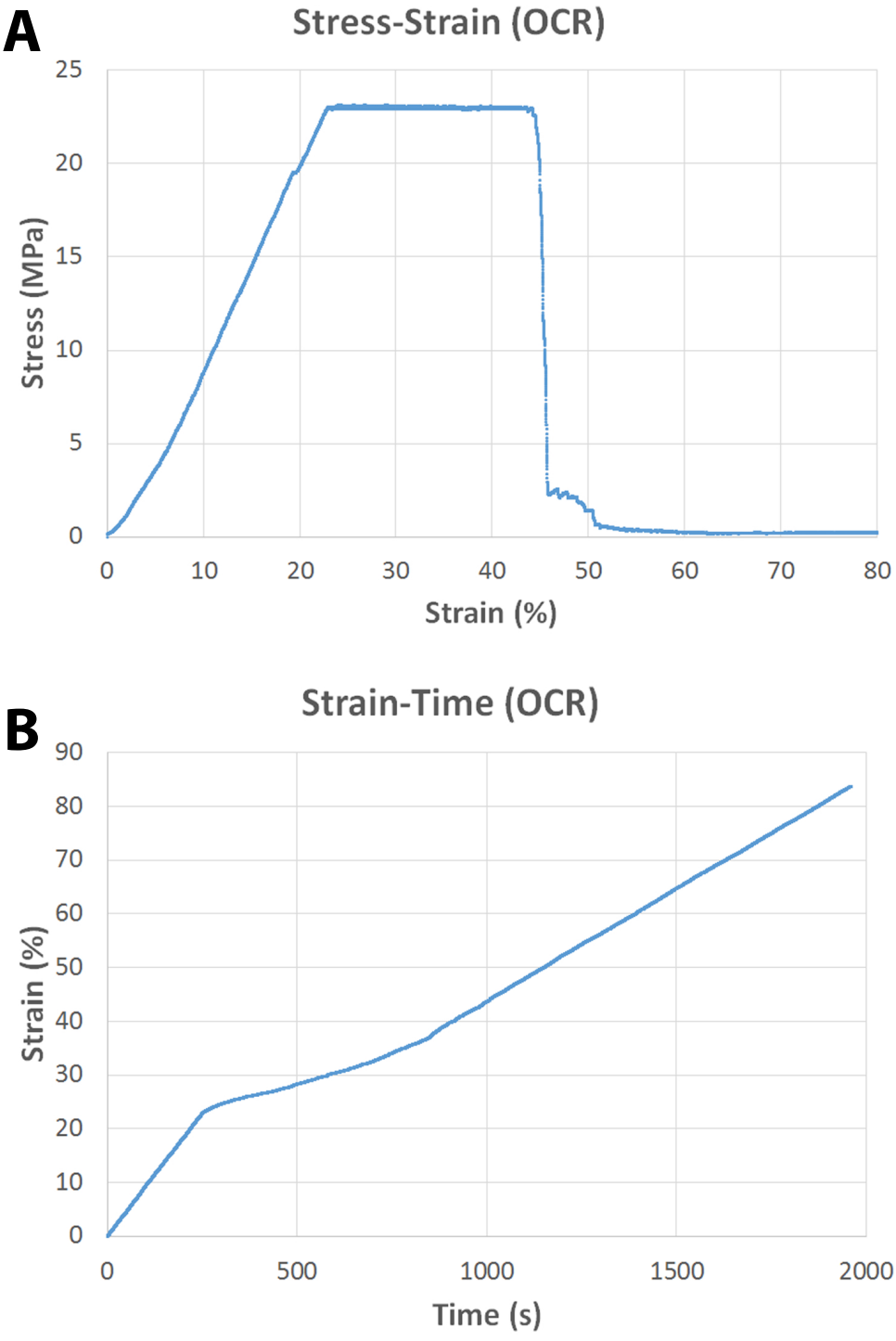

Figure 4.11: Representative Stress-Strain and Strain-Time charts an OCR sample.

Table 4.2: Average yield stress and yield strain values from tested tendons.

	Yield Strain (%)	Yield Stress (MPa)
HS	21.1 ± 3.5	27.8 ± 8.5
OCR	21.7 ± 4.9	30.3 ± 7.4
RR	22.5 ± 4.0	31.5 ± 7.2
Average	21.8 ± 4.2	30.7 ± 8.2

4.4.2 Macrostructural Rupture Properties

For all OCR and RR samples tested in this experiment, it was clear that ruptures occurred within the inter-grip region of loaded tendons, which means that failure was caused by loading rather than gripping damage propagation. The major difference between the RR and OCR ruptures was the rupture mode. OCR loading caused tearing and sliding of the tested tendons as they were separated into two parts, with no single failure location. RR samples, on the other hand, ripped apart in a cleaner fashion when they failed, with the rupture site being clearer in these samples.

The difference in macrostructural rupture features in different loading protocol can be indicative of the mechanical response of tendons to loading. The tearing and sliding breaking of tendons due to OCR loading treatment may indicate that they experienced higher intrafibrillar and interfibrillar shear shear levels than the other loading protocols. In this thesis, the level of shear was not measured. However, several methods to calculate shear were used in previous studies. Cheng and Screen[109] examined the levels of strain fields within the tendon matrix under tensile load, something that was achieved by examining the movement of fibrils and fibers through confocal microscopy. The results of Cheng and Screen's study[109] shows that significant sliding occurs in tendon fibers due to incrementing step straining of about 1% at a rate of 10%/s. Through notch tension testing, Szczesny et al.[38] was able to quantify the intrafibrillar shear stress in tendons. Either of the methods stated could be used in further studies to determine the amount of shear formed by overload creep.

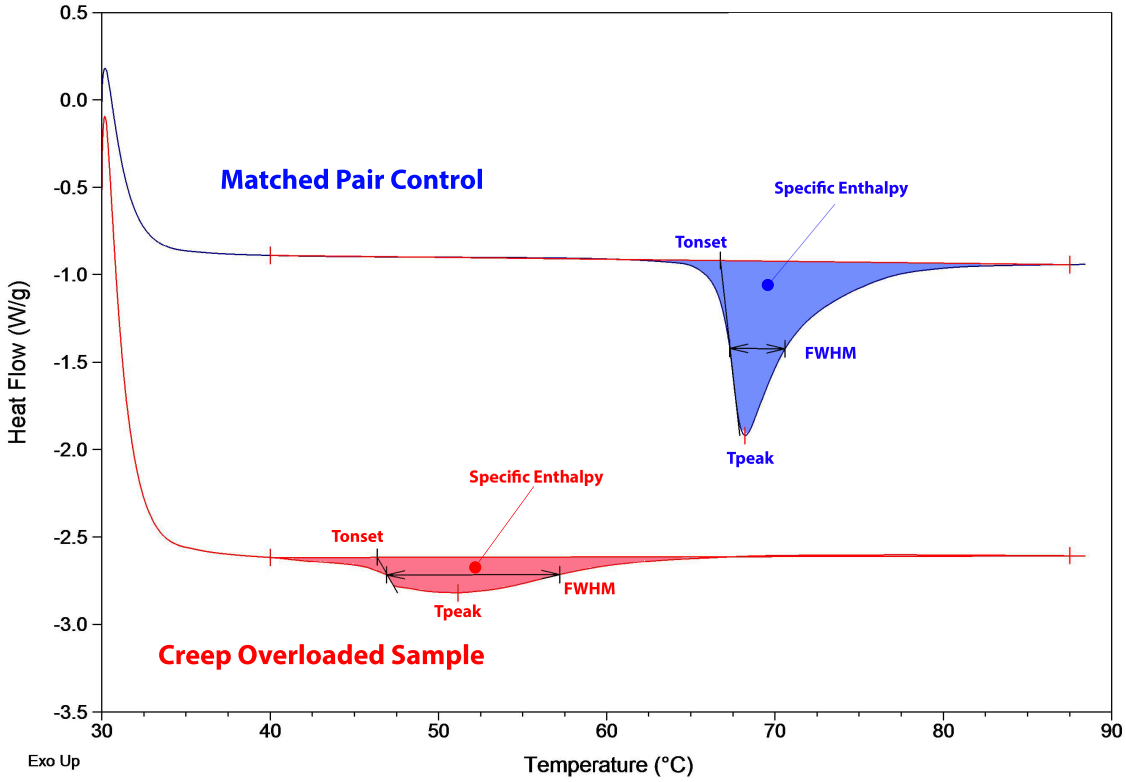

Figure 4.12: DSC analysis outcome showing the endotherms of both an OCR sample and its respective matched pair control.

4.4.3 DSC Thermoanalysis

Figures 4.12, 4.13 and 4.14 show representative examples of the DSC endotherms from different mechanical tests performed in this experiment. A summary of DSC results is shown in Table 4.3.

Matched-pair analysis of the DSC data indicated that T_{onset} values of both OCR and RR samples significantly dropped, when compared to their matched-pair controls(-18.5 $\pm$ 1.1 °C; $p < 0.0001$ and -19.0 $\pm$ 2.4 °C; $p < 0.0001$, respectively). T_{peak} values of the OCR and RR samples, when compared to their matched-pair controls,

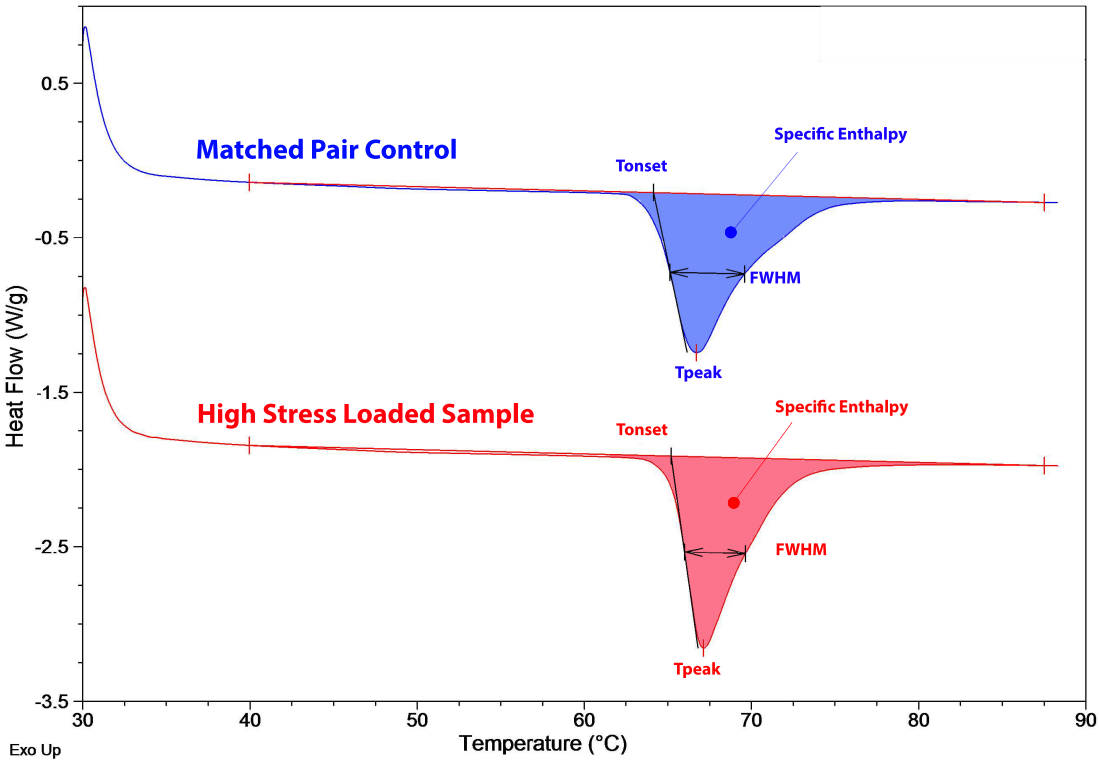

Figure 4.13: Representative DSC chart showing the endotherms of both an HS sample and its respective matched pair control.

Table 4.3: A summary of the first experiment's DSC thermoanalysis. All the thermal parameter results are shown relevant to Matched-pair control samples' DSC results.

	Water Content (%)	$\mathbf{T}_{onset}$ **(°C)**	$\mathbf{T}_{peak}$ **(°C)**	**Δh (J/g)**	**FWHM,(°C))**
C	72.7 ± 3.0	64.9 ± 0.8	67.5 ± 0.6	63.0 ± 6.1	4.5 ± 0.7
HS	73.4 ± 3.3	64.5 ± 0.8	66.8 ± 0.6	62.5 ± 4.9	4.7 ± 0.9
OCR	85.1 ± 2.6	46.4 ± 0.8	54.5 ±7.0	50.9 ± 13.6	16.0 ± 4.3
RR	85.0 ± 4.2	46.0 ± 1.6	49.9 ± 1.0	60.8 ± 5.7	13.4 ± 3.4

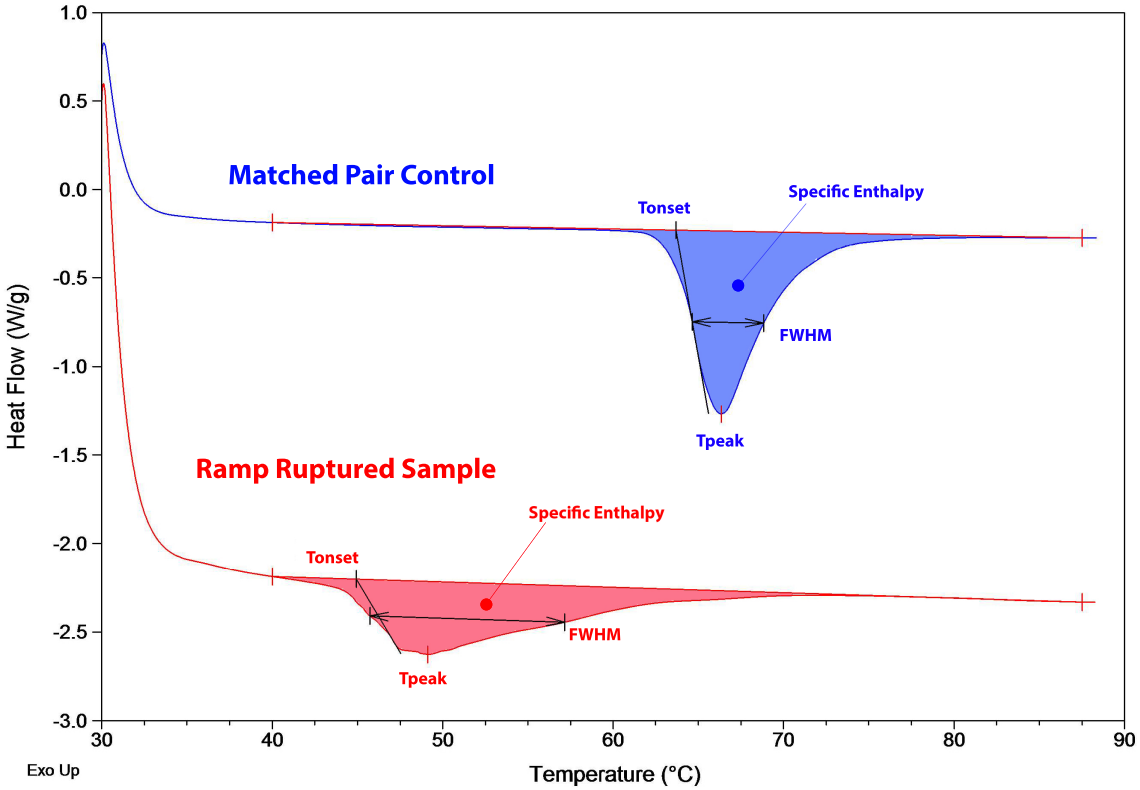

Figure 4.14: DSC analysis outcome showing the endotherms of both an RR sample and its respective matched pair control.

also showed significant drops (-13.0 ± 7.0 °C; p = 0.0156 and -17.5 ± 1.5 °C; p < 0.0001 respectively). FWHM values of the OCR and RR samples showed significant increases, in relation to their paired controls (+11.2 ± 3.9 °C; p < 0.0001 and +9.3 ± 3.4 °C; p = 0.0001) respectively.

Specific enthalpy readings from the OCR samples showed statistically significant drops relative to their paired controls(-12.9 ± 13.2; p = 0.0278). However, the standard deviation was large as half of the samples (n=4) showed a much smaller drop than the rest of the samples. Specific enthalpy readings from RR samples did not show a significant difference from the matched-pair controls (-2.9 ± 7.2 J/g; p =0.2999). Increases in the water content were also found for the OCR and RR samples relative

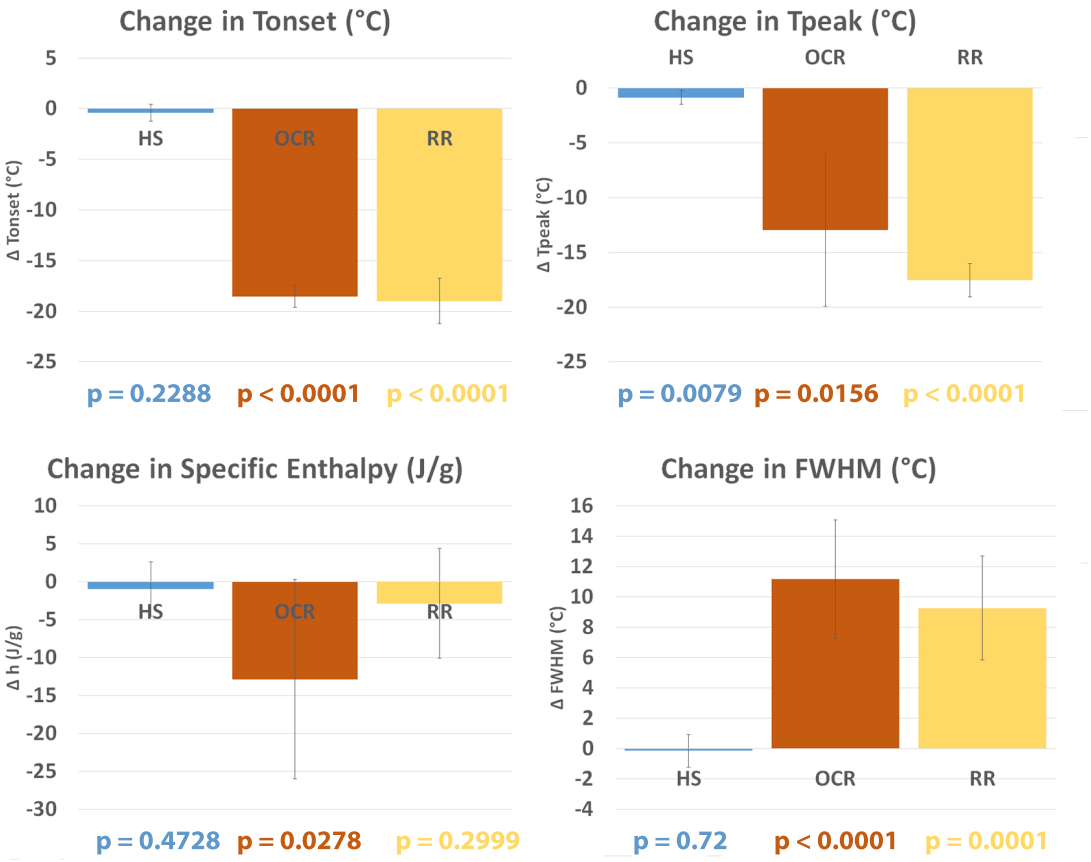

Figure 4.15: Comparison of the changes in the DSC thermal parameters in tendons loaded according to the three mechanical protocols compared to their respective match paired control.

to their paired unloaded controls (+13.6 ± 4.1 %; p < 0.0001 and +11.7 ± 3.6 %; p < 0.0001, respectively) (Figure 4.15).

One of the thermal parameters of the HS group's DSC analysis, T_{peak}, had a minor but a significant drop (-0.8 ± 0.6 °C; p =0.0079). T_{onset}, FWHM, and Δh values of HS samples were not significantly different from their matching controls.

A comparison of the thermal parameters results of the OCR and RR samples showed that changes to T_{onset}, T_{peak} and FWHM were similar (p > 0.05). The change in

specific enthalpy was lower for RR samples than that of OCR samples, but this failed to reach statistical significance ($p = 0.086$).

4.4.4 SEM Nanostructural Analysis

HS samples (n=4) and unloaded control samples (n=4) were analyzed under SEM. For all the samples tested, the HS samples showed little or no alternations to their fibril structure when compared to the unloaded control samples. In most scans of HS samples, fibrils were straight and had visible D-banding formation (Figure 4.16). In some very isolated cases, fibrils were found to have some kinking formation (Figure 4.17).

OCR samples (n=4) showed major changes in the structure of their fibrils. Across all scans from OCR samples, almost all fibrils featured heavy longitudinal kinking (Figures 4.18, 4.19, 4.20, 4.21 and 4.22). A majority of scanned fibrils had high levels of dissociation into sub-fibrils, with what seemed to look like blending formation of fibrils' components with each other (Figures 4.20 and 4.21). Another finding in OCR scans was the clear loss of D-banding of damaged fibrils (Figures 4.19 and 4.20). Unlike other previously observed discrete plasticity studies' results, the OCR group presented this nanostructural damage formation in a very uniform, highly homogeneous and severe fashion. The extensive and heavy presence of kinking formation and D-banding loss support this view.

All RR samples (n=4) contained significantly damaged fibrils. Unlike the OCR samples, however, the fibrillar damage formation was neither as extensive nor was it as homogeneous. A substantial amount of scanned fibrils was found to have signs of kinking with the D-banding still present (Figures 4.23 and 4.24). Other fibrils had a clear loss of D-banding and denser longitudinal kinking, along with the significant presence of fibrillar dissociation (Figure 4.25 and 4.26). The fibrillar damage formation in RR samples could be described as less homogeneous and severe than that of OCR samples.

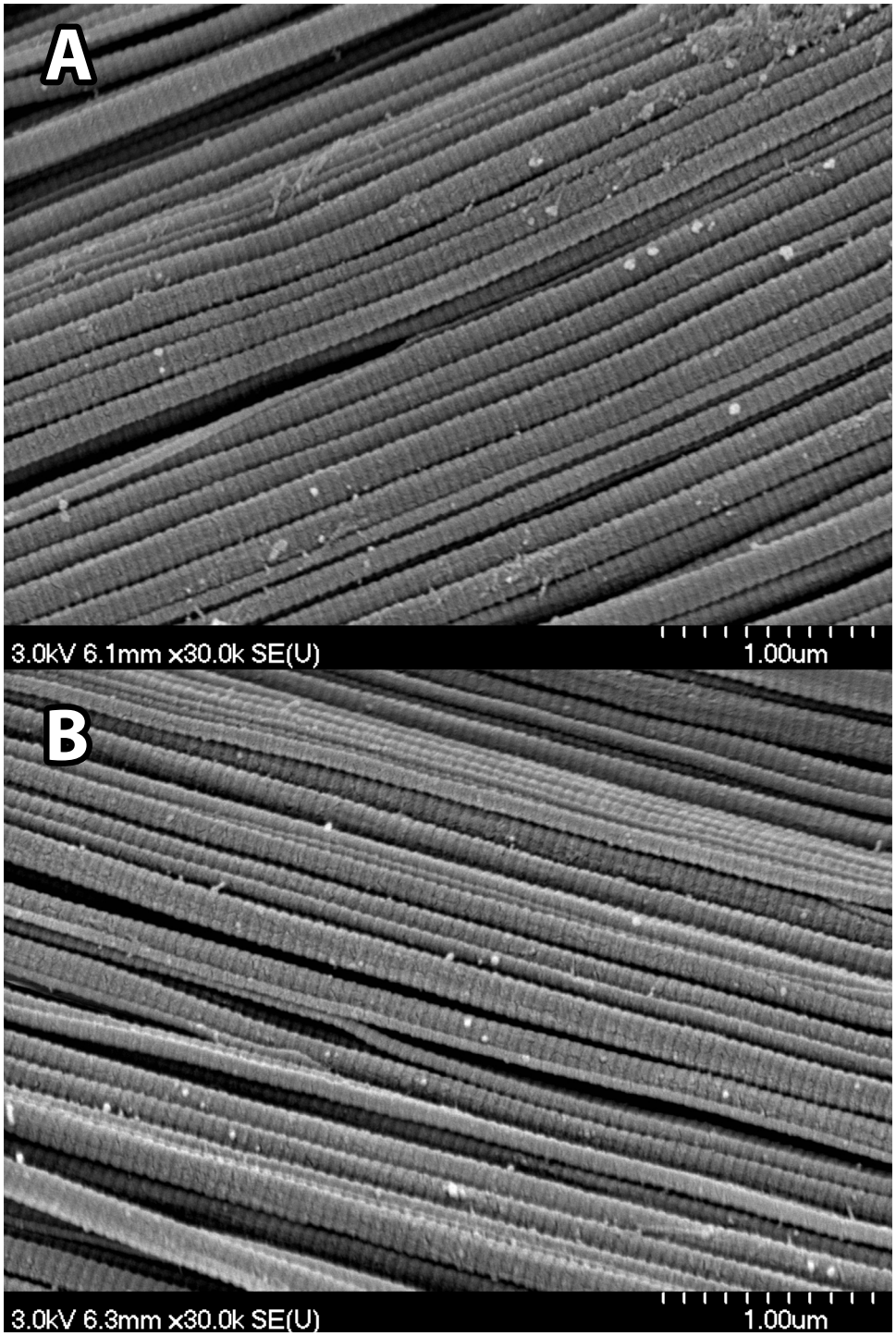

Figure 4.16: Representative SEM images of (A) unloaded control sample, and (B) HS sample. It can be clearly seen that in both scans, fibrils remained straight, with D-banding formation left unscathed, and a lack of any longitudinal kinking formation.

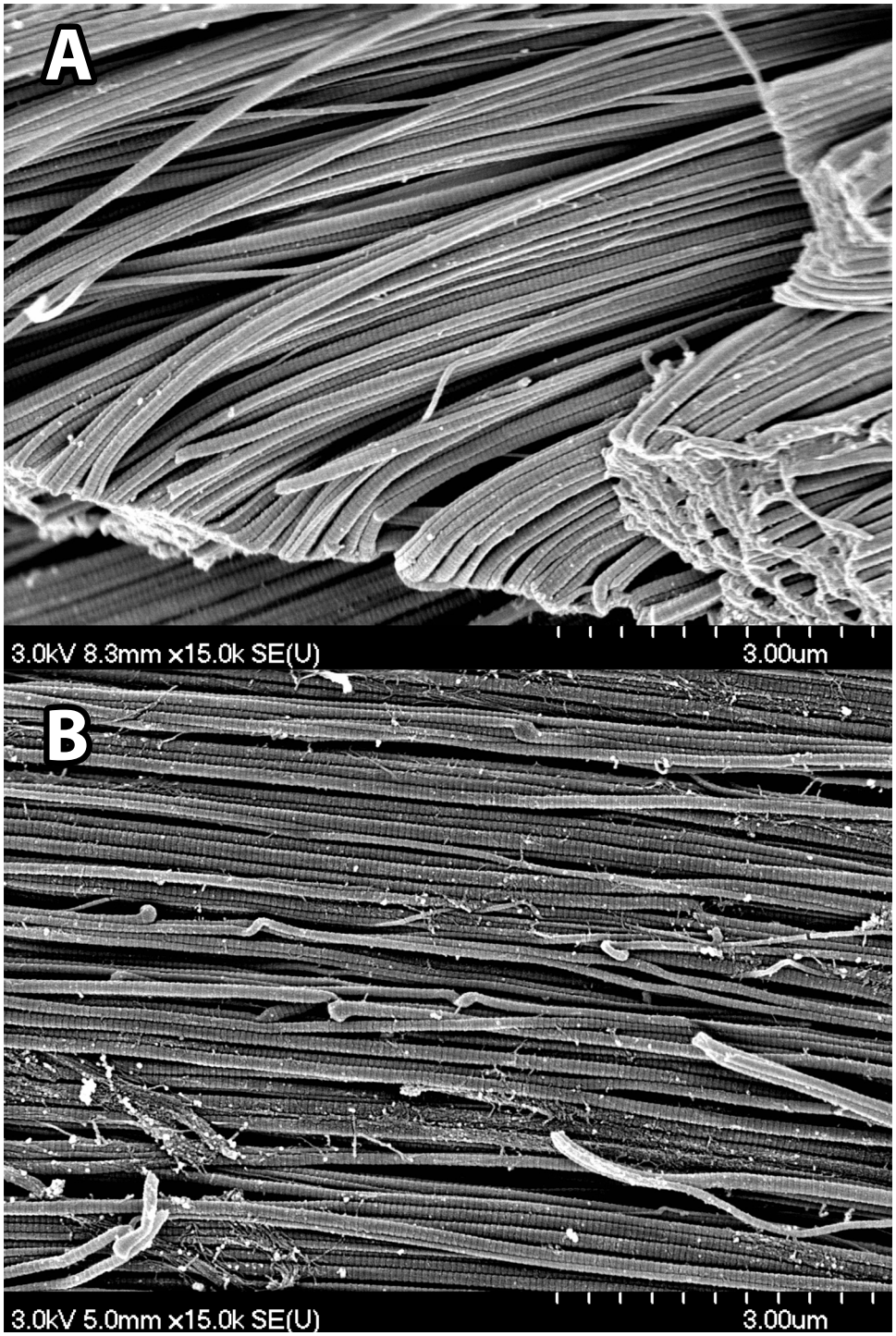

Figure 4.17: Representative SEM images of (A) unloaded control sample, and (B) HS sample, which does feature minor longitudinal kinking formation.

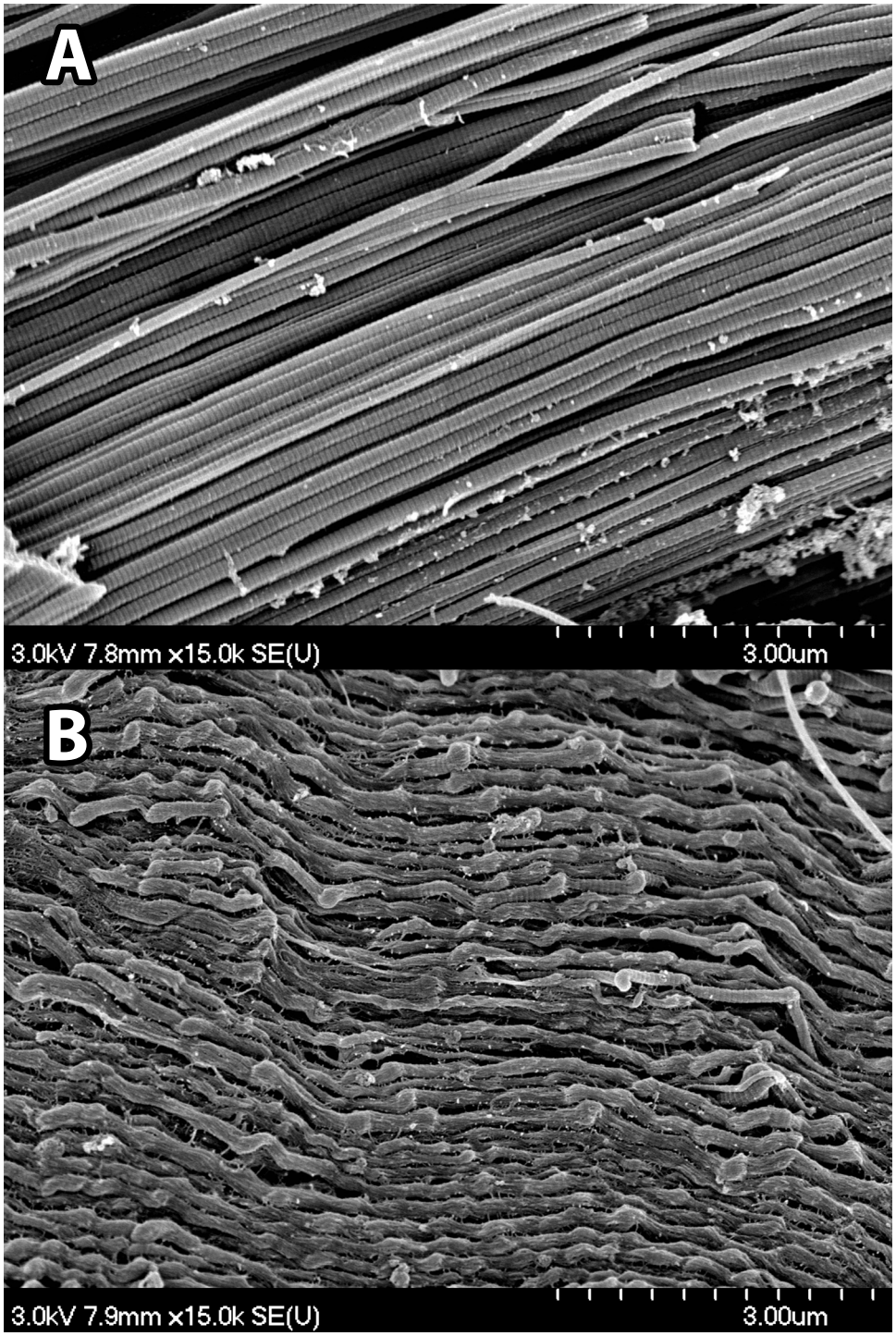

Figure 4.18: Representative SEM images of (A) unloaded control sample, and (B) an OCR sample. It is clear that all the fibrils in this image experienced a high amount of longitudinal kinking.

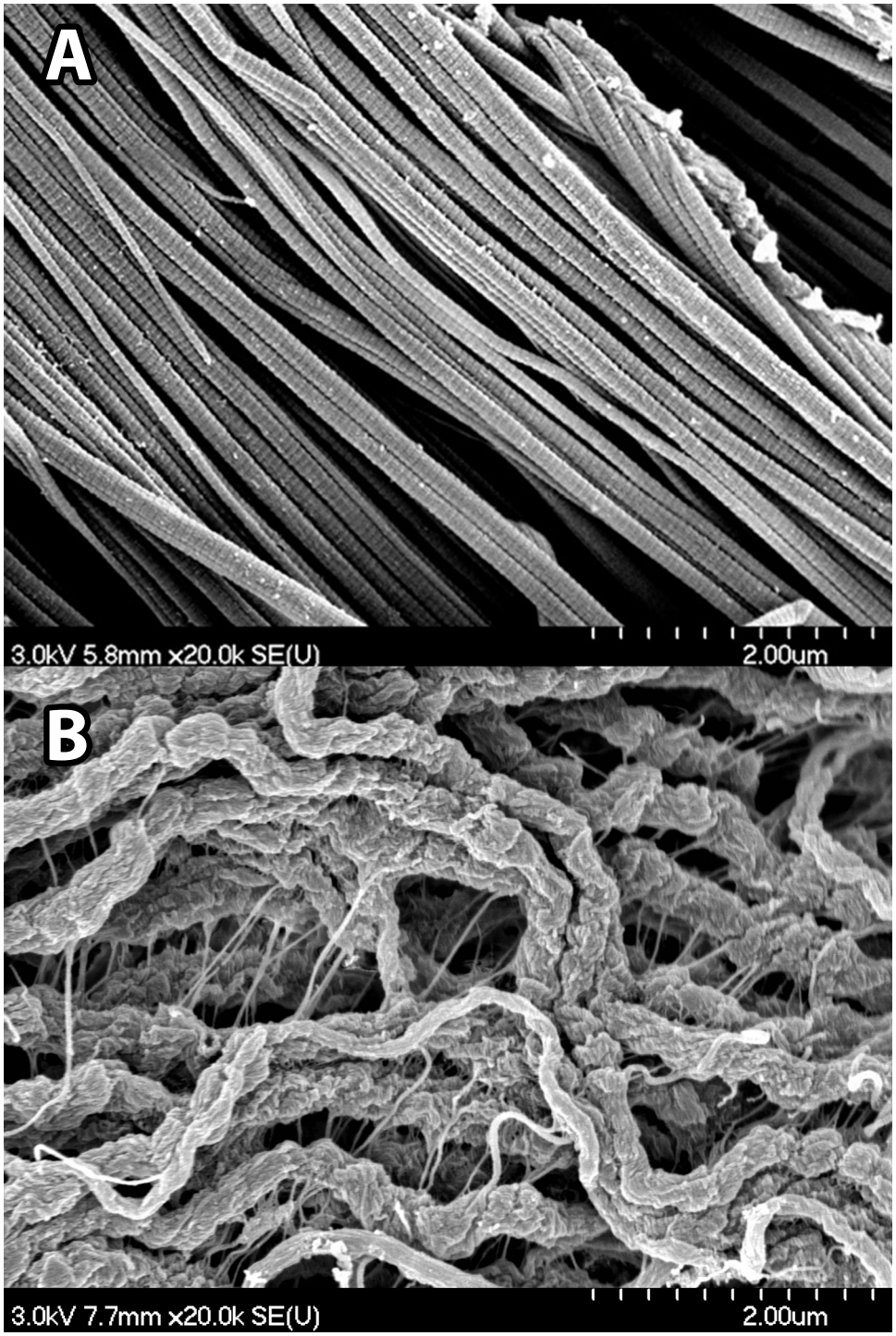

Figure 4.19: Representative SEM images of (A) unloaded control sample, and (B) an OCR sample. A total loss of the D-banding was found, along with the fibrils losing their straight structure, and with extensive kinking formation.

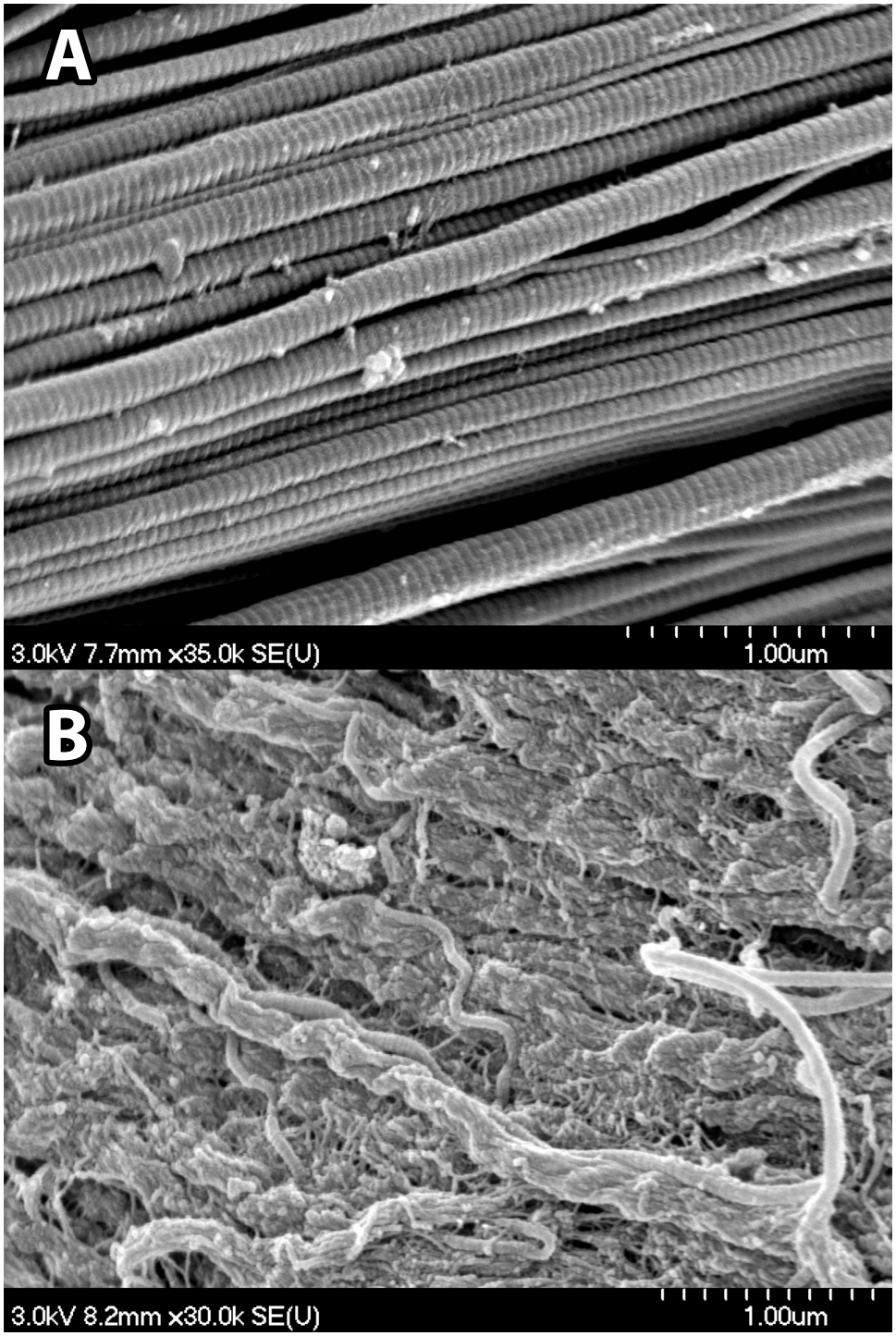

Figure 4.20: Representative SEM images of (A) unloaded control sample, and (B) an OCR sample. A total loss of the D-banding was found, along with the fibrils losing their straight structure, and with extensive kinking formation.

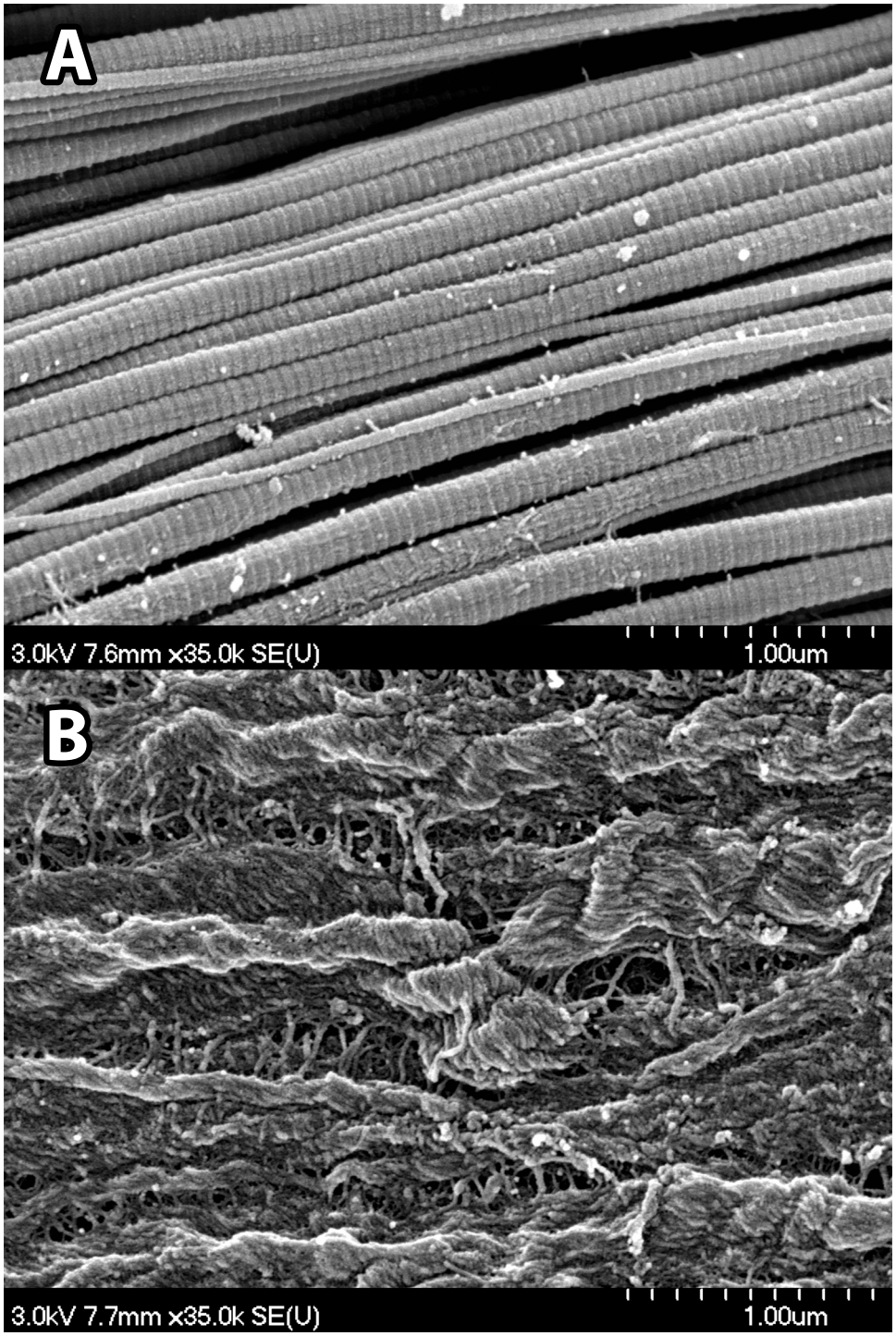

Figure 4.21: Representative SEM images of (A) unloaded control sample, and (B) an OCR sample. This scan shows an example of the fibrillar dissociation of the OCR fibrils.

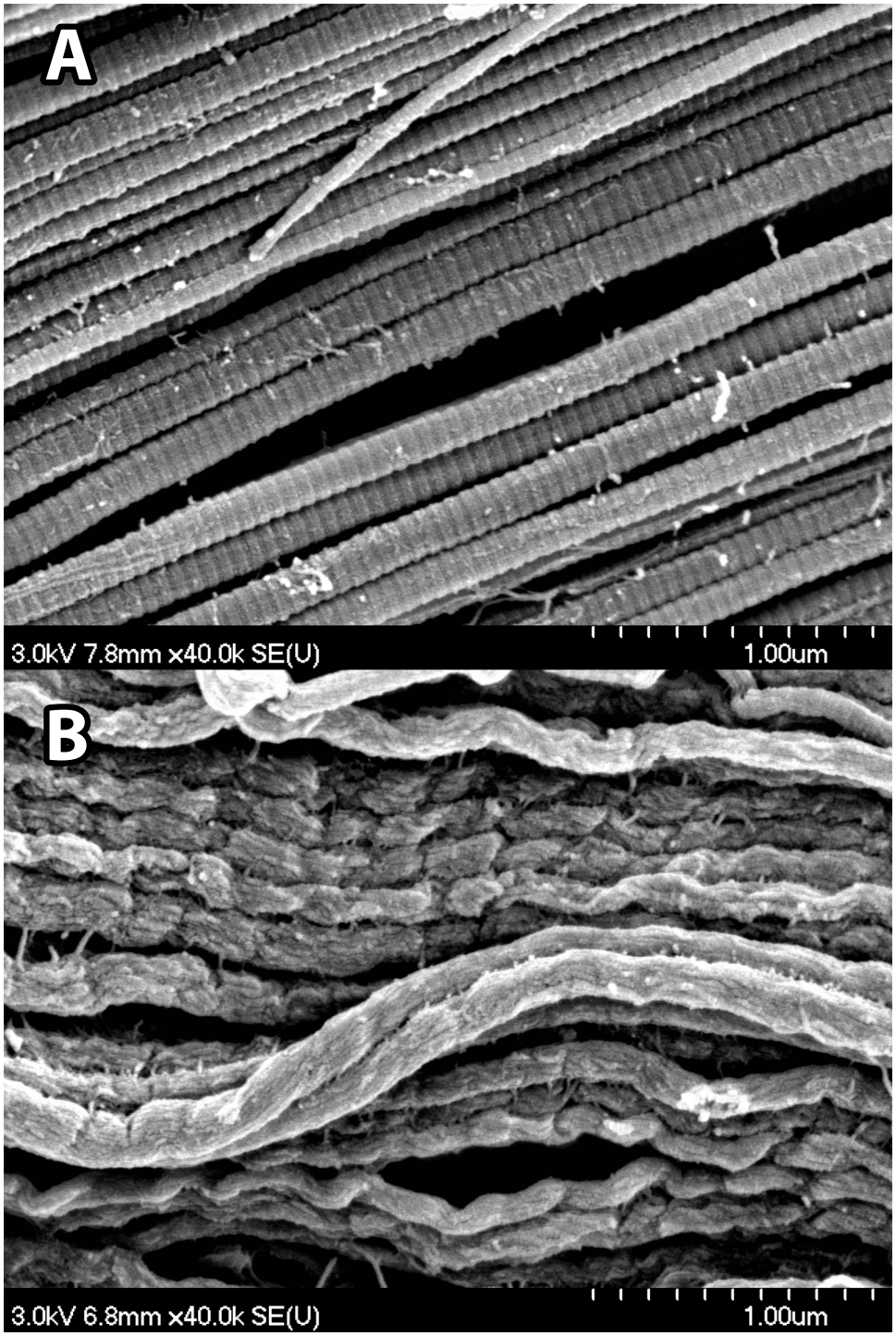

Figure 4.22: Representative SEM images of (A) unloaded control sample, and (B) an OCR sample. Showing all of the previously described nanostructural damage formation characteristics at a magnification of $\times$40,000.

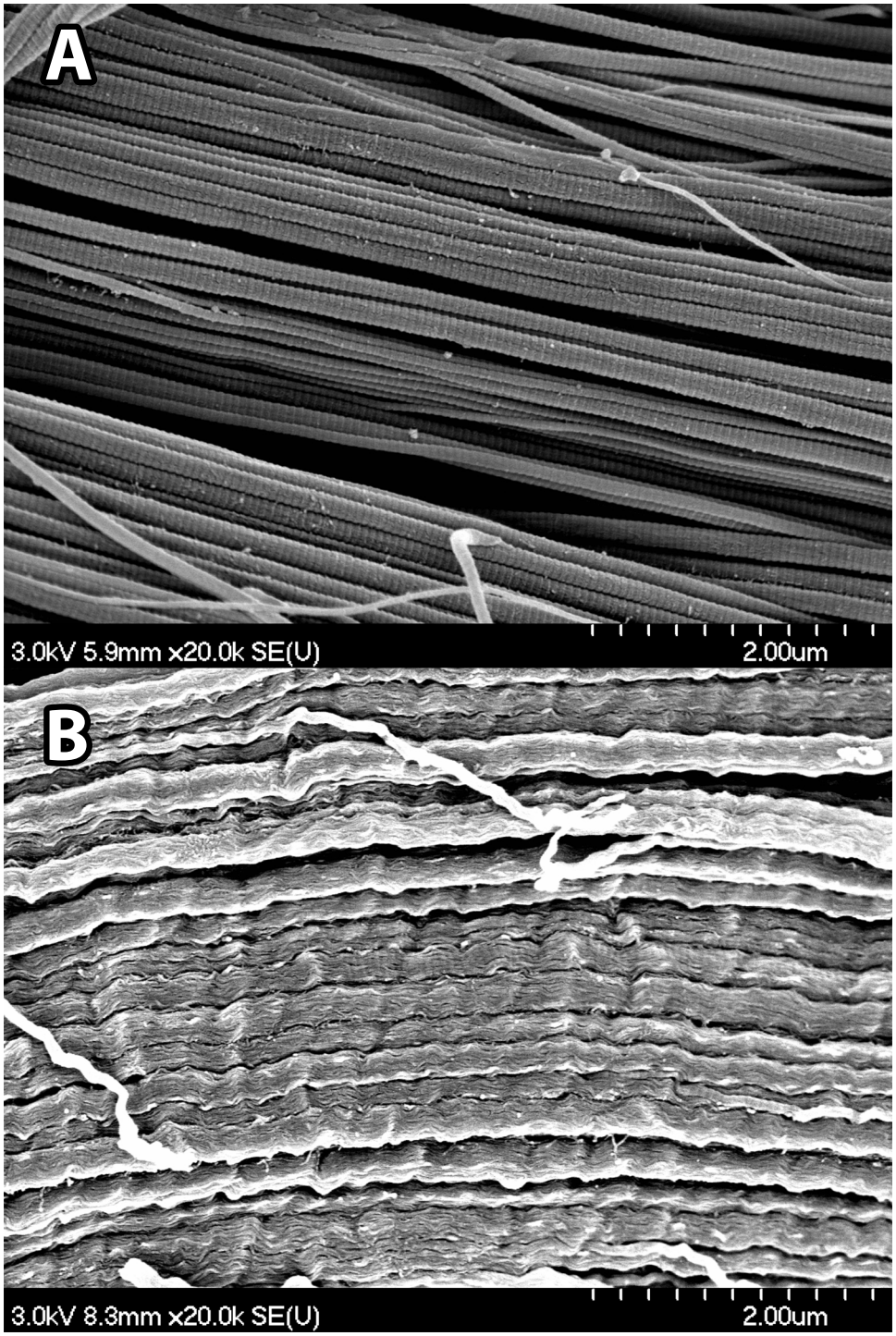

Figure 4.23: Representative SEM images of (A) unloaded control sample, and (B) an RR sample. The longitudinal kinking pattern was found to be similar to that previously reported by Veres et al.[78]. The D-banding is visible at this magnification level (20000x).

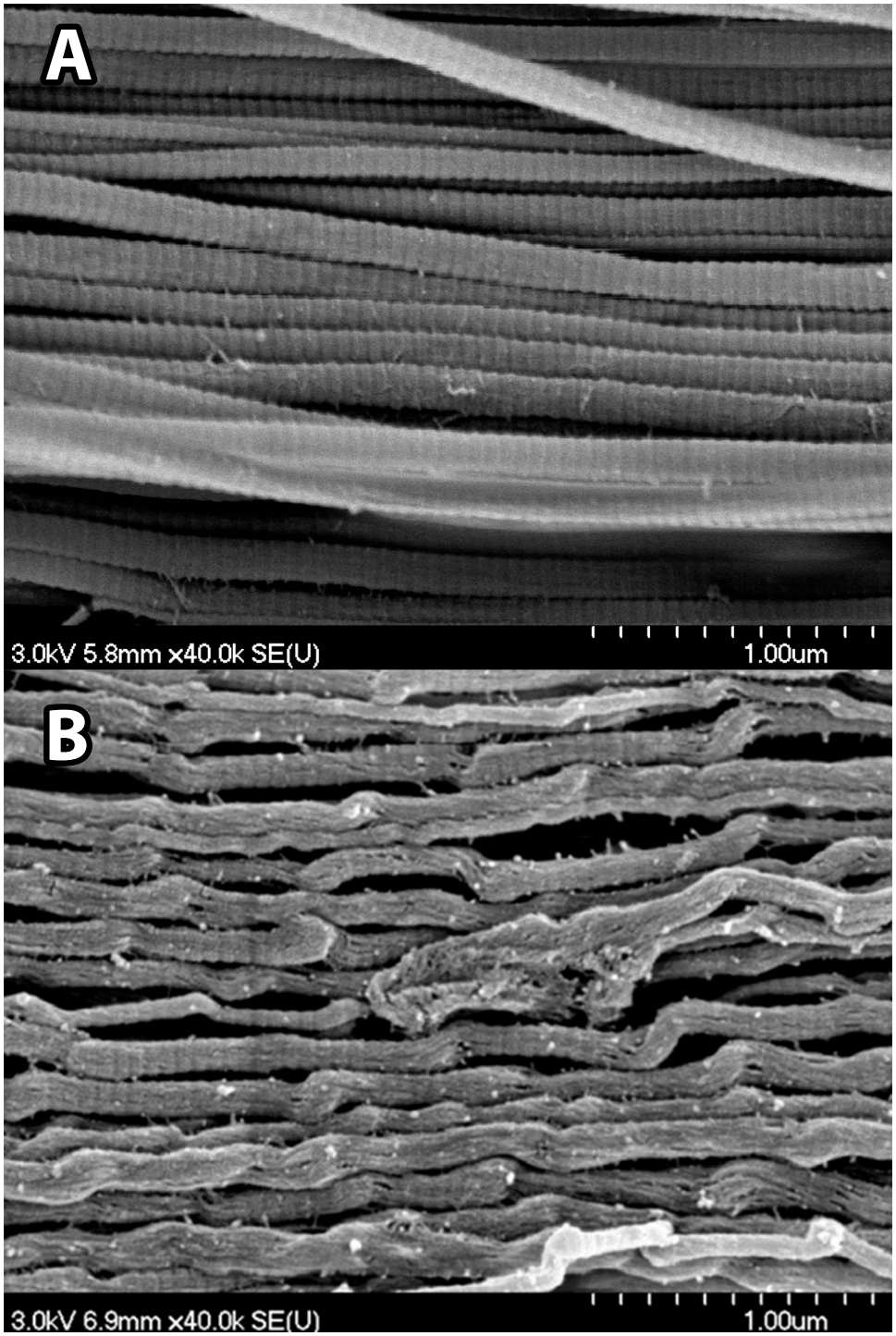

Figure 4.24: Representative SEM images of (A) unloaded control sample, and (B) an RR sample. The longitudinal kinking pattern was found to be similar to that previously reported by Veres et al.[78]. The D-banding is visible at this magnification level (40000x).

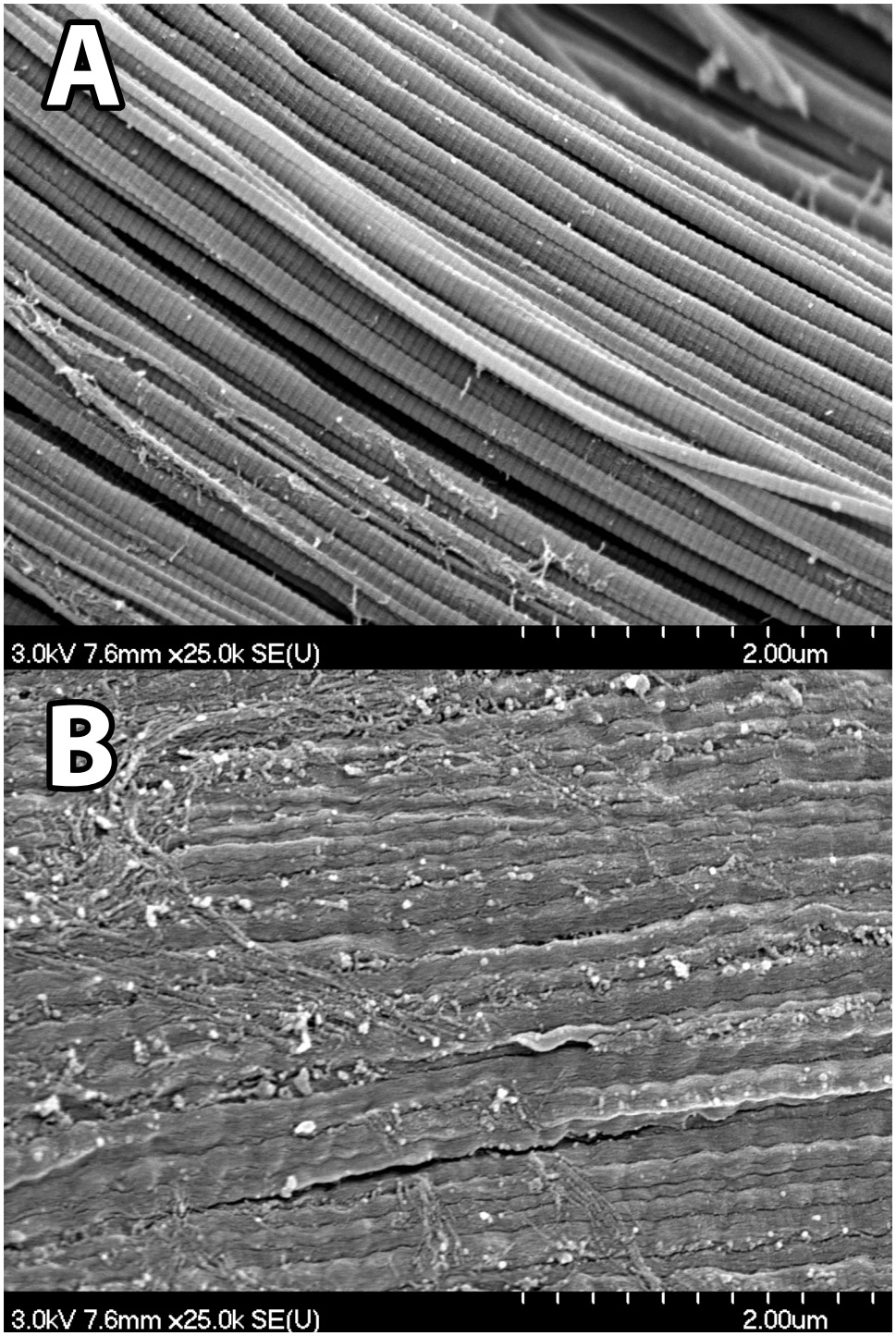

Figure 4.25: Representative SEM images of (A) unloaded control sample, and (B) an RR sample. This image shows dense formation of kinking and fibrillar dissociation of these tendons. The D-banding formation is also present in this image's fibrils.

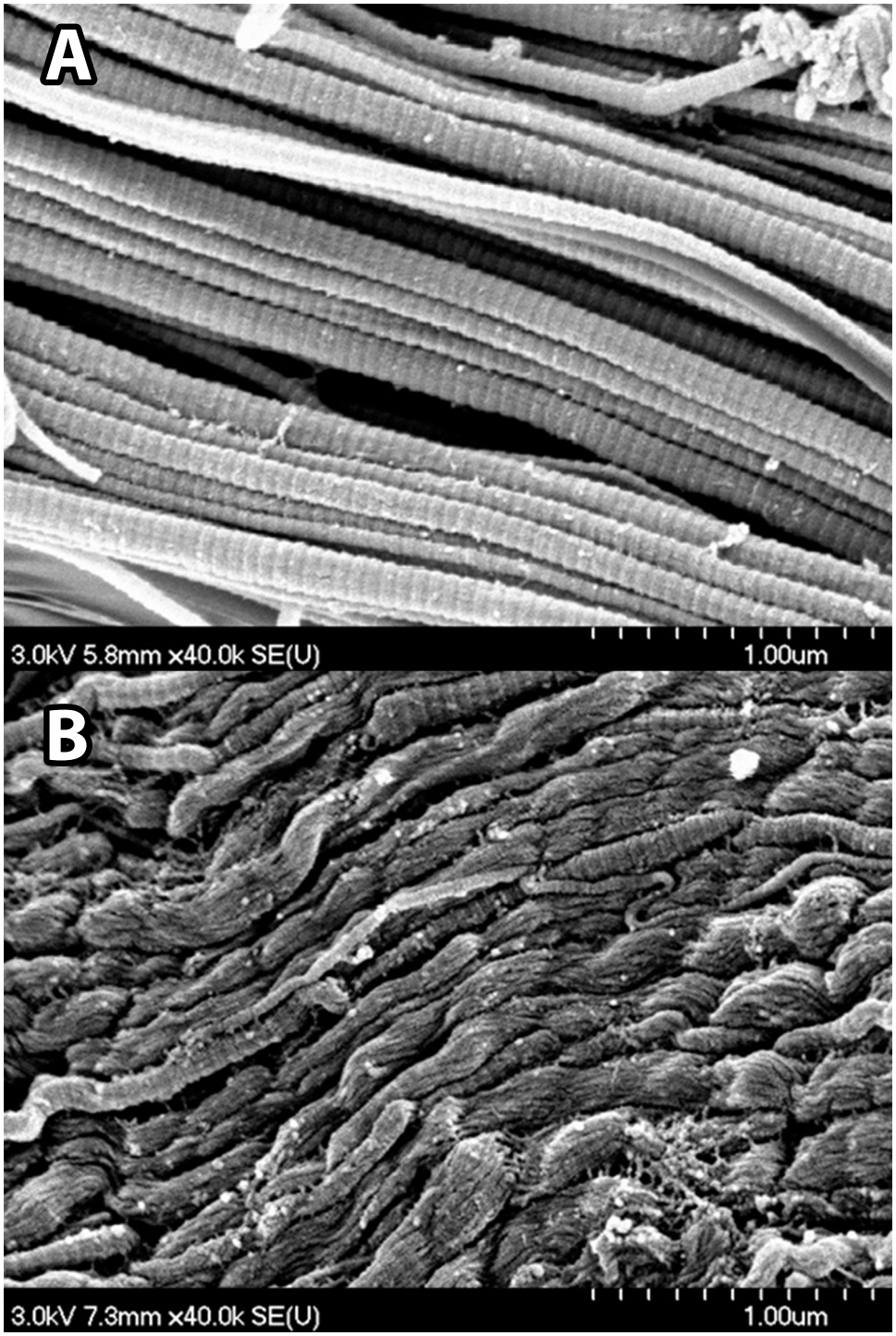

Figure 4.26: Representative SEM images of (A) unloaded control sample, and (B) an RR sample. This scan shows a clear mix of different fibrillar damage modes, including a dense formation of kinking and fibrillar dissociation of these tendons.

4.5 Discussion

4.5.1 The Relationship Between Fibrillar- and Molecular-level Structural Alterations

The structural interpretation of measured DSC parameters for the current study, is similar to the one used in previous studies[17,68,69,79]. Δh, also known as specific enthalpy, measures the thermal energy required to change collagen molecules from their native, triple-helical state into random α-chain coils. Δh measures hydrogen bonds breaking within the triple-helical structure of collagen and solvation of the separated α-chains, thus providing an indication of whether loading induced collagen denaturation occurred[17]. The T_{onset} parameter measures the initiation of the process of heat-induced collagen denaturation in tendon samples, and the T_{peak} parameter measures the temperature at which the maximum energy absorption occurs during denaturation. T_{peak} and T_{onset} depend on the conformational freedom of the α-chains. In the absence of chemical alterations such as crosslinking, solvent conditions, or amino acid side chain modifications, these can be used to measure disruption to molecular packing. Packing disruption causing an increase in the lateral spacing of molecules would reduce the kinetic energy needed by α-chains to break their restraining H-bonds, decreasing T_{onset} and possibly T_{peak}. FWHM is an indication of the range of molecular thermal stabilities in tendon samples[17], and hence an indication of the molecular packing heterogeneity within the specimen[68].

Looking at the outcome of the DSC analysis, both ramp rupture and overload creep rupture of tendons can cause significant disruption to their molecular packing. HS samples had a small yet significant decrease in T_{peak}, but not in any of the rest of tested DSC parameters, which might be an indication of a slight increase in the lateral spacing of collagen's molecules. On the fibrillar level, SEM analysis showed a common feature among all OCR and RR samples: the formation of longitudinal kinking in fibrils. This outcome is consistent with the previously described formation of longitudinal kinking in ramp overloaded tendons[56,79], as well as in cyclically overloaded

tendons[4,79]. On the other hand, the fibrils of HS samples remained straight and intact. When compared to each other, the formation of fibrillar kinking and dissociation was more significant, extensive and uniform in OCR samples than in RR samples. This is an interesting outcome, given that the comparison between OCR and RR samples in DSC did not show any significant differences. Direct visualization of fibrils suggests that extensive fibrillar dissociation and kinking can not occur without molecular packing disruption. This observation was also found in previous studies, where tendons were cyclically overloaded and analyzed using SEM[4] and later DSC[69]. In both of these studies, where the number of loading cycles and their stress levels were similar, results indicated a similar connection could be made between molecular packing disruption on one side, and fibrillar dissociation and kinking on the other side. Herod et al.[79] also found a similar outcome in their study on steer digital flexor/extensor tendons.

In previous studies, evidence of loading-induced collagen denaturation was found in ramp loaded steer tail tendons. Veres et al.[56] have shown using targeted enzymatic treatment that fibrils presenting kinking formation had significant amounts of denatured collagen in their structure[56]. Veres et al.[56] also showed that loss of D-banding was produced by the formation of a shell of denatured collagen on the outer surface of overloaded collagen fibrils. Willett et al.[68] reported that tendons' specific enthalpy, measured using DSC, does not drop due to ramp loading. This observation was used as an indication that intermolecular hydrogen bonds in tendons do not break due to loading, meaning that collagen denaturation is not likely to occur in ramp loaded tendons.

In this study, collagen denaturation in loaded tendons was thought to have occurred if two indicators, as used in previous studies were observed. These two indicators were the loss of fibril D-banding[56,79] and a significant drop in specific enthalpy in DSC[68,69]. Both indicators occurred in OCR samples, but not in RR samples, which had no significant change in specific enthalpy. In addition, it was found that D-banding loss was homogeneous and consistent over all scanned OCR fibrils, while in RR samples D-banding loss was rare and inconsistent. This indicates that loading-induced col-

lagen denaturation occurred in creep overloaded samples but not enough to register changes in ramp overloaded samples. The lack of significant amounts of collagen denaturation enough to register a change in specific enthalpy during DSC in RR samples is consistent with previous studies[68]. From this study, it appears that both the loss of fibrillar D-banding and the significant drop of specific enthalpy in the DSC, are linked to each other. This supports earlier observations by Veres et al.[56], which indicated that the D-banding loss occurs due to a shell of denatured collagen forming on fibrils. Overall, HS samples' fibrils showed intact D-banding, along with no significant drop in specific enthalpy, indicating that no collagen denaturation occurred due to loading to the yield point and then immediately unloading. This finding provides support to previous work, which showed that within the linear region, molecular sliding within tendons is reversible upon unloading[37].

The DSC thermoanalysis of tendons in this study did not take into account how far from the rupture site the DSC samples were taken. All samples used in the DSC and SEM analysis were collected from the inter-grip region of tendons. Willett et al.[68], in contrast to the current study's methodology, recorded the variation in molecular alterations with location from tendons' rupture sites. Willett et al.[68] have noted that molecular packing disruption was less significant the further away the tested sample was extracted from the rupture site. In the current study no recording how far away the DSC samples were from the rupture site, means that the exact distribution of molecular level damage along tendons can not be exactly determined. However, the extensiveness and uniformity of the OCR samples' fibrillar damage seen in SEM might point towards similar uniformity of molecular level alterations along the length of OCR loaded tendons. This observation remains to be further investigated in the future.

4.5.2 The Role of Strain Rate in Nanostructural Damage Formation

Ramp loading at low strain rates was previously known to cause different mechanical and structural responses in tendons. Haut et al.'s study[63] on rat tail tendons showed that under high strain rate ramp loading (∼720 %/s), tendons had greater ultimate strain than under lower strain rate ramp loading (∼3.6 %/s). Yamamoto et al.[64] studied the effect of higher rate (∼1250 %/s) vs. lower loading rates (∼151 %/s and ∼0.566 %/s) on the mechanical response of rabbit patellar tendons. The results from Yamamoto et al.[64] and Haut et al.[63] showed that both ultimate tensile strength and strain at failure increase at higher strain rates. Bovine tail tendons were noted by Willett et al.[68] to rip apart when they fail under higher loading rate (1000%/s), while lower loading rate (1%/s) caused tendons to rupture in a sliding fashion[68].

Considering all the previous studies, this experiment's results can now be compared to previous nanostructural studies, particularly studies which utilized both DSC and SEM. In those studies, tendons were loaded at faster strain rates than were used in this study. In the current study, ramp loading was conducted at 0.09%/s and the strain rate during static creep was even lower (0.02 to 0.04 %/s). Veres et al.[69] and Herod et al.[79] reported less substantial molecular packing disruption in loaded tendons than shown in this study. SEM analysis has shown that OCR samples had greater severity and homogeneity of fibrillar kinking and dissociation across all scanned fibrils compared to RR samples, as well as what was previously reported in faster ruptured tendons[4,56]. Table 4.4 shows the comparison of these results found by Willett et al.[68] with the current study's DSC results. The variations in T_{onset} and T_{peak} with loading rate indicates that reducing loading rate causes more significant disruption to a tendons' molecular packing.

A comparison of the specific enthalpy readings of the current study can be made with the results published by Willett et al.[68], as both the current study and Willett et al.'s study used the same DSC analysis method. Only OCR loading caused a statistically significant change in specific enthalpy. RR samples did not show significant changes

Table 4.4: The current study's DSC analysis results' changes along with the changes found in the DSC analysis from Willett et al.'s study[68]. All the changes were done in comparison to the matched pair, unloaded control samples' average DSC analysis.

	RR 1000 %/s (at rupture site)[68]	**RR 1 %/s (at rupture site)[68]**	**RR 0.09 %/s**	**OCR**
ΔT_{onset} (°C)	-3.1	-5.4	-19.0	-18.5
ΔT_{peak} (°C)	-.0.7	-2.7	-17.5	-13.0
ΔFWHM (°C)	+2.5	+3.6	+9.3	+11.2
Δh (J/g)	+1.6	+5.0	-2.9	-12.9

in enthalpy, similar to the results from Willett et al.[68] (loaded at 1%/s and 1000%/s). A similar outcome was found by Herod et al.[79] in ramp and cyclically loaded bovine forelimb tendons' DSC analysis. For ramp loading to rupture, the comparison shown here indicates that loading-induced denaturation of collagen can only occur in significant quantities during very low strain rate loading, such as in the case of creep loading. SEM analysis of OCR samples showed a higher prevalence of D-banding loss in fibrils than previously seen in tendons that were ramp loaded or cyclically loaded at higher strain rates, whether in this study or in other studies[4,56].

It can be clearly stated that nanostructural alterations in tendons are highly strain rate dependent. The effect of low strain rate loading on the nanostructure of tendons, as observed in this study, may explain differences in the macrostructural response of tendons to low strain rate loading, which were previously found in other studies. It was found that the creep loading of tendons caused a sliding and tearing at various regions, rather than a clean break. Cleaner breaks were observed in ramp ruptured samples. This difference was also noted by Willett et al.[68]. The homogeneity and severity of nanostructural damage in tendons exposed to creep loading may explain the sliding and tearing mode of failure in tendons at the macroscale level. The widespread formation of nanostructural damage may result in fibrils rupturing at multiple distributed sites within the inter-grip region of these tendons. This is expected to be the main cause of the sliding rupture mode observed in creep loaded tendons.

4.5.3 Possible Differences in Other Tendon Models

Cross-linking in tendons is thought to restrict intermolecular sliding[37,110], and may therefore alter molecular and fibrillar structure as a response to loading[37]. In a study done by Shepherd et al.[83] using bovine forelimb flexor and extensor tendons, cyclic creep loading of flexor tendons, which are highly cross-linked, were reported to withstand more cycles of loading than extensor tendons before rupture. Confocal imaging has shown a similar degree of damage in both flexor and extensor tendons at microscale levels, following cyclic creep loading[83]. Using the same tendon model, Herod et al.[79] studied differences in loading induced nanostructural damage in these tendons. In their study, Herod et al.[79] have determined that flexor tendons did not show significant nanostructural alterations, when exposed to either rupture or cyclic loading, unlike the positional extensor tendons. This happened despite the fact that extensor tendons were stronger and tougher than flexor tendons[79]. Using both AFM and second harmonic generation microscopy, Quigley[80] have found that individually ruptured fibrils extracted from bovine flexor tendons showed no structural alterations, while extensor fibrils experienced plastic damage.

It appears that this study's steer tail tendon model undergoes a similar mechanical and structural response to that of other positional tendons, probably as a direct result of them sharing similar cross-linking. It is clear that highly cross-linked tendons are less prone to nanostructural damage. However, given the severity and extensiveness of the nanostructural damage found in tendons that were creep loaded in this experiment, it is not far-fetched to believe that the higher cross-linked tendons might also experience nanostructural damage if loaded in a similar fashion.

Chapter 5

Suboverload Creep Rupture's Effect on the Nanostructure of Tendons

5.1 Introduction and Research Question

In the previous experiment, the effect of overload creep rupture on tendon nanostructure was investigated using thermoanalysis (DSC) and ultrastructural analysis (SEM). DSC analysis of overloaded and creep ruptured tendons showed that significant molecular packing disruption occurred. In addition, creep ruptured tendons demonstrated evidence of collagen denaturation, with significant decreases in enthalpy. Collagen fibrils in creep overloaded samples were found to have homogeneous and extensive fibrillar damage. This damage included longitudinal kinking, fibrillar dissociation into subfibrils and a complete disappearance of D-banding from fibrils.

Various studies have previously explored the effect of suboverload creep on the mechanical and structural properties of tendons. It is known from previous studies that static loading below the yield stress can cause tendons to rupture[58,82], and when applied for shorter durations can alter their mechanical properties[88]. However, whether

sustained loading at a low stress can cause nanostructural damage was not previously explored. Taking that in mind, the research question for this study is: can nanostructural damage, similar to that seen in overload creep occur in tendons due to suboverload creep? Suboverload creep, as stated in the literature review, is defined is sustained loading at a stress well below the tissue's yield point.

5.2 Hypotheses and Rationale

5.2.1 Hypotheses

Hypothesis 1: Static creep testing triggered at 10% strain can cause significant structural alterations within tendons.

Sub-hypothesis 1a: Structural alteration within tendons, as indicated by DSC, will depend on the duration of creep loading, with longer periods of creep causing greater alterations.

Sub-hypothesis 1b: Tendons that have undergone a static suboverload creep test and show changes in DSC will show disruption to fibrils under SEM. Tendons that do not show changes in DSC will not show structural changes relative to control samples in SEM.

5.2.2 Rationale

Rationale 1a: Previous studies have shown that tendons can rupture when they are exposed to creep loading at lower stress levels than their respective yield stress. Wang and Ker[82] have shown that creep rupture of wallaby tendons can occur at stresses as low as 14% of their yield stress. Wren et al.[58] have similarly shown that human Achilles tendons also rupture when subjected to sustained stresses within their linear region. Thornton et al.[88] have shown that suboverload creep can alter the mechanical properties of ligaments. The previous experiment in this thesis has

shown that creep rupture causes fibrillar and molecular level damage, which was both more significant and extensive than those found after tendon rupture at faster speeds, hinting that nanostructural damage is time-dependent. Hence, it is expected that the nanostructural alterations in tendons loaded at suboverload levels will depend on the duration of loading.

Rationale 1b: From previous studies[4,56,79], and from the previous experiment, fibrillar kinking and dissociation were linked to molecular packing disruption. From the previous experiment, fibrillar D-banding loss was linked to collagen denaturation. What can be taken from previous studies is that the damage formation in tendons' fibrillar structures is accompanied by alterations on the molecular level. Hence, it is expected that only samples that show significant molecular level alterations in DSC will end up showing fibrillar alterations in SEM.

5.3 Methodology

An overview of the experiment is shown in Figure 5.1.

5.3.1 Mechanical Loading Tests

Fifteen tendons from three different tails (five tendons per each tail) were prepared for each SCL test. The preparation and geometrical measurement processes were similar to those followed in the previous experiment (see section 4.3.1). A small piece of each tendon was extracted and stored as a matched pair control. As with the previous experiment, mechanical loading was conducted in a 37 °C, 0.15 M PBS bath. Tendons were gripped in the MCS rig and pre-loaded to 0.5 N before the mechanical loading test.

Tendons were subjected to ramp loading at 0.09 %/s to a strain of 10%. They were then creep loaded at the corresponding stress level. For each tail, the extracted five tendons were creep loaded for one of the following durations: 0.5, 1, 2, 4, or 5 hours.

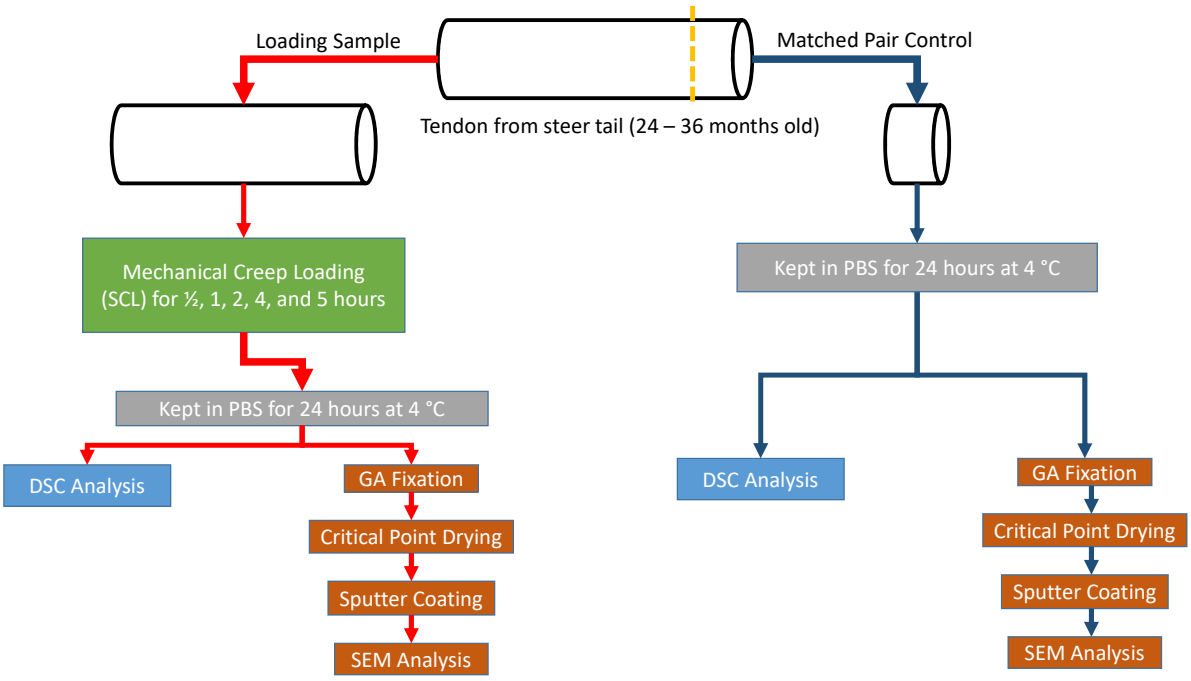

Figure 5.1: The flowchart of SCL experiment's methodology.

After the duration of creep loading was over, tested tendons were unloaded into their initial positions at 0.09 %/s.

5.3.2 Post-Test Mechanical Analysis

After each mechanical test, tendons were removed from the rig, their gripped ends were cut off, and samples were stored overnight in 5 ml of PBS, that were kept in at 4°C overnight. Force and displacement data were converted to stress and strain by

dividing values by the initial cross-sectional area and initial length respectively.

For all of the mechanical tests done in this experiment, stress-strain, stress-time, and strain-time charts were plotted. These plots were used to calculate the strain of each tendon at the start of primary, secondary, and tertiary regions of creep. The slope of the secondary creep phase was also calculated to find the strain rate during this portion of the test. The process of calculating these mechanical properties is shown in Figure 5.2. For each test, a straight line was manually drawn across the secondary creep region of the strain-time plot, the slope of this line was taken as the strain rate during secondary creep.

For all tests, ramp loading was done at an average strain rate of 0.09 ± 0.004 %/s and the extension rate during secondary creep was 0.0021 ± 0.0002 %/s. This is a lower rate than those previously used during rupture or overload tests of the same tendon model[56,68,69,78,79]. The extension rate during secondary creep for the SCL samples was significantly lower than that for the OCR samples.

5.3.3 Analysis of the Samples: SEM and DSC Tests

After storing all samples overnight, they were prepared for DSC and SEM analysis. The preparation of SCL samples for DSC analysis was the same to the method used in the OCR experiment. The procedure of DSC test was same to the one previously used in the first experiment. The analysis of the DSC results was also same to the previous test (section 4.3.4).

Specific enthalpy was determined after finding the dry mass of each sample. The mean wet mass of tested samples in this experiment was 12.7 ± 1.5 mg. The dry mass of the samples after 24 and 48 hours of drying in a vacuum desiccator was approximately 3.8 ± 0.5 mg.

The preparation of samples for SEM analysis, along with the SEM analysis procedure, was same to the one previously used in the OCR experiment. SEM analysis was first

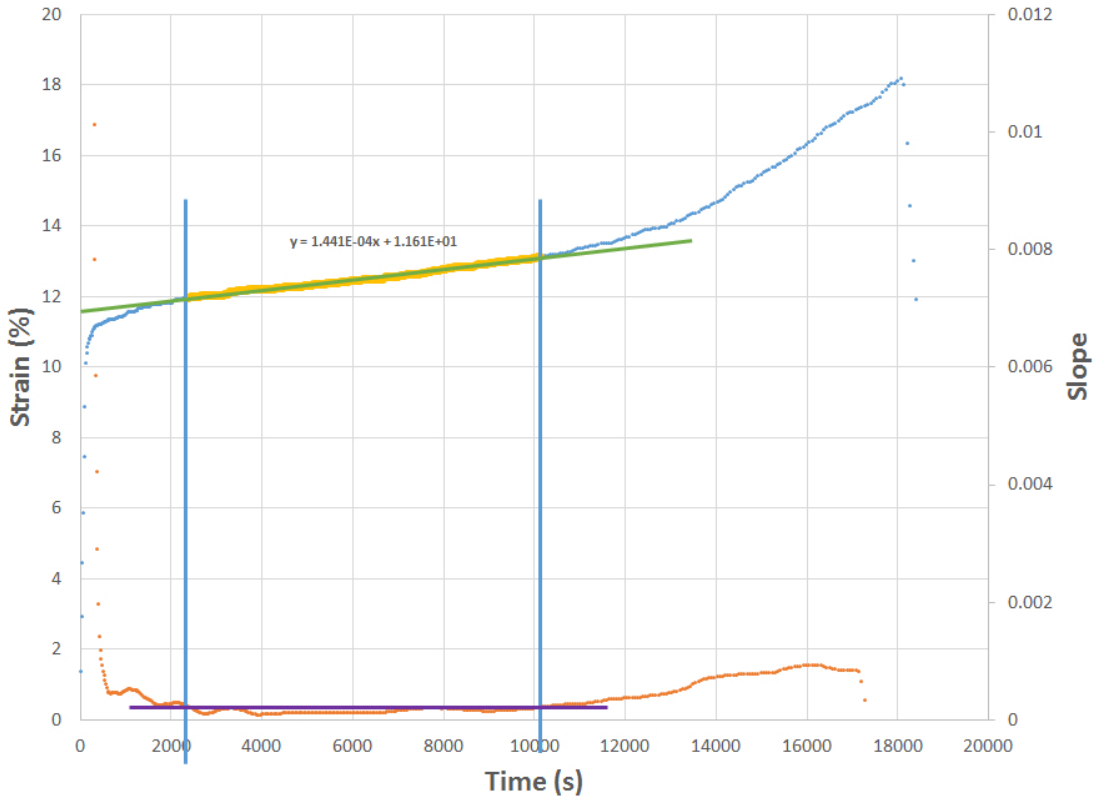

Figure 5.2: Illustration of the process of calculating the secondary creep loading start and end points. The strain-time curve (blue), the secondary creep phase manual estimation (green), the secondary creep phase (yellow), the slope readings (orange), and the strain rate within the secondary creep phase (purple) are all shown in the chart.

done in the 5 hours and 4 hours creep loaded samples. When analysis of 4 hour samples showed fibrillar damage, the two hours creep loaded samples were also scanned. Had two hour creep loaded samples also shown fibrillar damage, one hour samples were to be analyzed using SEM.

5.3.4 Statistical Analysis

To determine if tendons from the three animals were structurally similar and could, therefore, be viewed as independent samples, DSC data for matched-pair controls were compared using ANOVA, with their tail of origin set as the independent factor. Results of this analysis showed that there were no significant differences in the thermal parameters of the control samples, indicating that tendons from different tails were structurally similar to each other.

For this experiment, the statistical analysis took a different approach than that of the OCR experiment, as the goals of the SCL experiment were different. An analysis was done to find the relationship between macro-scale elongation (creep strain, ϵ_{creep}) of tendons within creep loading and the duration of creep loading. The strain was taken from the start of secondary creep to the end of test duration. Several fits were used in this analysis to determine the best possible fit for the resulting plot. Samples that ruptured during the test were not included in this analysis. Changes in DSC parameters were plotted against ϵ_{creep}. Relationships between these were tested using regression analysis. Fits were used to investigate the molecular damage's time dependence (sub-hypothesis 1a). These relationships were then compared to SEM scans, to investigate the relationship between molecular and fibrillar damage formations resulting from SCL (sub-hypothesis 1b).

5.4 Results

5.4.1 Mechanical Properties

For all plots given in the next two sections, the red points on the plots represent samples that reached the tertiary phase creep. A creep strain vs. creep duration chart was plotted for all the samples tested in this experiment (Figure 5.3). As shown in Table 5.1, the relationship between creep strain and creep duration was the best fit using a logarithmic. Shown in Figure 5.3, creep strain increased significantly after

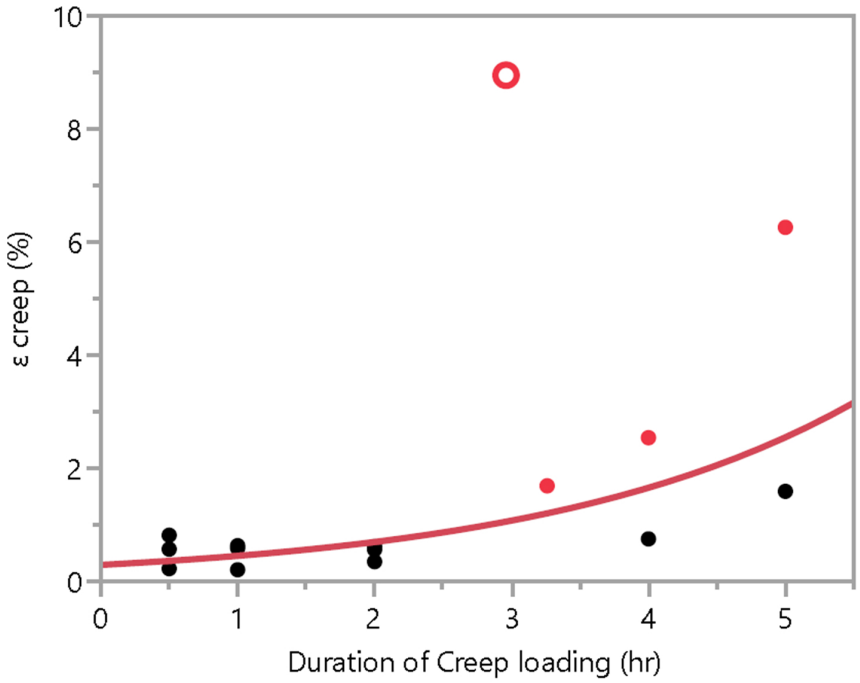

Figure 5.3: SCL creep strain vs. creep duration, showing the logarithmic fit. Samples shown by red points indicate those samples that entered tertiary creep. The point that is shown as a hollow circle ruptured and was excluded from the fit.

three hours, with several tendons entering tertiary creep after this time point. Two of the samples failed before they reached their target creep duration (four and five hours respectively). One of the samples was not included in the fit plot shown in Figure 5.3 but was included in the DSC analysis for this experiment.

5.4.2 DSC Thermoanalysis

Representative endotherms of tendons that were loaded for the different creep durations are shown in Figure 5.4. DSC analysis showed that the molecular level alterations

Table 5.1: Fit tests of creep strain vs. creep duration

Type of Fitting	R-Squared	p-value
Exponential	0.593	0.0013
Polynomial Fit to 2nd Degree	0.585	0.008
Polynomial Fit to 3rd Degree	0.591	0.025
Polynomial Fit to 4th Degree	0.596	0.062
Square	0.554	0.0023
Logarithmic	**0.610**	**0.001**

experienced varied with the duration of creep loading.

Plotting the DSC results against creep strain showed a linear relationship: samples that underwent greater creep had larger reductions in T_{onset} ($p < 0.0001$, $R^2 = 0.95$), and T_{peak} ($p < 0.0001$, $R^2 = 0.94$). This indicates that the lateral spacing of collagen molecules within tendons increased significantly with increasing elongation during creep (Figure 5.5A and B). The linear fit of ΔFWHM vs. ϵ_{creep} showed that samples that underwent greater creep had larger FWHM values ($p = 0.0004$, $R^2 = 0.63$)(Figure 5.5C). The analysis of specific enthalpy (Δh) vs. ϵ_{creep} showed no significant relationship (Figure 5.5D). A matched-pair statistical analysis of the specific enthalpy of all the SCL samples compared to unloaded controls showed a small but significant increase in specific enthalpy ($p = 0.0081$).

5.4.3 SEM Nanostructural Analysis

SEM analysis was performed on the five hour ($n = 2$), four hour ($n = 2$) and two hour creep loaded samples ($n = 3$) and their matched-pair controls. Imaging was done at a range of magnifications, reaching up to $\times$50000. The two five hours samples showed different degrees of damage. One of the samples had extensive longitudinal kinking

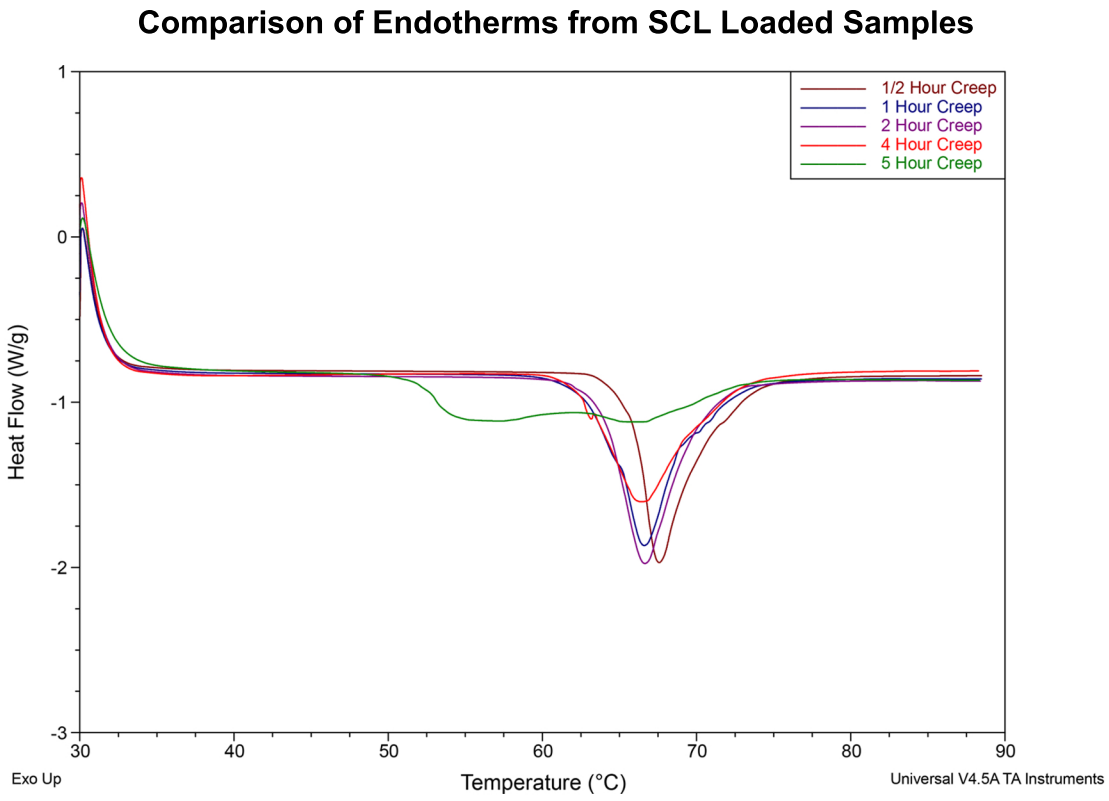

Figure 5.4: DSC Endotherms of tendons that underwent different durations of creep loading.

and fibrillar dissociation (Figure 5.6). Almost all fibrils viewed had intact D-banding (Figure 5.7 and 5.8). The second 5-hour creep sample showed some fibril damage, but it was less extensive and less severe. A majority of fibrils viewed in the second sample were not damaged, with clear D-banding and little to no kinking (Figures 5.9 and 5.10). It should be noted that the first five hour creep sample did reach the tertiary creep phase, while the second sample did not.

Damage to collagen fibrils was also found in the four hour creep samples. Scans of the four hour creep group showed at least some kinked and dissociated fibrils in both tested samples (Figures 5.11 and 5.12). While other scans showed just fibrillar dissociation without any signs of longitudinal kinking (Figure 5.13). Longitudinal kinking and

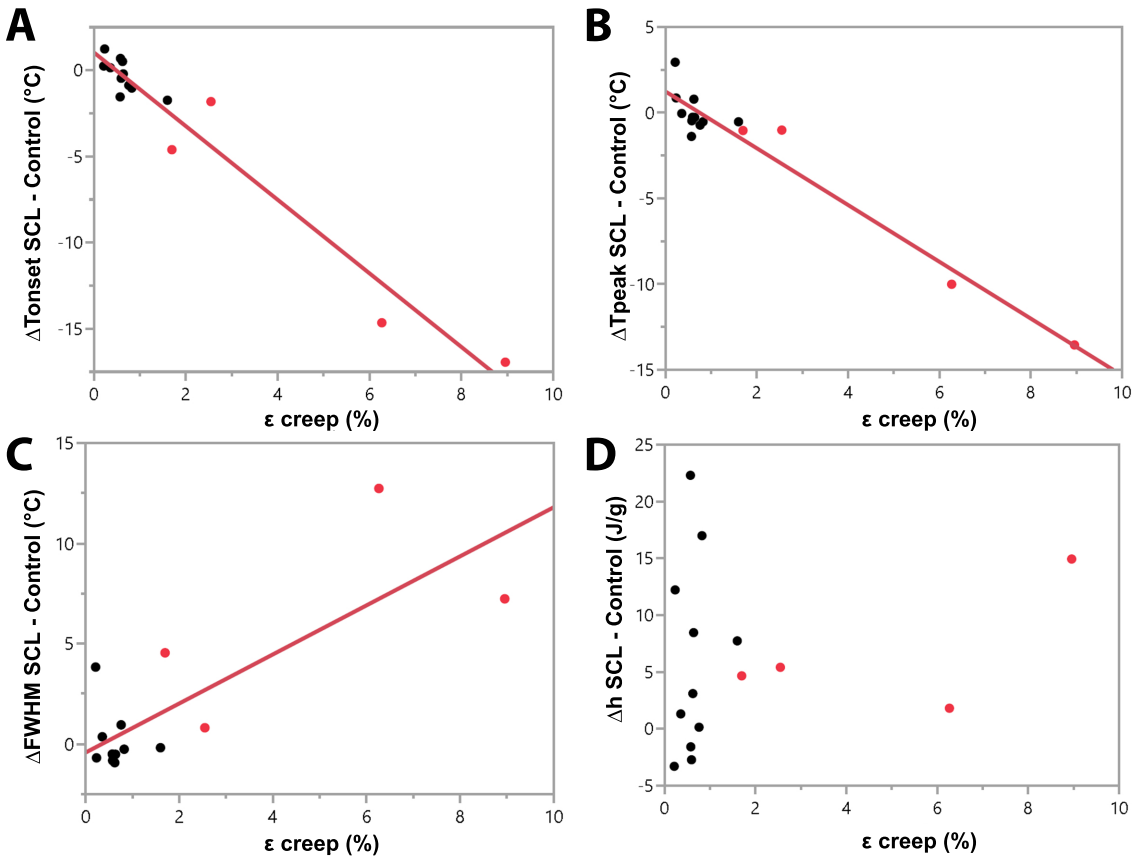

Figure 5.5: Plots representing the changes in (A) T_{onset}, (B) T_{peak}, (C) FWHM, and (D) Specific Enthalpy (Δh) vs. creep strain (ϵ_{creep}). Red points represent samples that reached tertiary creep.

fibrillar dissociation in the four hour creep loaded tendons were less extensive and severe than those observed in the five hour creep sample that reached tertiary creep. Other scanned fibrils were totally undamaged (Figures 5.11 and 5.12). Both damaged and undamaged fibrils had intact D-banding (Figure 5.13, 5.11, and 5.12).

Finally, SEM imaging of the two hour creep loaded samples showed no significant damage to their fibrils (Figures 5.14 and 5.15). Some of the scanned fibrils did show minor kinking, but this was not a common finding (Figure 5.16). Because the two hour samples did not show damage, the samples loaded for one hour and half an hour

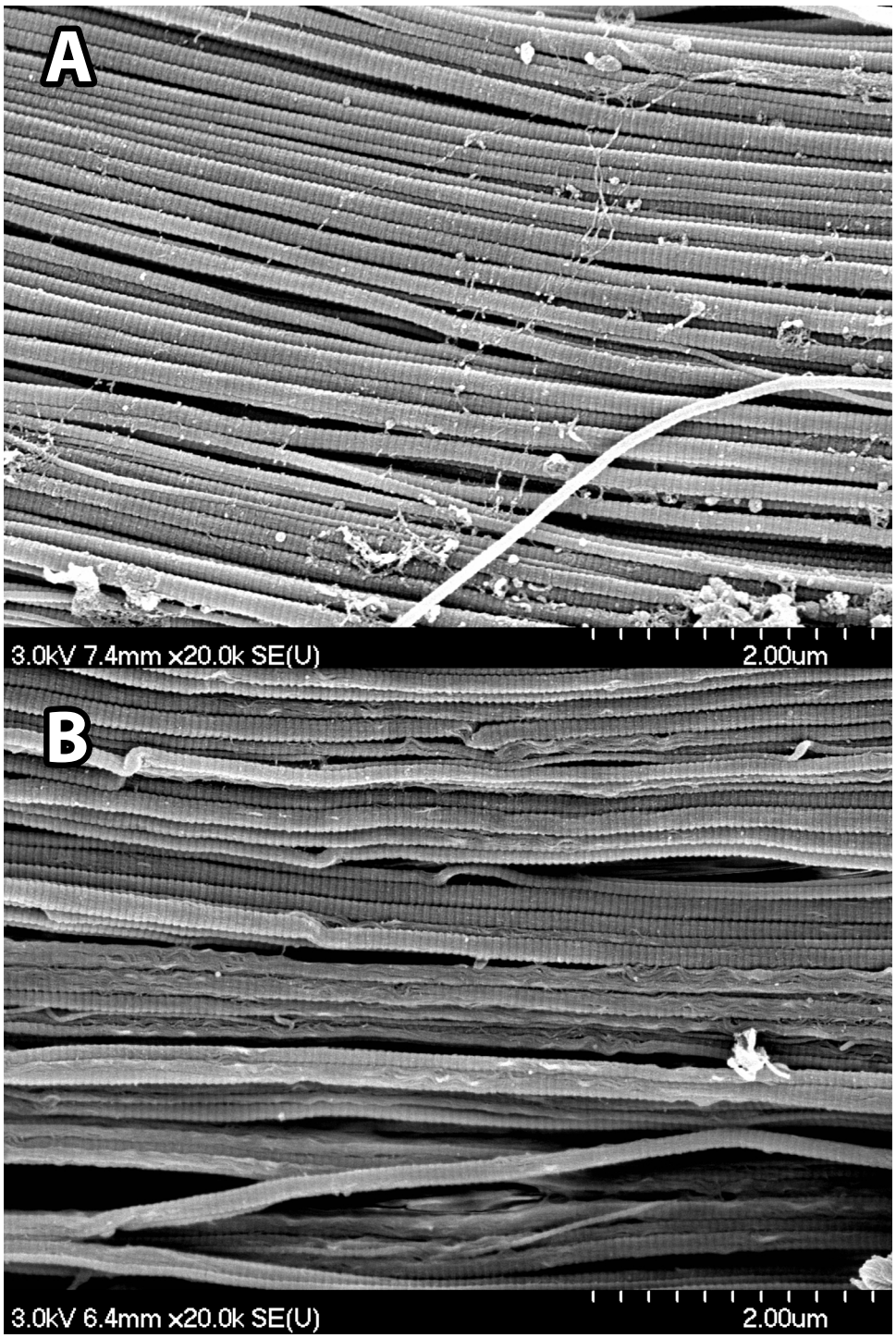

Figure 5.6: Representative SEM images of (A) Unloaded control sample, and (B) the first five hour SCL sample. The creep loaded sample had fibrils with clear D-banding, but also kinking and fibrillar dissociation.

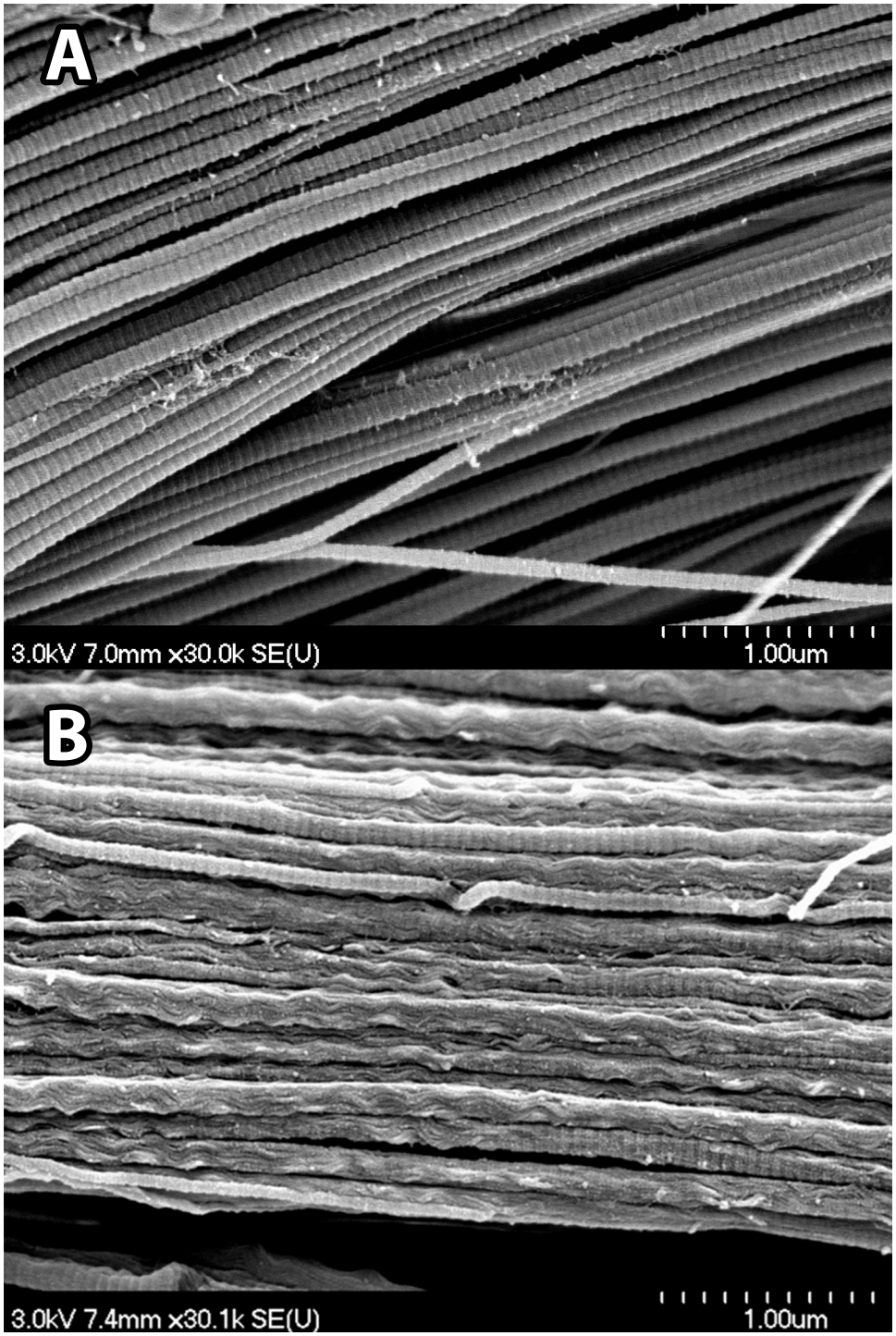

Figure 5.7: Representative SEM images of (A) Unloaded control sample, and (B) the first five hour SCL sample. The creep loaded sample had fibrils with clear D-banding formation, but also kinking and fibrillar dissociation.

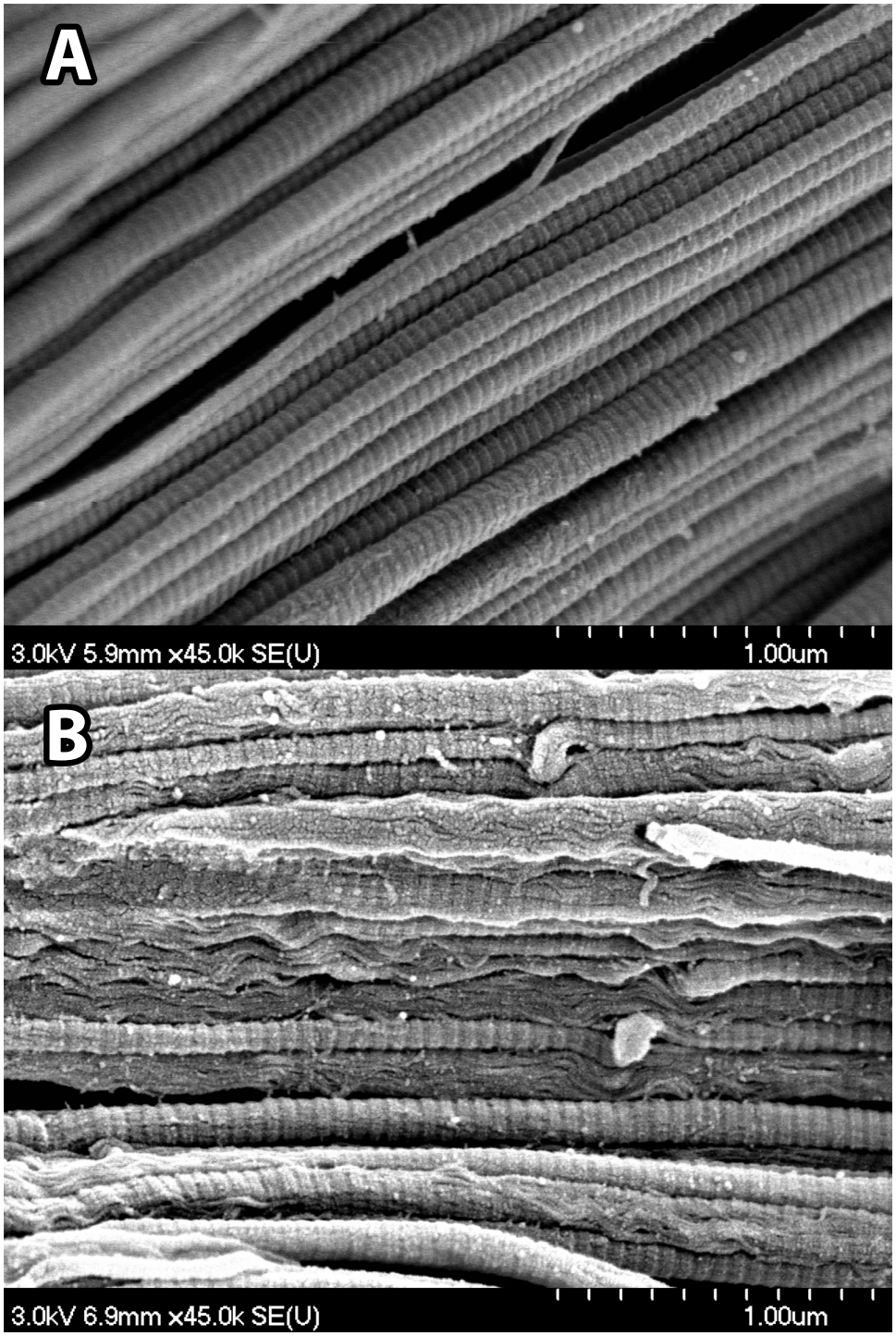

Figure 5.8: Representative SEM images of (A) Unloaded control sample, and (B) the first five hour SCL sample. This highly magnified image shows D-banding, longitudinal kinking, and significant fibrillar dissociation.

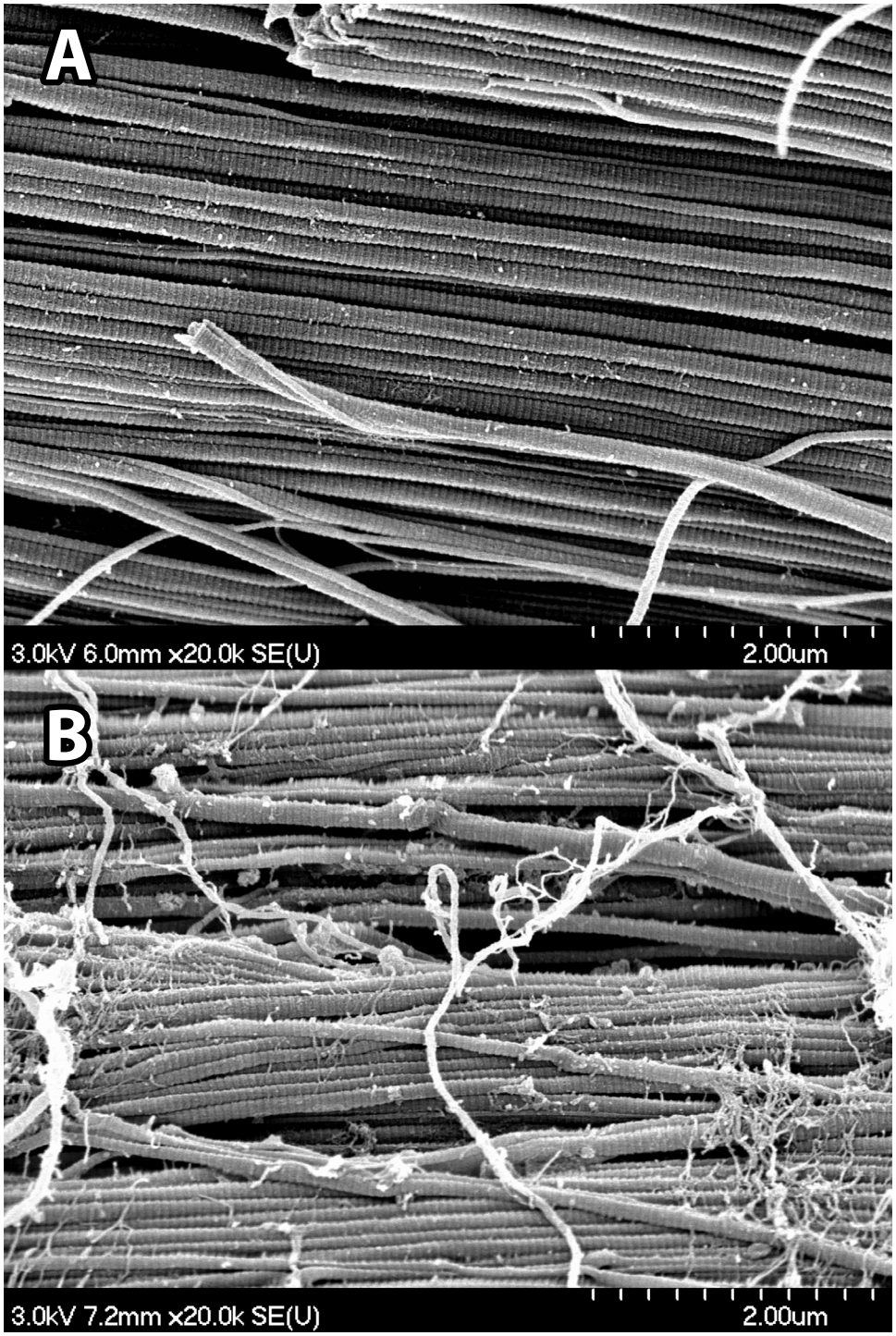

Figure 5.9: Representative SEM images of (A) Unloaded control sample, and (B) the second five hour SCL sample. B: While some longitudinal kinking was found, it was less severe and extensive than the first five hour creep sample (Figure 5.6).

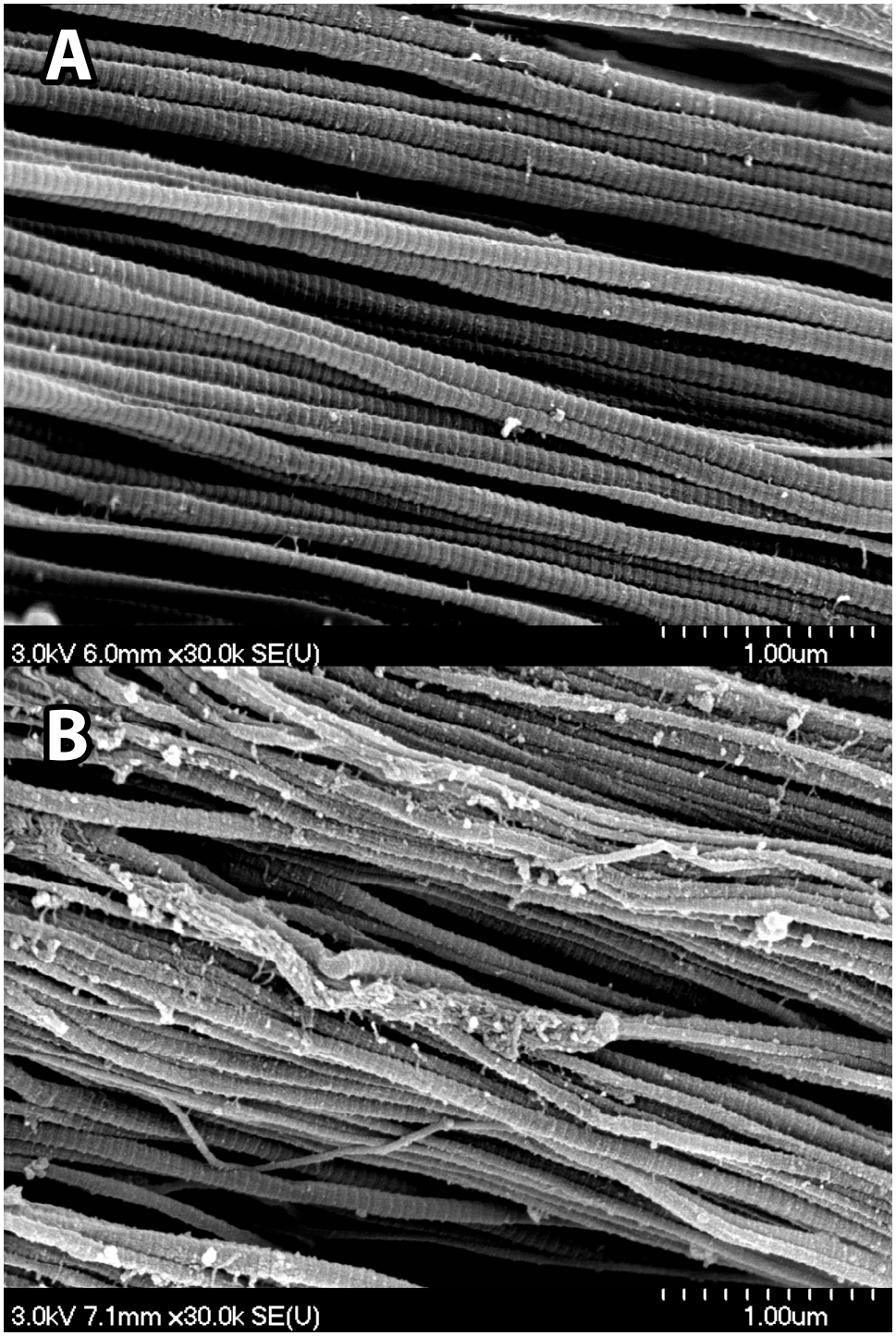

Figure 5.10: Representative SEM images of (A) Unloaded control sample, and (B) the second five hours SCL sample. B: Minor longitudinal kinking formation and fibrillar dissociation are present.

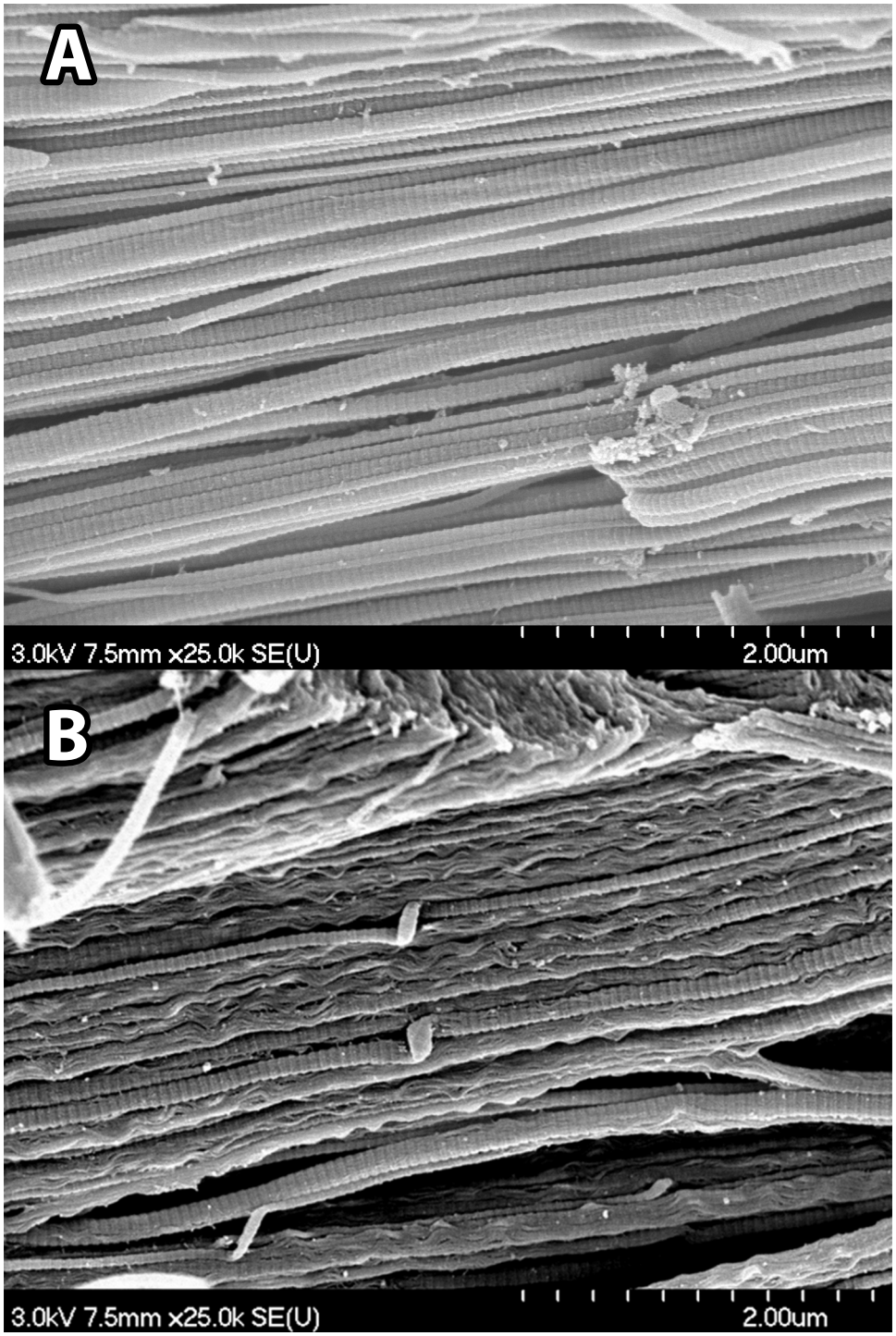

Figure 5.11: Representative SEM images of (A) Unloaded control sample, and (B) one of the four hour SCL sample. B: Clear kinking and fibrillar dissociation are present D-banding.

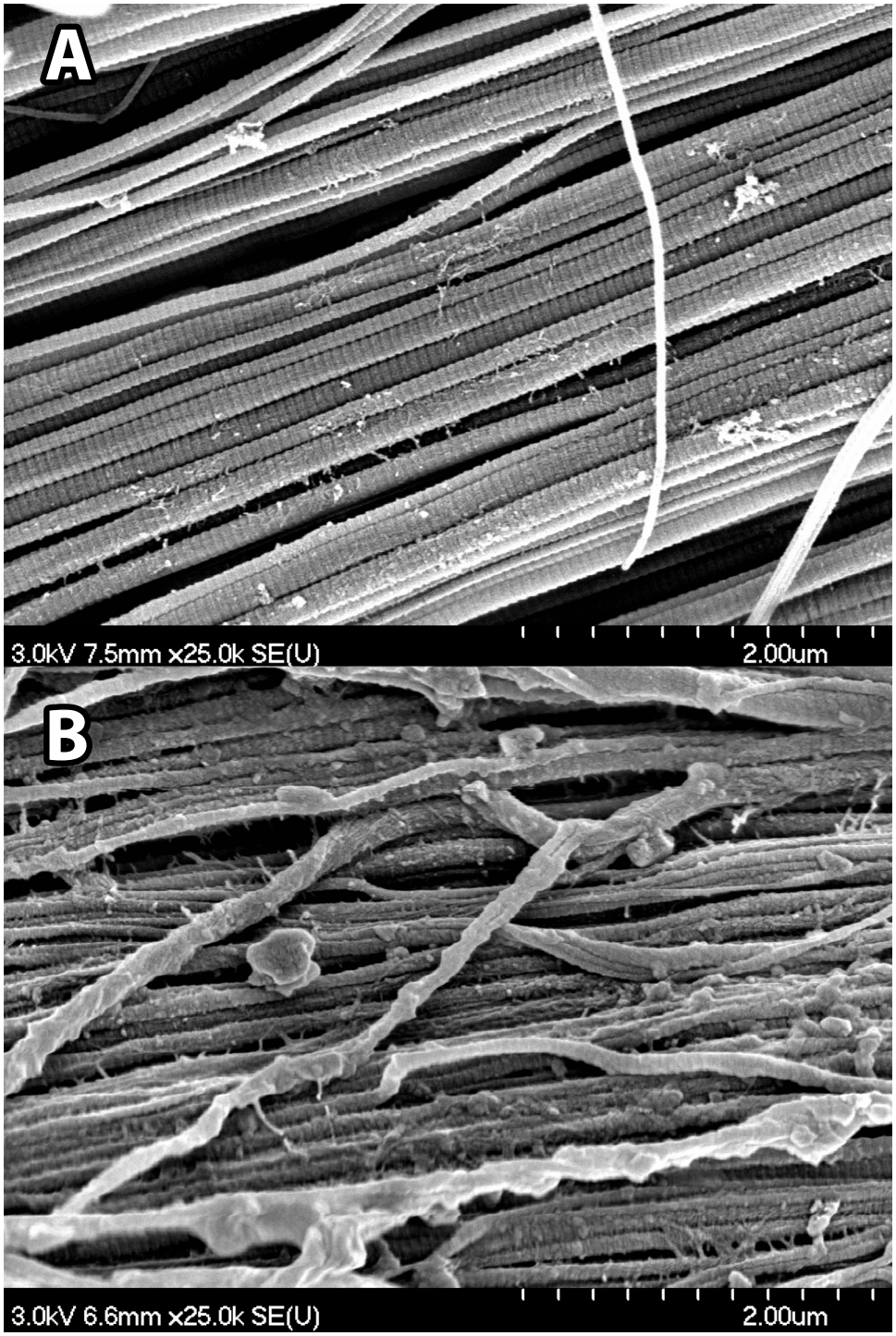

Figure 5.12: Representative SEM images of (A) Unloaded control sample, and (B) one of the four hour SCL sample. B: Minor but notable kinking of fibrils were found with intact D-banding.

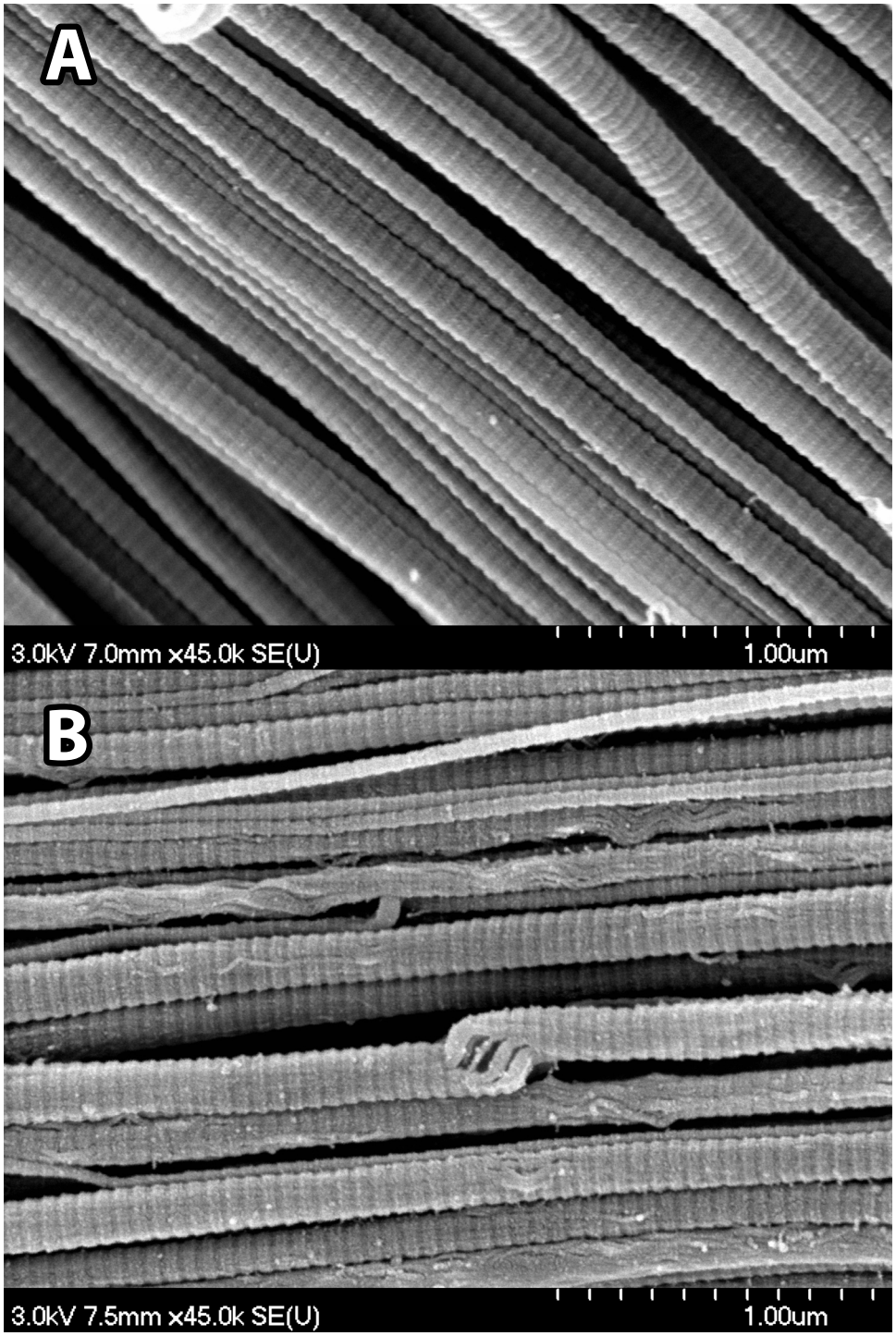

Figure 5.13: Representative SEM images of (A) Unloaded control sample, and (B) one of the four hour SCL sample. B: Minor but notable kinking of fibrils were found with intact D-banding.

samples were not imaged.

5.5 Discussion

5.5.1 Time Dependence of both Macroscale and Nanoscale damage formation

Creep deformation was found to have a logarithmic relationship with creep duration. DSC results suggest that molecular level alterations in tendon collagen begin to occur upon entry into the secondary creep loading phase. Most of the SCL showed certain levels of change in DSC compared to their matched pair controls. The extent of these changes, however, was dependent on strain, and in turn creep duration. Tendons that were creep loaded for more than three hours showed a significant amount of molecular-level damage, which was particularly true for tendons that reached the tertiary region of creep loading. Similarly, the fibril level damage observed in SEM was found to be significant in samples loaded for more than three hours only, with the four hour creep loaded samples showing less severity in damage than that seen in the five hour samples. Two hours of creep loading caused no observable damage in SEM. This set of results shows that tendons experience significant nanostructural damage upon entering the tertiary region.

5.5.2 The Relationship between Molecular and Fibrillar Damage

The results of the DSC and SEM analyses complemented each other, a finding that can be related to previous studies[69,79] and was touched upon in the previous experiment. In SCL samples, the molecular packing disruption was shown by T_{onset}, T_{peak}, and FWHM results indicating an increase in lateral spacing and spread of molecular thermal stabilities of the creep loaded tendons. Looking at the alterations seen in

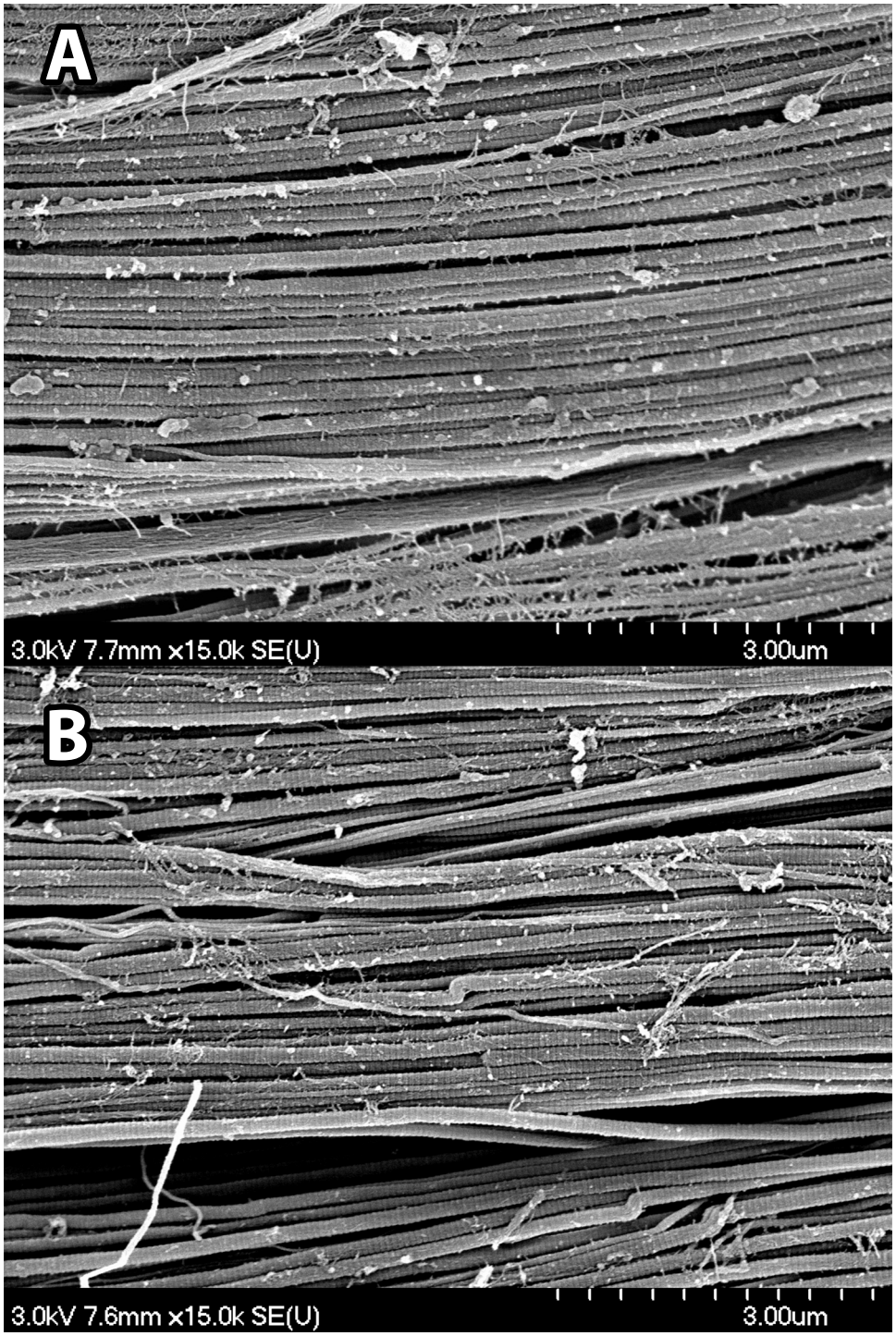

Figure 5.14: Representative SEM images of (A) Unloaded control sample, and (B) one of the two hour SCL samples. B: Only very minor evidence of kinking is apparent.

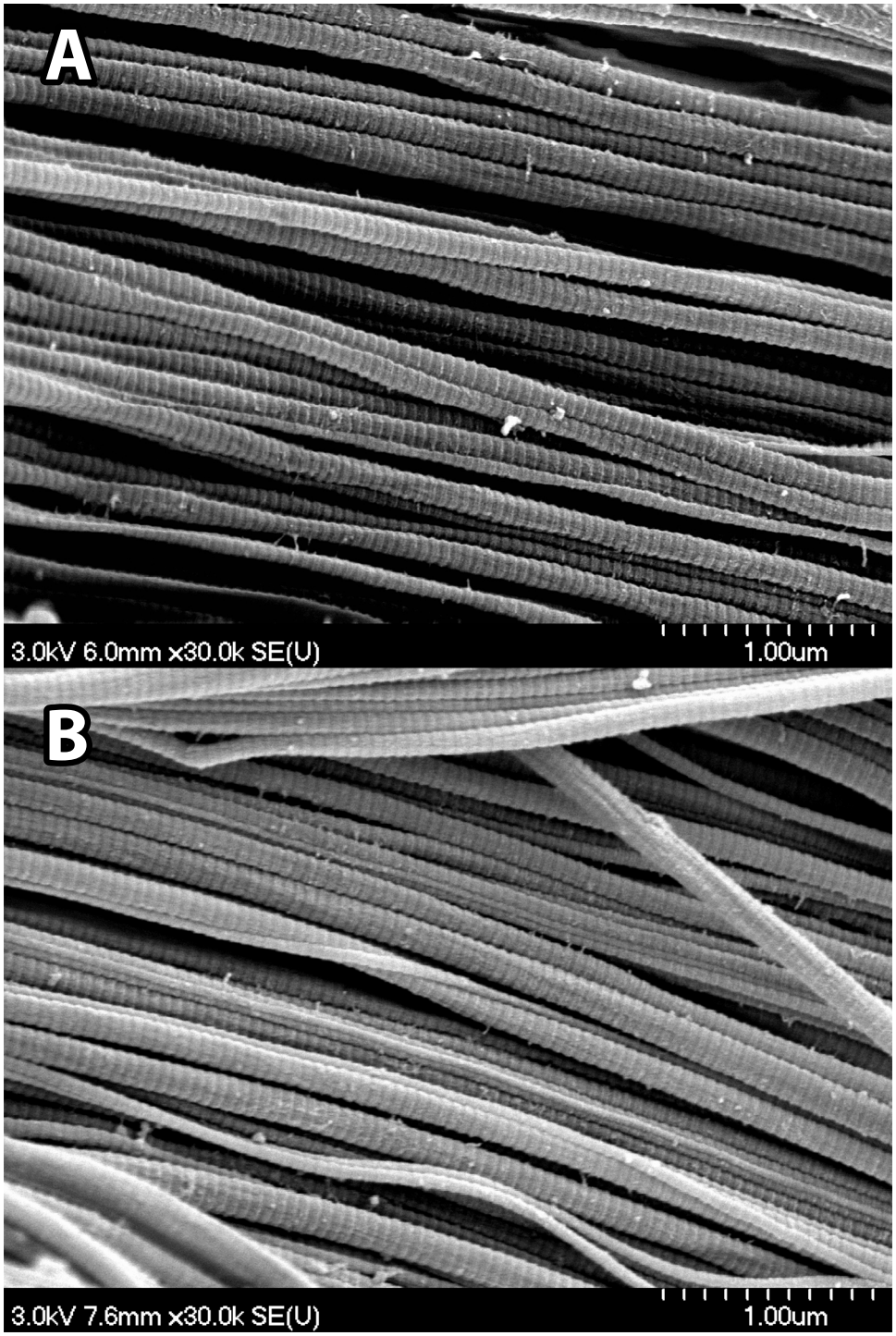

Figure 5.15: Representative SEM images of (A) Unloaded control sample, and (B) one of the two hour SCL samples. B: As was the case for most of the fibrils viewed, no damage is seen here.

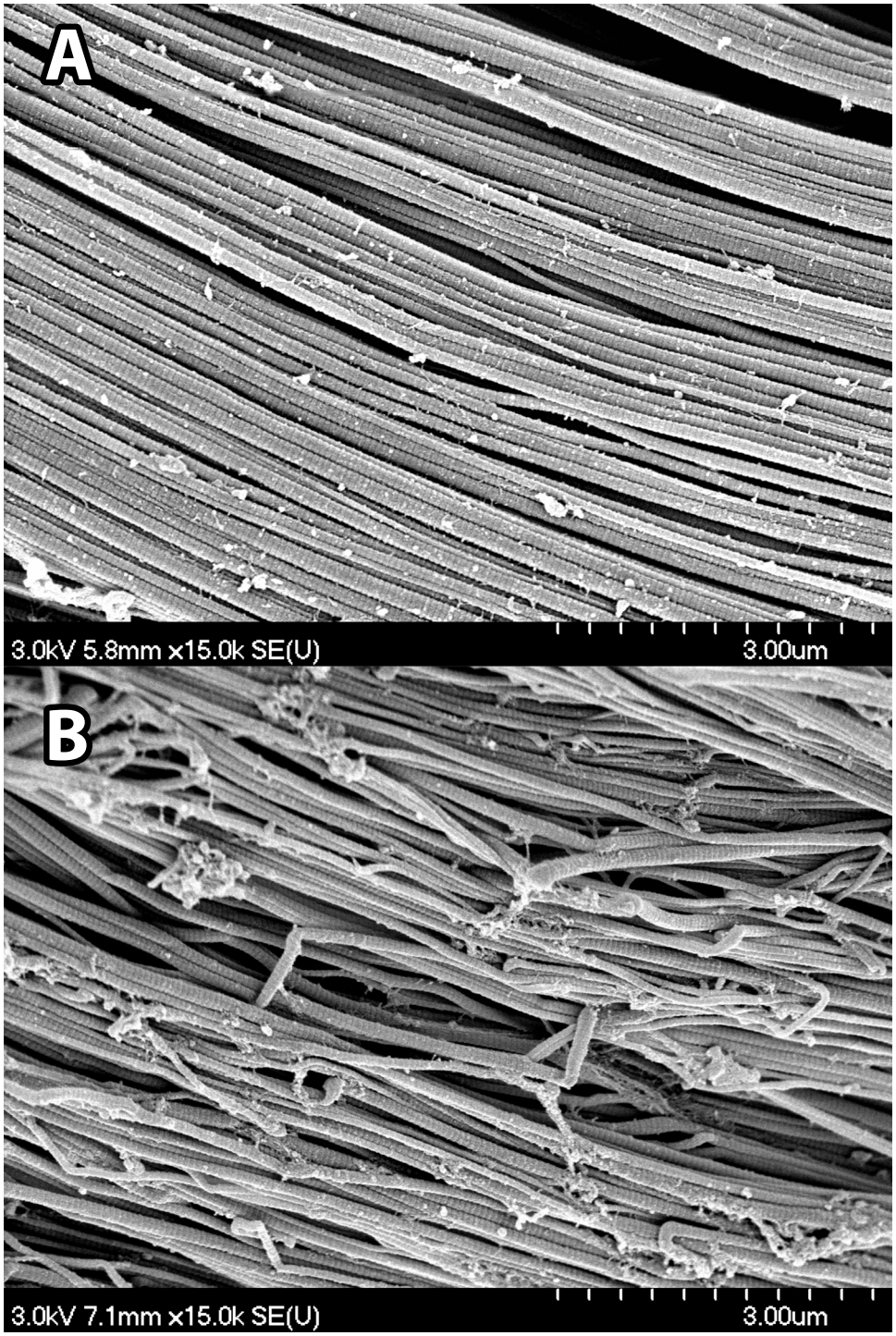

Figure 5.16: Representative SEM images of (A) Unloaded control sample, and (B) one of the two hour SCL samples. B: In this particular location significant kinking was found, though no regular longitudinal repeat pattern was present.

SEM, fibrils in SCL samples also had longitudinal kinking in both the 4 and 5 hour samples, along with fibrillar dissociation in these samples. This observation, along with observations from the previous experiment, indicates that molecular packing disruption is related to fibrillar kinking and dissociation. In essence, it appears that fibrillar dissociation and fibrillar kinking can not occur without significant molecular packing disruption. The relationship between D-banding and collagen denaturation was presented in the previous experiment and is further supported by the results of this experiment's results. These results from the OCR samples showed that significant collagen denaturation and significant loss of D-banding occurred concurrently, while all the other test samples did not show a significant drop in specific enthalpy, and also retained their D-banding.

The results from this study might shed light on the process of how fibrils dissociate. Fibrils consist of sub-fibrils, which in turn consist of micro-fibrils, within which collagen molecules are arranged[5]. It was noted in previous studies that sub-fibrils are wound around the fibril's axis[111–113]. Hashizume et al.[32] have studied the growth of collagen fibrils in osteosarcomic samples using atomic force microscopy (AFM), transmission electron microscopy (TEM), and SEM, providing an illustration of how subfibrils are wound along the axis of fibrils during their development. It appears, from the available results, that molecular unpacking is the major culprit behind fibrillar dissociation. Once assembled into a fibril, subfibrils can't unwind without significant damage to molecular packing.

It is not clear why the specific enthalpy of the SCL samples increased. One possible explanation could be related to the presence of some partially denatured collagen molecules existing within the tendons prior to mechanical loading[24]. With prolonged periods of stretching, these uncoiled α-chains might have been stretched to a point that realignment into collagen helices occurred, forming additional hydrogen bonding. This possibility, however, is minor, as the quantity of denatured collagen helices in native steer tail tendons is small ($\sim$1.5%)[24].

5.5.3 Creep Loading Induced Nanostructural Disruption

With the DSC and SEM results from the experiments in this thesis showing distinctive outcomes between OCR and SCL samples, it is important to examine how mechanical loading differences effect the nanostructural damage in tendons. In SCL samples, molecular packing disruption, and consequently fibrillar dissociation and longitudinal kinking occurred without detectable collagen denaturation. This indicates that molecular packing disruption and collagen denaturation might occur as independent processes. Looking at the current SEM analysis, fibrillar dissociation was consistently present with D-banding remaining largely intact, meaning that fibrils can be severely damaged, and possibly ruptured, without damaging the collagen helix. Since fibrillar dissociation appeared in both OCR and SCL tendons, it appears to be a strong indication that molecular unpacking can occur without stress level being a factor. This means that fibrillar dissociation and molecular unpacking are features of excessive loading duration, and are highly time dependent. Higher loading rate, both in RR samples and in previous studies, was found to cause fibrillar dissociation[4], which was also accompanied with molecular unpacking[68,69]. However, it is clear that lowering loading rate as in the current study causes significant increases in molecular unpacking.

In the first experiment, OCR and RR samples were loaded to the yield stress, while the SCL samples tested in the second experiment were not. Evidence of collagen denaturation was present in the OCR samples, but not in the SCL or RR samples. In a complete contrast, SCL samples actually experienced a significant but small increase in their specific enthalpy. The denaturation of collagen was previously linked to overloading tendons, particularly in the case of repeated overloading[56,79]. It appears that overload stress levels are required to cause significant breaking of hydrogen bonds, causing the denaturation of collagen, something that was not possible under SCL loading. This is consistent with previous X-ray diffraction work which showed that the D-banding period of fibrils is not altered when loading is limited to below the yield point, as shown by Folkhard et al[37] and Knorzer et al.[76]. Mosler et al.[28] used X-ray diffraction to analyze changes rat tail tendons creep loaded until rupture, with the

creep loading triggered at 5% strain level (suboverload creep). That study reported no changes to the D-period due to creep loading.

While stress level appears to be important to the occurrence of collagen denaturation in tendons, so too does loading rate. In the previous experiment, it was shown than OCR samples experienced collagen denaturation while RR samples did not, despite both being overloaded, implicating strain rate as an important factor. While low strain rate loading did not cause collagen denaturation in SCL samples, an argument could be made that points to the differences in methodologies used in the two experiments. Tendons in the first experiment were loaded to rupture, unlike tendons from the second experiment, which were loaded for set periods of times, after which they were unloaded. One could argue that eventual denaturation of collagen might have occurred if tendons were loaded under SCL to rupture.

Finally, it is worth suggesting what structural changes may take place during each phase of creep. Previous studies done by Folkhard et al.[37] and Sasaki et al.[36] have identified three main modes of molecular rearrangement, these are: (1) molecular elongation, (2) increase in the gap region between molecules along the fiber axis, and (3) the relative slippage of laterally adjoining molecules along the fiber axis. According to both Folkhard et al.[37] and Sasaki et al.[114], both of whom tested the effect of creep on tendons using X-ray diffraction, molecular rearrangement was found to occur due to static creep loading at stress levels higher than 10 MPa in tendons.

The primary creep phase is likely dominated by collagen fiber and fibril sliding, molecular alignment and straightening, and water. Confocal observation of tendon fascicles during stress relaxation has shown that significant fiber sliding occurs[95], and it is likely that this also occurs during ramp loading and continues during the primary phase of creep. X-ray diffraction indicates that molecular alignment and straightening occur during the initial phase of creep[114], which would not be expected to damage fibril structure and is consistent with SEM and DSC observations from the current study that no fibril damage occurs during primary creep. Creep loading has previously been found to cause water loss in both tendons and ligaments[115,116]. During primary creep, inter- and intra-fibrillar pressure would be generated by the applied tension, expelling

water allowing radial contraction and contributing to elongation.

In the secondary creep phase, fibrillar damage was detected in tendons that underwent suboverload creep, with the damage severity being dependent on duration of loading. The time dependence of fibrillar damage formation, as seen in this study's second experiment, coincides with previous work done by Sasaki et al.[114], which showed that molecular elongation is responsible for D-period change during the initial stages of creep loading, while the second two modes of molecular rearrangement are responsible for later D-period changes. At four hours of suboverload creep, collagen fibrils develop molecular packing disruption detectable in SEM and DSC analysis. Molecular packing disruption may be directly caused by loading induced molecular sliding within fibrils. Such an event would cause molecules to lose lateral cohesion, which could in turn cause their lateral spacing to increase. This may eventually cause fibrils to dissociate into subfibrils, something that was seen in SCL and OCR tendons. It appears that intrahelical hydrogen bonds are more inclined to break under overload creep, causing the unwinding of collagen molecules. As static loading continues, molecular sliding advances and molecular and fibrillar damage becomes more severe.

In the tertiary phase, collagen fibrils experience widespread damage, and become less effective in their load bearing function, causing an increase in the rate of damage to other fibrils. The widespread dissociation of fibrils seen in the OCR creep ruptured tendons and SCL tendons loaded for five hours suggests that once intrafibrillar cohesion is lost, fibrils have little tensile load bearing ability.

5.5.4 Structural Continuity of Collagen Fibrils

Whether fibrils are continuous or discontinuous over a tendon's length has been debated in the literature[7,38,47,86,118,119]. In a discontinuous model, fibrils are short in length compared to the tendon, and longitudinal force transmission occurs from one fibril to the adjacent fibril via non-collagenous components of the ECM, or labile connections between fibrils. In such a model fibrils are damaged via interfibrillar sliding[118]. A study by Mosler et al.[28] used X-ray diffraction analysis of tendons exposed

to creep after ramp loading to 5% to 10% strain. It was found that while creep loaded tendons elongated on the macroscale, the D-period did not change, which supports the discontinuity model of fibrils within tendons[28].

In the continuous fibril model, fibrils extend structurally from one end of the tendon to the other[7,47]. In this model, fibrils are the sole load bearing entity in tendons, hence they are also mechanically continuous, independent of their structural continuity[47]. If fibrils are continuous, then they are expected to fail through fibril breakage, which will occur by the means of reaching the fibrils' mechanical limit[47]. Support for the continuity of mature tendon fibrils can be based on different studies, which employed SEM of fracture surfaces[86] or serial TEM scanning[120]. The goal of these investigations was to either trace the fibrils or to determine the characteristic mechanical and structural properties of fibrils. As mentioned earlier, Svensson et al.[47] have recently published their investigation supporting the continuity of fibrils within tendons. This study took a statistical approach to measure the length of large numbers of fibrils in human and mouse tendons using serial block face-SEM. Fibril ends were rarely observed in mature tendons, indicating that fibrils are structurally continuous[47]. Other studies have found that fibrils' lengths are likely to exceed their critical length, which can be defined as the length at which material breaks rather than slips due to loading[47,86,120,121].

Further support for the continuity of fibrils might be deduced from discrete plasticity studies. Such investigations showed that plastic deformation occurs at discrete but widespread locations along tendons[4,56,69,79]. The same finding was also reported using atomic force microscopy (AFM) analysis on individually loaded fibrils. Quigley[80] showed in his study that individually ruptured fibrils failed the same as those damaged in whole tendon rupture. This means that the fibrillar discrete plasticity damage in tendons observed by Veres et al.[4,56] and Herod et al.[79] was likely not caused by interfibrillar sliding.

So what can be said on the continuity of fibrils within tendons, given this study's results? Creep overloaded tendons in this study presented severe and homogeneous fibrillar and molecular damage, which were more significant than found in previous

studies, in which fibrils were loaded at a significantly faster rate[4,56,69,79]. This indicates that inter-fibrillar sliding does not contribute to damage formation within tendons. In addition, creep overloaded tendons showed evidence of both molecular unpacking and collagen denaturation. This finding does not coincide with SCL samples, or the findings of previous studies[28,37,76]. The presence of both significant molecular and fibrillar damage in OCR samples supports the continuous model of tendons, as the force transmission must have occurred through a structural 'continuum' for it to cause the widespread damage in tendons at creep loading's slow extension rate. If fibrils were short and transmitted force through fibrillar sliding, as studies have suggested[38,40], slower stretching under both OCR and SCL should have reduced or halted any damage formation, as not enough shear stress would have been generated to cause fibrillar damage.

5.5.5 Physiological Relevance of this Study's Results

It is clear that nanostructural damage in tendons is possible under creep loading at both overload and sub-overload stress levels. Given the evidence from this study, the answer to the research question is that damage can be created at suboverload mechanical stress levels, but perhaps not within physiologically relevant conditions.

Different tendons have different morphological, anatomical, and physiological properties[87]. This means that different tendons may respond differently to creep loading than the steer tail tendons used in this study. In the previous experiment's discussion, the difference in crosslinking between tendons and how it might affect the structural response to creep loading was considered. Tendons are built to serve their particular physiological function[122]. Ker et al.[122] were able to estimate the maximum stress levels applied to different types of tendons in different species *in vivo* (Table 5.2). This was done through calculating the ratio of the CSA of muscles to that of tendons, multiplied by the muscular stress level, the later of which was found previously to reach a maximum of 0.3 MPa. Looking at that study's results, it can be clearly seen that tendons in humans and other mammals experience varying stress levels.

Table 5.2: Maximum Stress procured by human and cow tendons *in vivo*[122]. All the values presented are in MPa.

	Superficial Digital Flexor Tendons	Digital Flexor Tendons	Digital Extensor Tendons
Cow	69	15 - 46	8 - 11

	Achilles Tendons	Digital Flexor Tendons	Digital Extensor Tendons
Human	67	16, 23	11,13

When investigating the physiologic relevance of suboverload creep applied to tendons, it is beneficial to look at *in vivo* muscular activity studies. Prolonged or static muscle contraction may impose creep loading on the connected tendon. Studies have found a correlation between static muscular activity, and the development of discomfort and/or pain in the neck and shoulder regions[123–128]. It has been shown by Ostensvik et al.[126] that workers in the forestry industry were more likely to develop discomfort and pain when they had a higher number of static trapezius muscle activities of more than 10 minutes per hour. It was also reported in a recent study by Hanvold et al.[128] that workers who had a high level of sustained muscle activity over a period of time were more likely to develop neck and shoulder pain. Prolonged periods of static loading defined in this study was defined as static muscle activity as longer than four minutes for periods of more than 50% of the working day[128]. In several studies, the maximum voluntary contraction (MVC) was investigated using electromyogrpahy (EMG). Jensen et al.[124] studied trapezius muscle activity in industrial sewing machine workers. They found that the average static contraction of the trapezius muscle in these workers was 9% of MVC during the working day, with this average contraction being constant throughout the day[124]. An earlier study done on chocolate packing factory workers that also used EMG analysis was conducted by Veiersted et al.[123]. This study stated that trapezius muscle activity reached an average static contraction of around 5% MVC, for durations greater than 17 minutes[123]. Workers participating in this study were more likely to report neck and shoulder pain with higher static EMG levels[123]. Besides factory workers, a similar pattern was also found in people who work as cleaners or janitors. This can be seen in a study done by Søgaard et al.[127], which investigated the amount of static muscle activity experienced by cleaners.

This study found that cleaners spent around 65% of the 8 hour work day with their trunk flexed more than 20°, with EMG analysis reporting a static contraction of the trapezius at 10% MVC[127]. Sustained loading for long periods of time has also been detected, albeit with lower contraction levels (∼4% of MVC), in white collar jobs, specially ones involving prolonged computer work without arm support[125].

Sustained muscular activity, as described earlier, may expose tendons to static creep loading. However, stress levels would likely be much lower than those used in this study's SCL experiment. There seems to be a correlation between high levels of static muscular loading and the development of neck and shoulder pain. With the knowledge that static suboverload creep loading can cause nanostructural damage to tendons *in vitro*, there could be a possible connection between the development of neck and shoulder pain and similar damage *in vivo*.

Knowing that nanostructural damage is formed in tendons by static creep loading might indicate that nanostructural damage can also form during cyclical creep loading. According to Hess et al.[129] and Wren et al.[58], most clinically reported tendon injuries occur as a result of microtrauma, that arises from repetitive or cyclic loading[130,131]. In previous *in vitro* cyclic loading tests, high frequency loading was done at relatively high stress levels. These studies have shown that tendon fibers are structurally disrupted due to cyclic loading[83], as well as presenting macro-scale structural damage[58]. It might also be the case that nanostructural damage might occur in cyclically creep loaded tendons too. Discrete plasticity was indeed detected in cyclically loaded steer CDETs by Herod et al.[79], but not in their SDFT counterparts. This outcome suggests certain similarities in the damage formation process in both static and cyclic creep loaded tendons.

Chapter 6

Summary and Conclusion

6.1 Summary of Results

This study, which includes two experiments, culminates in five main points. First, creep loading tendons causes them to incur intensive and homogeneous molecular packing disruption, which was more significant than what was observed in tendons loaded at higher strain rates. DSC analysis indicated that a significant increase in the lateral spacing of collagen molecules within fibrils occurs due to creep loading, which leads to the dissociation of fibrils into subfibrils. Overload creep was found to cause extensive longitudinal kinking of collagen fibrils within tendons, while suboverload creep did not cause extensive kinking.

Second, overload creep appear to cause intensive collagen denaturation, in contrast with tendons overloaded at faster strain rates, or subjected to suboverload creep. The loss of fibrillar D-banding in tendons caused by overload was homogeneous. Since loss of D-banding was only observed when specific enthalpy was reduced, it indicates that loss of D-banding is a sign of collagen denaturation, which in turn could mean that collagen denaturation was homogeneous along the length of fibrils in the creep overloaded tendons. Both longitudinal kinking and collagen denaturation appear to occur significantly only in tendons that are overloaded, with lowering of strain rate

affecting the homogeneity and spread of damage.

Third, molecular packing disruption and collagen denaturation appear to be processes that are distinct from each other. While molecular unpacking can occur without collagen denaturation, as seen in the suboverloaded creep samples, collagen denaturation can not occur without some level of molecular unpacking occurring, as seen in ramp rupture and overload creep samples. Dissociation of fibrils may indicate that divalent thermally labile crosslinks between subfibrils rarely form.

Fourth, the results from this study suggest that fibrils are mechanically continuous in buildup within tendons. Support for this statement stems from the homogeneity and high severity of damage in the fibrils of all extremely low strain rate loaded tendons. Interfibrillar sliding does not appear to be the major cause of damage formation, or the major force transmission factor in tendons. Instead, fibrils appear to bear the tensile load directly, undergoing extensive damage before causing macroscale failure due to slippage.

Fifth, it was shown that with sufficient duration of creep loading, tendons can undergo nanostructural damage at suboverload stress levels.

6.2 Significance

This study was a natural continuation of previous studies that investigated the effect of loading on tendon nanostructure[4,56,68,69,79]. To the author's knowledge, no other studies were done to explore the effect of static creep loading on the nanostructure of tendons using SEM and DSC analysis. The results and deductions of this study will allow the enhancement of our collective understanding of how tendons respond to loading at the nanostructural level. The comparison between the nanostructural alterations in tendons caused by different types of tensile loading sheds light on previously unclear structural properties of tendons. Particularly interesting is the finding of the presence of widespread and intensive nanostructural alterations in tendons creep loaded at overload levels, which was more severe than the damage levels found

in faster ramp loaded tendons. This study's findings also support previous studies confirming that fibrils are structurally continuous, which will help in explaining the response of tendons and possibly ligaments to mechanical loading.

While it is experienced at the current study's durations and stress levels, understanding the nanostructural damage caused in tendons by creep loading might provide an insight into how repetitive intervals of static suboverload creep may affect tendons *in vivo*. This study's findings might help further investigation into how tendon damage can occur in real life situations, which may help in developing better targeted therapies to hasten the tendon healing.

6.3 Next Steps

The next logical step after this research study would be to investigate the effect of creep loading on different tendon models. From previous studies, it is known that the structural response of tendons is largely affected by their crosslinking[57,79]. Steer tail tendons are positional tendons and contain low crosslinking. Hence, a priority should be placed on testing the effect of low strain rate loading on tendons with greater crosslinking. It is known that tendons with more crosslinking are more likely to be exposed to different types of loading *in vivo*, which includes static creep loading. It is suggested by the author that a good example of such investigation would be to analyze the differences in the effects of overload creep on steer forelimb flexor and extensor tendons, using the same methodology as the first experiment (OCR, RR and HS). This investigation should be followed with a similar methodology to that done in the second experiment (SCL) on flexor and extensor tendons. This second experiment would be particularly important if both flexor and extensor tendons were found to incur significant nanostructural alterations due to overload creep.

Collagen denaturation in creep loaded tendons was investigated in this study using both DSC and SEM analysis. However, additional investigation using trypsin digestion would be helpful, in order to support this study's observations. There was a

notable inconsistency in the DSC results from the OCR tendons. Creep overloading tendons caused significant collagen denaturation, as indicated by the significant change in the specific enthalpy readings of creep overloaded tendons, when compared to unloaded control samples. However, there was a large standard deviation in the specific enthalpy values recorded. This variability occurred because four samples showed significantly larger specific enthalpy changes than the other four samples in that group. A possible experiment could be done using the same tendon model, and applying the same overload and suboverload crep mechanisms, but with different post-loading analysis methods. Analysis of these loaded tendons and their controls could be done using trypsin digestion of these samples, followed with SEM analysis, as done by Veres et al.[56]. Trypsin digestion would cause the removal of denatured collagen. A comparison between the amount of denatured collagen in loaded and unloaded samples could then be made. This would provide more complete answer to the question of whether tendons experience collagen denaturation during overload creep.

Bibliography

[1] Rigby BJ, Hirai N, and Spikes JD. The mechanical properties of rat tail tendon. *The Journal of General Physiology* 1959;43:265–283.

[2] Birch HL. Tendon matrix composition and turnover in relation to functional requirements. *International journal of experimental pathology* 2007;88(4):241–8.

[3] Puxkandl R, Zizak I, Paris O, et al. Viscoelastic properties of collagen: synchrotron radiation investigations and structural model. *Philosophical transactions of the Royal Society of London. Series B, Biological sciences* 2002; 357(1418):191–197.

[4] Veres SP, Harrison JM, and Lee JM. Repeated subrupture overload causes progression of nanoscaled discrete plasticity damage in tendon collagen fibrils. *Journal of Orthopaedic Research* 2013;31(5):731–737.

[5] Rowe R. The Structure of the Rat Tendon. *Connective tissue research* 1985; 14:9–20.

[6] Kastelic J, Galeski A, and Baer E. The Multicomposite Structure of Tendon. *Connective Tissue Research* 1978;6(1):11–23.

[7] Ker RF. Mechanics of tendon, from an engineering perspective. *International Journal of Fatigue* 2007;29(6):1001–1009.

[8] Screen HRC, Bader DL, Lee DA, et al. Local strain measurement within tendon. *Strain* 2004;40(4):157–163.

[9] Torp S, Baer E, and Friedman B. Effects of age and of mechanical deformation on the ultracture of tendon. *Colston Papers* 1975;26(223-250):223–251.

[10] Gautieri A, Vesentini S, Redaelli A, et al. Viscoelastic properties of model segments of collagen molecules. *Matrix Biology* 2012;31(2):141–149.

[11] Kastelic J and Baer E. Deformation in Tendon Collagen. *Symposium of the Society for Experimental Biology* 198;(34):397–435.

[12] Kirkendall DT and Garrett WE. Function and biomechanics of tendons. *Scandinavian journal of medicine & science in sports* 1997;7(2):62–66.

[13] Wess TJ. Collagen Fibril Form and Function. *Advances in protein chemistry* 2005;70:341 – 375.

[14] Kuo CK, Marturano JE, and Tuan RS. Novel strategies in tendon and ligament tissue engineering: Advanced biomaterials and regeneration motifs. *Sports medicine, arthroscopy, rehabilitation, therapy & technology : SMARTT* 2010; 2:20.

[15] Kadler KE, Holmes DF, Trotter Ja, et al. Collagen fibril formation. *The Biochemical journal* 1996;316 (Pt 1:1–11.

[16] McCarthy MM and Hannafin Ja. The mature athlete: aging tendon and ligament. *Sports health* 2014;6(1):41–8.

[17] Miles C and Ghelashvili M. Polymer-in-a-box mechanism for the thermal stabilization of collagen molecules in fibers. *Biophysical journal* 1999;76:3243 – 3252.

[18] Tresoldi I, Oliva F, and Benvenuto M. Tendon's ultrastructure. *Muscles, Ligaments and Tendons Journal* 2013;3(1):2–6.

[19] Sopakayang R, De Vita R, Kwansa A, et al. Elastic and viscoelastic properties of a type I collagen fiber. *Journal of Theoretical Biology* 2012;293:197–205.

[20] Thorpe CT, R H, and Screen C. Tendon structure and composition. In *Metabolic Influences on Risk for Tendon Disorders*, January, pages 229–238. ISBN 9783319339412 2016;.

[21] Eriksen HA, Pajala A, Leppilahti J, et al. Increased content of type III collagen at the rupture site of human Achilles tendon. *Journal of Orthopaedic Research* 2002;20(6):1352–1357.

[22] Kadler KE, Hojima Y, and Prockop DJ. Collagen fibrils in vitro grow from pointed tips in the C- to N-terminal direction. *The Biochemical journal* 1990; 268(2):339–343.

[23] Riley GP, Harrall RL, Constant CR, et al. Tendon degeneration and chronic shoulder pain: changes in the collagen composition of the human rotator cuff

tendons in rotator cuff tendinitis. *Annals of the Rheumatic Diseases* 1994; 53(6):359–66.

[24] Willett TL, Labow RS, Avery NC, et al. Increased Proteolysis of Collagen in an InVitro Tensile Overload Tendon Model. *Annals of Biomedical Engineering* 2007;35(11):1961–1972.

[25] Baldwin SJ, Quigley AS, Clegg C, et al. Nanomechanical Mapping of Hydrated Rat Tail Tendon Collagen I Fibrils. *Biophysical journal* 2014;107(October):1–8.

[26] Rumian A, Wallace AL, and Birch HL. Tendons and ligaments are anatomically distinct but overlap in molecular and morphological featuresa comparative study in an ovine model. *Journal of orthopaedic research* 2007;(April):458–464.

[27] Canty EG and Kadler KE. Procollagen trafficking, processing and fibrillogenesis. *Journal of cell science* 2005;118(Pt 7):1341–1353.

[28] Mosler E, Folkhard W, Knörzer E, et al. Stress-induced molecular rearrangement in tendon collagen. *Journal of Molecular Biology* 1985;182(4):589–596.

[29] Silver FH, Freeman JW, and Seehra GP. Collagen self-assembly and the development of tendon mechanical properties. *Journal of Biomechanics* 2003; 36(10):1529–1553.

[30] Barnard K, Light ND, Sims TJ, et al. Chemistry of the collagen cross-links. Origin and partial characterization of a putative mature cross-link of collagen. *The Biochemical Journal* 1987;244(2):303–9.

[31] Gutsmann T, Fantner GE, Venturoni M, et al. Evidence that collagen fibrils in tendons are inhomogeneously structured in a tubelike manner. *Biophysical journal* 2003;84(4):2593–2598.

[32] Hashizume H, Hitomi J, and Ushiki T. Growth of Collagen Fibrils Produced by Human Osteosarcoma Cells: High-Resolution Scanning Electron Microscopy. *Archive of the Histological Cytology* 1999;62(4):327 – 335.

[33] Bozec L, Van der Heijden G, and Horton M. Collagen Fibrils: nanoscale ropes. *Biophysical Journal* 2007;92:70 – 75.

[34] Ottani V, Martini D, Franchi M, et al. Hierarchial structures in fibrillary collagens. *Micron.* 2002;33:587 – 596.

[35] Zhao T, Weinhold PS, Lee NY, et al. Some observations on the subfibrillar structure of collagen fibrils as noted during treatment with NKISK and cathepsin G with mechanical agitation. *Journal of electron microscopy* 2011;60(2):177–82.

[36] Sasaki N and Odajima S. Elongation mechanism of collagen fibrils and force-strain relations of tendon at each level of structural hierarchy. *Journal of Biomechanics* 1996;29(9):1131–1136.

[37] Folkhard W, Mosler E, Geercken W, et al. Quantitative-Analysis of the Molecular Sliding Mechanism in Native Tendon Collagen - Time-Resolved Dynamic Studies Using Synchrotron Radiation. *International Journal of Biological Macromolecules* 1987;9(3):169–175.

[38] Szczesny SE, Caplan JL, Pedersen P, et al. Quantification of Interfibrillar Shear Stress in Aligned Soft Collagenous Tissues via Notch Tension Testing. *Scientific reports* 2015;5(October):14649.

[39] Rigozzi S, Stemmer A, Müller R, et al. Mechanical response of individual collagen fibrils in loaded tendon as measured by atomic force microscopy. *Journal of Structural Biology* 2011;176(1):9–15.

[40] Szczesny SE, Fetchko KL, Dodge GR, et al. Evidence that interfibrillar load transfer in tendon is supported by small diameter fibrils and not extrafibrillar tissue components 2017.

[41] Cribb AM and Scott JE. Tendon response to tensile stress: an ultrastructural investigation of collagen:proteoglycan interactions in stressed tendon. *J. Anat* 1995;187(2):423–428.

[42] Redaelli A, Vesentini S, Soncini M, et al. Possible role of decorin glycosaminoglycans in fibril to fibril force transfer in relative mature tendons - A computational study from molecular to microstructural level. *Journal of Biomechanics* 2003; 36(10):1555–1569.

[43] Raspanti M, Alessandrini A, Ottani V, et al. Direct Visualization of Collagen-Bound Proteoglycans by Tapping-Mode Atomic Force Microscopy. *Journal of Structural Biology* 1997;119(2):118–122.

[44] Svensson RB, Hassenkam T, Hansen P, et al. Tensile force transmission in human patellar tendon fascicles is not mediated by glycosaminoglycans. *Connective tissue research* 2011;52(5):415–21.

[45] Fessel G and Snedeker JG. Equivalent stiffness after glycosaminoglycan depletion in tendon - an ultra-structural finite element model and corresponding experiments. *Journal of Theoretical Biology* 2011;268(1):77–83.

[46] Szczesny SE and Elliott DM. Interfibrillar shear stress is the loading mechanism of collagen fibrils in tendon. *Acta Biomater* 2014;10(6):2582–2590.

[47] Svensson RB, Herchenhan A, Starborg T, et al. Evidence of structurally continuous collagen fibrils in tendon. *Acta Biomaterialia* 2017;.

[48] Betsch D and Baer E. Structure and Mechanical Properties of Rat Tail Tendon. *Biorheology* 1980;17(6):83 – 94.

[49] Bailey AJ, Robins SP, and Balian G. Biological significance of the intermolecular crosslinks of collagen. *Nature* 1974;251(5471):105–109.

[50] Bailey AJ and Sims TJ. Chemistry of the collagen cross-links. *Biochemistry Journal* 1976;153:211–215.

[51] Avery NC and Bailey aJ. Enzymic and non-enzymic cross-linking mechanisms in relation to turnover of collagen: relevance to aging and exercise. *Scandinavian journal of medicine & science in sports* 2005;15(4):231–40.

[52] Willett TL, Labow RS, Aldous IG, et al. Changes in collagen with aging maintain molecular stability after overload: evidence from an in vitro tendon model. *Journal of biomechanical engineering* 2010;132(3):031002.

[53] Lee JM. Tissue mechanics. In *Wiley Encyclopedia of Biomedical Engineering*. John Wiley and Sons, Inc. 2006;.

[54] Bella J, Brodsky B, and Berman HM. Hydration structure of a collagen peptide. *Structure* 1995;3(9):893–906.

[55] Masic A, Bertinetti L, Schuetz R, et al. Osmotic Pressure Induced Tensile Forces in Tendon Collagen. *Nature communications* 2015;6:5942.

[56] Veres SP and Lee JM. Designed to fail: a novel mode of collagen fibril disruption and its relevance to tissue toughness. *Biophysical journal* 2012;102(12):2876–84.

[57] Shepherd JH, Riley GP, and Screen HRC. Early stage fatigue damage occurs in bovine tendon fascicles in the absence of changes in mechanics at either the gross or micro-structural level. *Journal of the mechanical behavior of biomedical materials* 2014;38:1–9.

[58] Wren TaL, Lindsey DP, Beaupré GS, et al. Effects of Creep and Cyclic Loading on the Mechanical Properties and Failure of Human Achilles Tendons. *Annals of Biomedical Engineering* 2003;31(6):710–717.

[59] Duenwald SE, Vanderby R, and Lakes RS. Viscoelastic relaxation and recovery of tendon. *Annals of Biomedical Engineering* 2009;37(6):1131–1140.

[60] Machiraju C, Phan aV, Pearsall aW, et al. Viscoelastic studies of human subscapularis tendon: Relaxation test and a Wiechert model. *Computer Methods and Programs in Biomedicine* 2006;83(1):29–33.

[61] Pearson SJ, Burgess K, and Onambele GNL. Creep and the in vivo assessment of human patellar tendon mechanical properties. *Clinical biomechanics (Bristol, Avon)* 2007;22(6):712–7.

[62] Knudson D. *Fundamentals of Biomechanics*, volume 86. Springer 2000.

[63] Haut RC. Age-dependent influence of strain rate on the tensile failure of rat-tail tendon. *Journal of biomechanical engineering* 1983;105(3):296–9.

[64] Yamamoto N and Hayashi K. Mechanical properties of rabbit patellar tendon at high strain rate. *Bio-medical materials and engineering* 1998;8(2):83–90.

[65] Shen ZL, Kahn H, Ballarini R, et al. Viscoelastic properties of isolated collagen fibrils. *Biophysical Journal* 2011;100(12):3008–3015.

[66] Ciarletta P, Micera S, Accoto D, et al. A novel microstructural approach in tendon viscoelastic modelling at the fibrillar level. *Journal of Biomechanics* 2006;39(11):2034–2042.

[67] Donahue TL, Gregersen C, Hull ML, et al. Comparison of viscoelastic, structural, and material properties of double-looped anterior cruciate ligament grafts made from bovine digital extensor and human hamstring tendons. *Journal of biomechanical engineering* 2001;123(2):162–169.

[68] Willett TL, Labow RS, and Lee JM. Mechanical overload decreases the thermal stability of collagen in an in vitro tensile overload tendon model. *Journal of Orthopaedic Research* 2008;26(12):1605–1610.

[69] Veres SP, Harrison JM, and Lee JM. Mechanically overloading collagen fibrils uncoils collagen molecules, placing them in a stable, denatured state. *Matrix biology : journal of the International Society for Matrix Biology* 2014;33:54–9.

[70] Hansen P, Bojsen-Moller J, Aagaard P, et al. Mechanical properties of the human patellar tendon, in vivo. *Clinical biomechanics (Bristol, Avon)* 2006; 21(1):54–8.

[71] Fratzl P, Mis K, Iv Z, et al. Fibrillar Structure and Mechanical Properties of Collagen. *Journal of structural biology* 1997;122(1-2):119–122.

[72] Misof K, Rapp G, and Fratzl P. A New Molecular Model for Collagen Elasticity

Based on Synchroton X-Ray Scattering Evidence. *Biophysical journal* 1997; 72(March):1376 – 1381.

[73] Maganaris CN, Narici MV, Almekinders LC, et al. Biomechanics and pathophysiology of overuse tendon injuries: Ideas on insertional tendinopathy. *Sports Medicine* 2004;34(14):1005–1017.

[74] Danto MI and Woo SL. The mechanical properties of skeletally mature rabbit anterior cruciate ligament and patellar tendon over a range of strain rates. *Journal of Orthopaedic Research* 1993;11(1):58–67.

[75] Nemetschek T, Jonak R, Meinel A, et al. Kinckdeformationen an Kollagen. *Arch. orthop. Unfall-Chir* 1977;89:249 – 257.

[76] Knörzer E, Folkhard W, Geercken W, et al. New Aspects of the Etiology of Tendon Rupture. *Archives of Orthopaedic and Traumatic Surgery* 1986;105(2):113–120.

[77] Steven FS, Minns RJ, and Finlay JB. Evidence for the local denaturation of collagen fibrils during the mechanical rupture of human tendons. *Injury* 1975; 6(4):317–319.

[78] Veres SP, Harrison JM, and Lee JM. Cross-link stabilization does not affect the response of collagen molecules, fibrils, or tendons to tensile overload. *Journal of Orthopaedic Research* 2013;31(12):1907–1913.

[79] Herod TW, Chambers NC, and Veres SP. Collagen fibrils in functionally distinct tendons have differing structural responses to tendon rupture and fatigue loading. *Acta Biomaterialia* 2016;42:296–307.

[80] Quigley AS. *Collagen fibrils from physiologically distinct tendons follow unique paths to failure.* Dalhousie graduate theses, Dalhousie University 2016.

[81] Kopp J, Bonnet M, and Renou JP. Effect of collagen crosslinking on collagen-water interactions (a DSC investigation). *Matrix (Stuttgart, Germany)* 1989; 9(6):443–450.

[82] Wang XT and Ker RF. Creep rupture in wallaby tail tendons. *J Exp Biol* 1995; 198(August):831–845.

[83] Shepherd JH, Legerlotz K, Demirci T, et al. Functionally distinct tendon fascicles exhibit different creep and stress relaxation behaviour. *Proceedings of the Institution of Mechanical Engineers. Part H, Journal of engineering in medicine* 2013;228(1):49–59.

[84] Folkhard W, Geercken W, Knörzer E, et al. Structural dynamic of native tendon collagen. *J Mol Biol* 1987;193(2):405 – 407.

[85] Zec ML, Thistlethwaite P, Frank CB, et al. Characterization of the fatigue behavior of the medial collateral ligament utilizing traditional and novel mechanical variables for the assessment of damage accumulation. *Journal of biomechanical engineering* 2010;132(1):011001.

[86] Provenzano PP and Vanderby R. Collagen fibril morphology and organization: implications for force transmission in ligament and tendon. *Matrix biology : journal of the International Society for Matrix Biology* 2006;25(2):71–84.

[87] Amiel D, Frank C, and Harwood F. Tendons and ligaments: a morphological and biochemical comparison. *Journal of Orthopaedic Research* 1984;1(3):257 – 265.

[88] Thornton GM, Shrive NG, and Frank CB. Ligament creep recruits fibres at low stresses and can lead to modulus-reducing fibre damage at higher creep stresses: A study in rabbit medial collateral ligament model. *Journal of Orthopaedic Research* 2002;20(5):967–974.

[89] Sopakayang R and De Vita R. A mathematical model for creep, relaxation and strain stiffening in parallel-fibered collagenous tissues. *Medical Engineering and Physics* 2011;33(9):1056–1063.

[90] Solomonow M. Ligaments: A source of work-related musculoskeletal disorders. *Journal of Electromyography and Kinesiology* 2004;14(1):49–60.

[91] Provenzano P, Lakes R, Keenan T, et al. Nonlinear ligament viscoelasticity. *Annals of Biomedical Engineering* 2001;29(10):908–914.

[92] Johnson GA, Tramaglini DM, Levine RE, et al. Tensile and viscoelastic properties of human patellar tendon. *Journal of orthopaedic research : official publication of the Orthopaedic Research Society* 1994;12(6):796–803.

[93] Kubo K, Kawakami Y, Kanehisa H, et al. Measurement of viscoelastic properties of tendon structures in vivo. *Scandinavian journal of medicine & science in sports* 2002;12(1):3–8.

[94] Thornton GM, Oliynyk a, Frank CB, et al. Ligament creep cannot be predicted from stress relaxation at low stress: A biomechanical study of the rabbit medial collateral ligament. *Journal of Orthopaedic Research* 1997;15(5):652–656.

[95] Screen HRC. Investigating load relaxation mechanics in tendon. *Journal of the Mechanical Behavior of Biomedical Materials* 2008;1(1):51–58.

[96] Thornton GM, Schwab TD, and Oxland TR. Cyclic loading causes faster rupture and strain rate than static loading in medial collateral ligament at high stress. *Clinical Biomechanics* 2007;22(8):932–940.

[97] Ker RF, Wang XT, and Pike aV. Fatigue quality of mammalian tendons. *The Journal of experimental biology* 2000;203(Pt 8):1317–1327.

[98] Arumugam V, Naresh MD, Somanathan N, et al. Effect of strain rate on the fracture behaviour of collagen. *Journal of Materials Science* 1992;27(10):2649–2652.

[99] Wang XT, Ker RF, and Alexander R. Fatigue Rupture of Wallaby Tail Tendons. *J. Exp. Biol.* 1995;198(3):847–852.

[100] Bella J and Berman HM. Crystallographic evidence for C alpha-H...O=C hydrogen bonds in a collagen triple helix. *Journal of molecular biology* 1996; 264(4):734–742.

[101] Mason P. The viscoelasticity and structure of keratin and collagen. *Kolloid-Zeitschrift und Zeitschrift für Polymere* 1965;202(2):139–147.

[102] Jozsa LG and Kannus P. *Human Tendons: Anatomy, Physiology, and Pathology*. Human Kinetics, Champaign, IL 1997.

[103] Huang H, Zhang J, Sun K, et al. Effects of repetitive multiple freeze-thaw cycles on the biomechanical properties of human flexor digitorum superficialis and flexor pollicis longus tendons. *Clinical biomechanics (Bristol, Avon)* 2011; 26(4):419–23.

[104] Ng BH, Chou SM, Lim BH, et al. The changes in the tensile properties of tendons after freeze storage in saline solution. *Proceedings of the Institution of Mechanical Engineers. Part H, Journal of engineering in medicine* 2005;219(6):387–392.

[105] Monaco J. Orthopedic Consideration In Pregnancy. *Prim Care Update Ob/Gyns* 1996;3(6):197 – 200.

[106] Ireland ML and Garrick JG. The Effects of Pregnancy on the Musculoskeletal System. *Clinical Orthopaedics & Related Research* 2000;372:169–179.

[107] Wells SM, Pierlot CM, and Moeller aD. Physiological remodeling of the mitral valve during pregnancy. *AJP: Heart and Circulatory Physiology* 2012; 303(7):H878–H892.

[108] Fitzgerald CM and Segal NA. *Musculoskeletal Health in Pregnancy and Postpartum for Clinicians*. Springer International, Cham 2015.

[109] Cheng V and Screen H. The micro-structural strain response of tendon. *Journal of Materials Science* 2007;42:8957–8965.

[110] Fratzl P. Collagen: Structure and mechanics, an introduction. In *Collagen*, pages 1–13. Springer, Boston, MA. ISBN 9780387739052 2008;.

[111] Cisneros DA, Hung C, Franz CM, et al. Observing growth steps of collagen self-assembly by time-lapse high-resolution atomic force microscopy. *Journal of Structural Biology* 2006;154(3):232–245.

[112] Orgel JPRO, Irving TC, Miller A, et al. Microfibrillar structure of type I collagen in situ. *Proceedings of the National Academy of Sciences of the United States of America* 2006;103(24):9001.

[113] Holmes DF, Graham HK, Trotter JA, et al. STEM/TEM studies of collagen fibril assembly. *Micron* 2001;32(3):273–285.

[114] Sasaki N, Shukunami N, Matsushima N, et al. Time-resolved X-ray diffraction from tendon collagen during creep using synchrotron radiation. *Journal of Biomechanics* 1999;32(3):285–292.

[115] Hannafin JA and Arnoczky SP. Effect of cyclic and static tensile loading on water content and solute diffusion in canine flexor tendons: an in vitro study. *Journal of orthopaedic research : official publication of the Orthopaedic Research Society* 1994;12(3):350–356.

[116] Thielke RJ, Vanderby R, and Grood ES. Volumetric changes in ligaments under tension. *Proc. ASME Bioeng. Conf.* 1995;29(197).

[117] Chimich D, Shrive N, Frank C, et al. Water content alters viscoelastic behaviour of the normal adolescent rabbit medial collateral ligament. *Journal of Biomechanics* 1992;25(8):831–837.

[118] Svensson RB, Coupp C, and Magnusson SP. Mechanical Properties of the Aging Tendon. In *Mechanical Properties of Aging Soft Tissues*, pages 135 – 165. ISBN 978-3-319-03969-5 2015;.

[119] Svensson RB, Mulder H, Kovanen V, et al. Fracture mechanics of collagen fibrils: Influence of natural cross-links. *Biophysical Journal* 2013;104(11):2476–2484.

[120] Craig AS, Birtles MJ, Conway JF, et al. An estimate of the mean length of

collagen fibrils in rat tail-tendon as a function of age. *Connective tissue research* 1989;19(1):51–62.

[121] Silver FH, Christiansen DL, Snowhill PB, et al. Role of storage on changes in the mechanical properties of tendon and self-assembled collagen fibers. *Connective tissue research* 2000;41(2):155–164.

[122] Ker RF, Alexander RM, and Bennett MB. Why are mammalian tendons so thick? *Journal of Zoology* 1988;216:309–324.

[123] Veiersted, K B, Westgaard, R H, and Andersen P. Pattern of muscle activity during stereotype work and its relation to muscle pain. *International Archives of Occupational and Environmental Health* 1990;62:31–41.

[124] Jensen BR, Schibye B, Søgaard K, et al. Shoulder muscle load and muscle fatigue among industrial sewing-machine operators. *European Journal of Applied Physiology and Occupational Physiology* 1993;67(5):467–475.

[125] Aaras A, Fostervold KI, Ro O, et al. Postural load during VDU work: a comparison between various work postures. *Ergonomics* 1997;40(11):1255–1268.

[126] Østensvik T, Veiersted KB, and Nilsen P. A method to quantify frequency and duration of sustained low-level muscle activity as a risk factor for musculoskeletal discomfort. *Journal of Electromyography and Kinesiology* 2009; 19(2):283–294.

[127] Søgaard K, Fallentin N, and Nielsen J. Work load during floor cleaning. The effect of cleaning methods and work technique. *European journal of applied physiology and occupational physiology* 1996;73(1-2):73–81.

[128] Hanvold TN, Wærsted M, Mengshoel AM, et al. The effect of work-related sustained trapezius muscle activity on the development of neck and shoulder pain among young adults. *Scandinavian Journal of Work, Environment & Health* 2013;39(4):390–400.

[129] Hess GP, Cappiello WL, Poole RM, et al. Prevention and treatment of overuse tendon injuries. *Sports medicine (Auckland, N.Z.)* 1989;8(6):371–384.

[130] Lin TW, Cardenas L, and Soslowsky LJ. Biomechanics of tendon injury and repair. *Journal of Biomechanics* 2004;37(6):865–877.

[131] Schechtman H and Bader DL. In vitro fatigue of human tendons. *Journal of Biomechanics* 1997;30(8):829–835.